NPL REPORT
DQL-AC 010

Improvements in the provision of standards for underwater acoustics at simulated ocean conditions

GRAHAM A BEAMISS,
GARY HAYMAN,
STEPHEN P ROBINSON
and ALEX D THOMPSON

NOT RESTRICTED

DECEMBER 2004

Improvements in the provision of standards for underwater acoustics at simulated ocean conditions

by

Graham A. Beamiss, Gary Hayman,
Stephen P. Robinson and Alex D. Thompson

ABSTRACT

In this report, a description is given of the improvements made to the provision of standards for underwater acoustics at simulated ocean conditions by the UK National Physical Laboratory. The improved techniques now employed to make acoustic measurements in the APV facility are described, and results obtained using the techniques are presented.

The engineering modifications made to enhance the mounting and positioning of devices within the test chamber have improved the operational performance of the facility. In addition, improvements have been made to the procedures for the calibration of acoustic transducers and hydrophones by both absolute and relative methods, dramatically increasing the speed of measurements, and to the measurement of transducer electrical impedance. Work has also been undertaken to determine the acoustic properties of the APV test chamber with parameters determined such as the echo-free time as a function of position, reverberation time, ambient noise levels, and the performance of the acoustic absorbers in providing echo-reduction. A novel technique based on signal modelling has been used to extend the frequency range of operation of the APV down in frequency for calibration of high-Q projectors. Finally, the traceability of open-water calibrations at the Wraysbury facility is described. Particular emphasis is placed on methods to account for the variation in response of reference transducers with temperature, and an assessment is made of the current limitations and planned improvements.

ISSN 1744- 0599

National Physical Laboratory
Teddington, Middlesex TW11 0LW

Approved on behalf of Managing Director, NPL, by Dr B. Zeqiri,
authorised by Director for Quality of Life Division.

CONTENTS

1. INTRODUCTION

1.1 BACKGROUND

1.1.1 Underwater acoustic calibration

In underwater acoustics, electroacoustic transducers are typically used to generate and detect acoustic fields. Such transducers are most often characterised in terms of absolute sensitivity levels (important as source level and receive sensitivity are often used to determine range or detection limits) and device directivity (important for beam forming and for noise rejection). If the transducer specification is to be unambiguous, quantitative measurements of these parameters must be made, and for these measurements to be meaningful, they must be traceable to common standards of measurement [1-3]. The only National Metrology Institute in Europe that is actively involved in underwater acoustics and able to provide such traceable measurements in is NPL [4, 5].

NPL currently provide a range of calibration and testing services for the underwater acoustics community under the auspices of the DTI National Measurement System (NMS) Acoustic Metrology Programme. Traceable measurements under free-field conditions are provided at frequencies from 1 kHz to 1 MHz using NPL's suite of facilities that include laboratory tanks, the largest of which is a circular wooden tank of 5.5 metres diameter and 5 metres deep, equipped with a precision positioning system There is also an open-water facility located on a reservoir about 8 miles from NPL, the reservoir being approximately 2 kilometres long by 1 kilometre wide, with a typical depth of 22 metres. All free-field calibrations and testing carried out in the open tanks and the open-water facility are limited to ambient temperatures and depths of a few metres, conditions which are not necessarily representative of the transducer operating conditions in the ocean.

1.1.2 Simulated ocean conditions

As applications require transducers to operate at ever increasing depths, the need to conduct acoustic measurements under ocean conditions is growing. Clearly, one option is to undertake sea-trials, but although such exercises are inevitably required for testing of large systems, they are very expensive and the environmental conditions are limited to the prevailing temperature in the ocean and the (often limited) depth obtainable with the tether management system used on the vessel. For cost-effective testing and validation, a shore-based laboratory alternative is required to replace some of the activities undertaken on sea-trials, and to provide increased confidence in transducer performance before commitment is made to the expense of measurements at sea.

As an alternative, the conditions in the ocean may be partly simulated by use of small laboratory pressure vessels, allowing the testing of acoustic devices at elevated hydrostatic pressures to simulate depth. These pressure vessels are typically made of steel and are small in size, restricting the range of measurements that can be conducted within them, and in particular, corrupting any acoustic measurements with reflections from the vessel boundaries, making free-field measurements impossible. If the pressure pot is made from a material such as glass fibre, it may even appear acoustically "transparent" when submerged in water at low frequencies (below a few kilohertz). Such a small pressure pot can then be used for free-field testing in laboratory tanks and open water facilities to simulate the effect of water depth. However, the transparency to the acoustic field is only an approximation that is valid for low frequencies and such pressure pots cannot in general accommodate measurements conducted at higher frequencies [1].

To enable free-field measurements to be made at simulated ocean conditions requires a pressure vessel large enough to allow free-field conditions to be realised by use of time-gating techniques. The ability to provide positional control for the transducers and hydrophones under test is also required. To simulate ocean conditions, the test chamber must be capable of being sealed and pressurised to simulate ocean depth, and the temperature of the water must be controllable over the range of temperatures commonly found in the ocean. To simulate the complete range of conditions in the ocean, including the hydrostatic pressures observed at full ocean depth of 6,000 m, in a vessel large enough to undertake free-field measurements at frequencies as low as a hundred hertz, is very difficult to achieve technically and would be very expensive. Inevitably, a compromise must be reached between available budget, finite size, operating frequency range, maximum operating pressure and operating temperature range.

1.1.3 The NPL Acoustic Pressure Vessel

The NPL Acoustic Pressure Vessel (APV) addresses the above requirement by providing the capability to carry out free-field acoustic testing of transducers at simulated ocean conditions from a few kilohertz up to 500 kHz [6-8]. The APV is a unique facility within Europe, being the only available acoustic test facility of this type, and it forms an essential part of the UK's National Measurement System for underwater acoustics [9].

The APV provides industry with traceable calibrations and tests for underwater acoustic devices under closely controlled environmental conditions. The water temperature can be varied over the range 2 °C to 35 °C, and a hydrostatic pressure may be applied of up to 7 MPa (equivalent to a water depth of approximately 700 metres). A full operational specification is detailed in Appendix 1 of this report.

Figure 1.1 shows a plant-room view of the APV, which is enclosed by a layer of black thermal insulation. The test chamber is sited on anti-vibration mounts and has strategically positioned sound-absorbing wedges within the vessels interior [10-11]. In addition, various pumps, valves, filters and pipelines can also be seen in the foreground of the photo.

Figure 1.1 Acoustic Pressure Vessel.

1.2 SCOPE OF APV IMPROVEMENT WORK

Though the APV was demonstrated to work satisfactorily as an operational facility, the work to establish the APV facility highlighted a number of areas that would benefit from improvement and upgrading. These were described in NPL Report CMAM 76 [9] and are reproduced here:

1. Incorporating adjustment to the height of the transducers, preferably under automatic control, to improve alignment for directional transducers;
2. Increasing the flexibility of the transducer mounting in general so that a greater variety of devices can be accommodated;
3. Increasing the flexibility in the use of the extension cradle;
4. Increase the variety of cable sizes that can be accommodated;
5. Establish the capability to mount large panels within the APV for testing properties of materials;
6. In the longer term, establish the capability to scan a transducer along axes orthogonal to the main tank axis.
7. Improve the implementation of the free-field reciprocity method to reduce uncertainties and increase speed;

8. Improve the speed and flexibility of relative calibrations in the APV and assess accuracies;
9. Increase the flexibility of impedance measurement to enable measurements to be taken using tone-burst signals;
10. Fully characterise the performance of the current reference transducers with temperature and pressure at NPL;
11. Characterise the acoustic properties of the APV more fully in terms of reverberation time, echo free time, echo reduction of anechoic lining, background noise levels, etc;
12. Investigate techniques to extend the lower frequency range of measurements;
13. Undertake comparisons of measurements in the APV with those in other facilities (eg USA, China);
14. Perform a systematic assessment of commercial designs of hydrophone and identify devices suitable as reference devices for simulated ocean conditions, in particular for frequencies greater than 200 kHz;
15. Develop experimental techniques to enable the characterisation of materials in the form of panels as a function of temperature and pressure using parametric array and/or linear acoustics.

Although considerable progress has been made with addressing items 5, 14 and 15, the results of this work are reported elsewhere and so do not form part of this report. Funding was not available to address items 6 and 13 during the period since NPL Report CMAM 76 was written.

However, work to address items 1-5 ands 7-12 has been undertaken as part of the 2001 - 2004 NMS Acoustical Metrology Programme funded by the National Metrology Directorate of the UK Department of Trade and Industry. It is the results of this work that are described in this report.

1.3 WRAYSBURY OPEN-WATER ACOUSTIC TEST FACILITY

A major dissemination route for the UK underwater acoustic primary standard is NPL's open-water calibration facility based on a reservoir at Wraysbury, about 8 miles from the main NPL laboratories in Teddington. The facility consists of a calibration raft in the centre of a 1 km x 2 km fresh water reservoir with an average water depth of over 20 m and can be seen in Figure 1.2. Here, free-field calibrations and measurements are undertaken in the frequency range from below 1 kHz to 350 kHz to characterise the performance of acoustic transducers or complete sonar systems. The calibration raft has three separate, fully instrumented measurement stations, with hoists and handling equipment capable of deploying large sonar arrays up to 1.5 tonne. The facility is integrated into the provision of acoustical standards under the auspices of the National Measurement System, providing a high volume of calibrations traceable back to primary standards maintained at NPL Teddington.

However, the calibrations that are undertaken at Wraysbury have some limitations. Being an open-water site, there is no control over the water temperature, and the reference projectors which have traditionally been used at Wraysbury have sensitivities which are dependent on temperature. Historically, this has led to the need for time-consuming absolute calibrations to be undertaken periodically throughout the year by the free-field reciprocity method in order to check the transducer sensitivities. Due mainly to time constraints, these calibrations are only practical at a few temperatures in the typical seasonal variation of 4 °C to 21 °C.

Relatively large components have then been included in the uncertainty budget to account for drift in the reference sensitivities with temperature.

Figure 1.2 The Acoustic Calibration Facility located on Wraysbury reservoir.

Another limitation is posed by the restriction on the depth of immersion to only 5 metres. Along with the limitations of the on-board signal-processing techniques routinely used, this restricts the lower frequency range to only 1 kHz. With suitable improvements to the facility and experimental procedures, it should be possible to extend the lower frequency range for free-field measurements to below 1 kHz.

With the above in mind, as part of the 2001-2004 NMS Acoustical Metrology Programme funded by the National Measurement System Directorate (NMSD) of the UK Department of Trade and Industry, NPL undertook a brief study to determine the limitations of the current facility and how the traceability of calibrations undertaken at Wraysbury may be improved with the adoption of different methodologies. Since much of this is related to methods of accounting for the variation in reference transducer sensitivity with temperature, this work was undertaken as part of the programme to provide improved dissemination of standards for simulated ocean conditions, and the results are reported here.

1.4 REPORT STRUCTURE

In this report, a description is presented of the work conducted to address the issues outlined in sections 1.2 and 1.3.

Chapter 2 details the engineering improvements that have been carried out to enhance the mounting and positioning of devices within the test chamber, and describes how these improve the operational performance of the facility.

Chapter 3 describes the work undertaken to improve the methods of measuring the electrical impedance of transducers in the APV. Chapter 4 documents the improvements that have been implemented to address issues relating to conducting free-field reciprocity calibrations within the APV. Improvements were carried out to all aspects of the procedure including the hardware, software and measurement procedure and some example results are shown. Chapter 5 describes the implementation of more rapid relative calibration methods in the APV, which include the use of reference hydrophones and projectors previously calibrated by the free-field reciprocity method.

Chapter 6 discusses the work in determining the acoustic properties of the APV test chamber including, echo-free time, reverberation time, ambient noise levels and of the performance of the acoustic absorbers in providing echo-reduction. Chapter 7 depicts the work undertaken to attempt to extend the frequency range of measurements in the APV and Chapter 8 describes the results of the study to assess the improvements required to the traceability of calibrations provided by the Wraysbury open-water facility. The final chapter summarises the report and makes some suggestions for future work.

2. IMPROVEMENTS TO FACILITY HARDWARE

2.1 PRIOR LIMITATIONS

Having gained operational experience of the APV facility following its commissioning in 2000, it became apparent that a number of issues required addressing to improve the quality of the technical work undertaken and to make the facility more user-friendly and time-efficient to use. Of course, the logistics of operating a facility such as the APV are such that it takes longer to produce measurement results than is typical for an open-tank facility. For example, the time required to change water temperature, pressurise the chamber, and remove and replace the port lids all add to the time normally taken for acoustic measurements.

At the beginning of the current NMS program no height adjustment of transducers or artefacts retained within the test chamber was possible on any of the existing mounting stages and hydrophone rotation from the large lid suffered from backlash which had to be removed. The transducer mounting in general lacked flexibility and there was difficulty in accommodating common commercially available devices, which frequently meant that modifications to existing mounts were required to provide a temporary solution. The two mounting cradles accessible through the small port currently have very limited functionality; they are only able to support devices with no ability to provide such movement as rotation or lateral translation. Transducer cables in the range 5 to 20 millimetres diameter are able to be pressure sealed and it is possible to pass connectors of up to 38 millimetres through either of the two test chamber lids. This could potentially cause problems if artefacts for testing have cable diameters or integral connectors that fall outside of this specification. The requirement to provide a measurement service for the characterisation of panel materials has grown considerably from the time that the APV was first put into service at the NPL. Therefore it became important that there should be an ability to support large panels within the test chamber. The remainder of this chapter details these issues and where appropriate, the measures taken to address them.

2.2 VERTICAL HEIGHT ADJUSTER

All the mounting of devices and artefacts for test using the APV facility is conducted in the laboratory area on the mezzanine floor level, and suitable fixtures such as mounting poles are used for securing the devices to the appropriate mounting stages [9]. For the vast majority of work where two or more acoustic devices are used, it is desirable to have all of the devices positioned on the central axis of the APV as this generally maximises the echo-free time available for a given transducer separation. In the past, it had only been possible to achieve this by manually calculating the required heights from physical measurement made of the vessel's interior and applying any appropriate height offsets to the devices during the initial mounting process that was carried out in the laboratory, with no further height adjustments being possible once the devices were in the test chamber. Applying the correct height offset is an important consideration for work carried out in the APV as there is no vertical reference point that relates to all three mounting stages, each mounting point being at a different height to the other two. In practice, this is adequate for the majority of low-frequency measurement work conducted in the APV using transducers which are nominally omnidirectional.

Although this is acceptable for most work in the APV conducted at these lower frequencies, it is not always the case for devices that are more directional and operate at hundreds of kilohertz. For devices of this nature, the need for acoustic alignment is increased, and with this in mind, the implementation of a vertical height adjuster was deemed necessary. A specification was drawn up for a system to move any artefact vertically through approximately 200 millimetres while being positioned underneath the large lid, this movement being possible while the test chamber is at the maximum simulated depth. Although the solution, shown below in Figure 2.1, was from an engineering aspect quite a straightforward solution, it still required significant modifications be made to the hardware associated with the large lid. The solution required stripping down the entire large lid rotary system and removing the existing rotator shaft that feeds through the lid. This was required since the shaft was modified by boring a large hole through its length. An extension piece was fabricated and then welded onto the top of the tube to facilitate the insertion of a new thinner shaft through the bore. The new shaft mates to the drive motor sited on top of the existing rotator box, and at the bottom, a new standard mounting flange (manufactured to the same specification to the existing flange) was secured on to the shaft. This mounting flange is important as it provides the interface to which devices are located. The original locking nut assembly that prevents the shaft from extruding through the lid when pressure is applied to the test chamber has been retained, with new seals being introduced to the vessel to maintain a pressure seal around the new shaft, even when traversing while the test chamber is in a state of pressurisation.

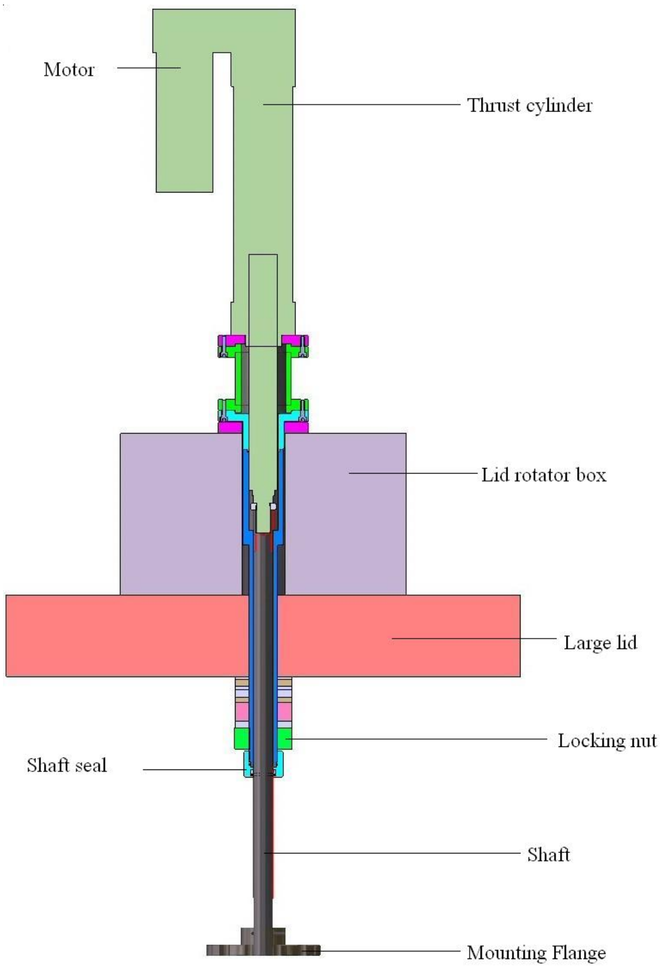

Figure 2.1 Cross-sectional schematic view of the vertical height adjuster incorporated into the large lid

The vertical height adjuster can be controlled by three methods of operation: from the front of its control panel via two buttons that control the direction of movement; via a pendant controller; and finally, operation can be actioned and monitored through one of the PC's that control the suite of acoustic measurement software. Positional accuracy is in the range of 0.1 millimetres and is also repeatable to within 0.1 millimetres. Although currently only manually controlled, there is scope to further enhance the functionality of the vertical height adjuster by integrating the operational control into the suite of acoustic measurement software, this would allow automatic maximisation of any acoustic signals and also allow for scanning to take place in the vertical axis for devices that are attached to the large lid mounting flange.

2.3 LID ROTATOR

The lid rotator in its current form is identical to that first commissioned at NPL. The current rotator system employed uses fifty-year-old technology and the rotational movement is supplied via a Scientific-Atlanta system that was typically designed to rotate antennas or flag poles. The only upgrading that took place at the time of commissioning was to replace the internal motor and provide a new control box for the unit. Generally, it performs its task of rotating devices mounted to the large lid rotator shaft adequately, but with significant levels of backlash in the movement of the rotator. In addition, several other problems have occurred, generally consisting of the rotator binding with the lid seals which in-turn causes the drive motor to stall during a move; when this happens, there is no way of continuing the desired rotation. In such a case, before a move can be completed, the rotator must be freed by reversing the direction of travel. This could potentially result in abandoning an acoustic measurement and re-starting once the rotator shaft has been freed (the most common type of acoustic measurement requiring the rotation of the large lid is directional response through which device beam patterns are measured). One of the added complications is that there is no feedback from the motor encoder to the control system to flag that a move is either incomplete or unfinished. This is of concern as there would be no warning to the operator if the stalling of the motor was in fact caused by some other cause such as a device cable snagging around an obstacle in the large lid area.

To investigate these issues, the rotator assembly and large lid was examined, with the lid rotator assembly being completely dismantled. A visual inspection of the internal components suggested several options to resolve the problem. Although the ideal solution would involve installation of a completely new rotator system along with the implementation of new sealing techniques to provide the pressure seal between the lid and rotator shaft, it was clear that with relatively minor physical modifications the rotator system, it could be made to function in a way which met operational requirements and was more reliable and resistant to failure due to binding of seals.

It was decided that the original system and sealing technology would be retained with modifications being carried out to the rotator. The improvements will include the addition of a new positional reader that will feed back to the controller the exact angular position of the rotator shaft. It will also be possible to interrogate it to confirm that a desired move is being implemented correctly and it has not stalled during the movement. The physical modifications and additions required for this are relatively minor with all the new hardware being sited on the top surface of the existing rotator box. The visual inspection conducted indicated that the seals bind on the rotator shaft when they age significantly. The condition of the seals cannot be determined without stripping down the large lid as the pressure seal is still made with this level of seal wear and so no other indication of seal wear is available. Therefore, although the current sealing technique employed between the rotator shaft and large lid will be retained, a new planned maintenance routine has been introduced to eliminate the binding problem.

The option that included replacing the existing Scientific-Atlanta rotator with a new form of rotator that has no backlash associated with it was discarded due to the level of engineering required and the significant cost associated with it. The implementation of new sealing technology would require machining the large lid to house the new seals. It was decided that there was an element of risk associated with this, as the worst-case result would be that the lid would not retain a pressure seal, leaving no ability to pressurise the test chamber until further modification work had been performed to rectify such problems.

Currently, the physical implementation of the new hardware for the large lid rotator is in progress and it is anticipated that the work will be completed by early 2005.

2.4 INTERNAL SLIDEWAY

The internal slideway system operated within the test chamber is the original system that has been used for the vessel's entire life and operates the two mounting stages accessible through the small port. Propulsion is provided through a series of drive shafts and gearing mechanisms that interface with a motor positioned externally at one end of the APV. The primary mounting stage known as the main cradle can be seen below in Figure 2.2 along with the azimuth motor that allows for limited rotation of the cradle when installed. The two drive shafts that run across the width of the mounting stage can also be seen, one of which is connected to a fibre gear (shown in the top right of the photograph) that meshes with the rack providing the ability for the mounting stages to be traversed down the length of the chamber. Fibre has historically been the material of choice for that particular gear so that a weakness is deliberately built into the slideway. This means that in the event of excess resistance being imposed upon the slideway, the fibre gear would fail gracefully, thereby protecting the rest of the drive mechanism.

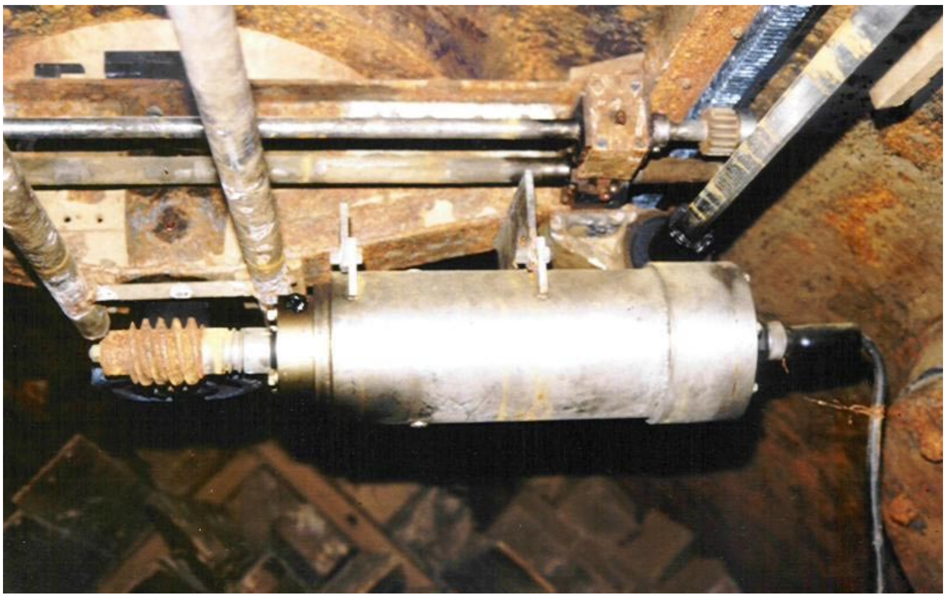

Figure 2.2 Test chambers internal slideway

The system is of an antiquated nature requiring a number of shafts and gears to work in conjunction with each other allowing the slideway to traverse without incurring any operational problems such as the slideway sticking, stalling, or in the worst case, stripping a fibre gear. A number of causes can lead to this happening and include transducer cables getting caught up on the internal structure of the vessel or slideway, objects such as rust or lime-scale deposits getting between either the vessel wall and the slideway or the fibre gear and track. Finally, it is possible for the two sides of the slideway to get misaligned over a period of time due to backlash becoming evident in one or both of the fibre gears.

It is outside of the scope of current work to consider anything other than a rigorous regime of planned preventative maintenance to retain this existing slideway in good working order, due to the significant cost of designing and installing a replacement system. Many complications exist in potentially replacing the system, as it would most likely involve a completely new suite of components that could include the use of hydraulics to drive a new slideway and would likely involve attaching items to the fabric of the vessel. Any such work would incur strict procedures to be followed to ensure that the vessels integrity was not compromised. With this in mind and through a detailed investigation, a thorough maintenance plan was drawn up that should keep the existing slideway functioning to an acceptable level for the immediate future.

2.5 MOUNTING POLES FOR TRANSDUCERS AND HYDROPHONES

For initial work undertaken in the APV, very limited mounting poles and rigging were available. The vessel did not come supplied with a suite of mounting poles and brackets and any such mounts would have been unlikely to have interfaced with NPL transducers or those most commonly used by UK industry, since the vessel was originally operated at the Naval Underwater Warfare Center (NUWC) where devices of a physically different geometry are generally used. During this early period of operation at NPL, rigging was manufactured to suit devices and artefacts on an *ad-hoc* basis with the core of the mounting capability for standard types of hydrophones coming from redundant aluminium mounting poles obtained from one of the NPL open tank facilities.

From the experience gained using existing redundant poles, it has been possible to produce a specification for the supply of a suite of mounting poles that will provide easier mounting of the transducers most commonly used in the APV. When supplied, the mounts will provide greater flexibility of mounting, allowing acoustic devices to be easily interchanged between the various mounting points within the test chamber, namely the large lid mounts and the two mounting cradles that are accessible through he small port. A suite of short poles that are nominally 150 millimetres long and designed to mate specifically with a particular type of transducer or hydrophone will be supplied. The non-hydrophone end of the short pole will interface with lengths of bar that are compatible with all of the mounting stages with a quick release mechanism securing them. This approach to the mounting issue will facilitate easy and quick relocation of devices between the different mounting stages and will reduce device mounting times due to no longer needing to completely disassemble a mount assembly to either relocate devices or mount new ones. The short pole of a device will be replaced by one appropriate for the new device being mounted. The design process has been completed and the suite of mounting poles should be manufactured and supplied by Autumn 2004.

2.6 DUAL HYDROPHONE MOUNT

The addition of the dual hydrophone mount to the existing suite of device mounts has proved to be one of the most significant improvements to the operational side of calibration and experimental work. The ease of use of the mount has enabled measurements to be undertaken that would otherwise be prohibitively time-consuming. Prior to the commissioning of the dual hydrophone mount, it was only possible to mount one acoustic device through the large port, directly below the centre of the large lid.

The dual hydrophone mount shown below in Figure 2.3 is manufactured from stainless steel and is assembled from three sections consisting of an arbour that mounts directly to the standard mounting flange and two slotted arms that clamp together around it at an appropriate height for the work being undertaken. It has the capacity to securely hold several devices at user-defined positions along the length of the slotted arms by means of the hydrophone pole clamps that can be seen in the diagram below. In addition to this, the bottom of the arbour terminates in a mount suitable for securing heavy panels that might be used during materials characterisation in the APV [12, 13].

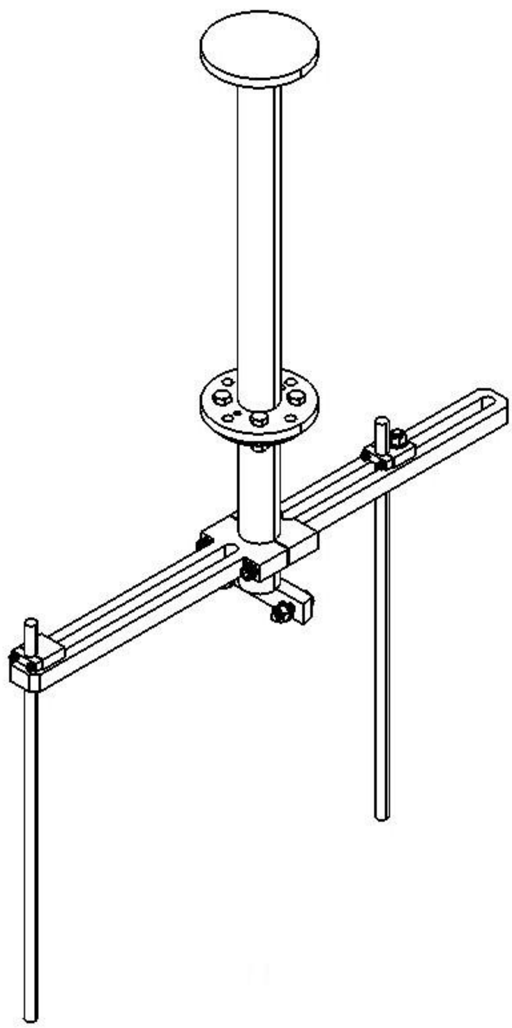

Figure 2.3 Dual hydrophone mount

The dual hydrophone mount lends itself to several measurement applications in addition to the panel characterisation work. It is extensively used to enable three transducer reciprocity calibrations to be conducted in a far more efficient way than was previously possible: this will be discussed in greater detail Chapter 4. It can also be utilised for measurement techniques that only require two devices to be present. For example, this mount will enable two “unknown” devices to be mounted in the test chamber at one time and when one of the two devices is not being characterised, it can be rotated through 180° so that its presence will not interfere with measurements being conducted on the second device. This is particularly useful when calibrations are being conducted at a series of pressures, as the whole suite of measurements can be conducted at the desired pressures without the need to de-pressurise the test chamber and re-mount devices. This can potentially save a considerable amount of time, since it reduces the time-consuming procedure required to firstly prepare the test chamber for pressurisation and secondly, to revisit the pressures of interest for a second time.

2.7 POTENTIAL IMPROVEMENTS

Other potential improvements have been identified over the period that the facility has been in operation. Some of these could potentially be implemented, while others either fall outside of the current scope of work or are not financially feasible.

The potential improvement that is worthy of future investigation is the implementation of bulkhead connectors positioned in the existing compression gland assemblies. This would allow cables of acoustic devices to be terminated on the test chamber side of a lid and would mean that the device cable would not be subjected to the clamping pressure exerted through the compression gland assemblies currently in use. This could be beneficial for some delicate cables such as thin fibre optic cables. Some transducer cables, particularly the softer ones made of neoprene rubber, will not stand up to being repeatedly compressed. Transducer and hydrophone cables are manufactured from different materials and some experience a relatively short life expectancy when repeatedly compressed, most notably when the operating temperature of the vessel is high. The implementation of bulkhead connectors would eliminate this problem and also prevent the possibility of cables being extruded while the test chamber is seeing an increase in hydrostatic pressure. On the laboratory side of the lid, an additional cable would be required to run from the bulkhead connector to the relevant piece of instrumentation. However, there are a couple of considerations if this type of feed through was to be used. The electrical loading of the additional cable being applied on the laboratory side of the lid would have to be accounted for if measurement results are to be accurate, as indeed would the bulkhead connector itself. Also there may be issues of compatibility, i.e. any devices using this type of feed through would need to be terminated with the correct connector to mate with the bulkhead connector.

Other modifications or improvements that may be carried out could include changes to the facility control system where all non-acoustic tasks are performed. Useful modifications would improve the versatility of some of the pre-programmed sequences that currently control such tasks as the pressurisation cycles, where, for example, an option of leaving the lid seals de-pressurised would enhance the operational functionality of the system. Another example of a beneficial software upgrade would be to have a form of automatic top-up routine associated with the Head Tank. This would be useful as the Head Tank has a relatively small water storage capacity of approximately 1000 litres and some calibration routines such as those involved in the characterisation of panel materials require significant volumes of water to be used, leading to regular and time-consuming filling of the Head Tank.

There were other possible improvements acknowledged in the former NMS programme but were considered too ambitious to be undertaken at this time [9]. They included increasing the flexibility of the extension cradle to allow it to move independently of the main cradle and for it to be able to be "swung" away to the side of the tank. A longer-term enhancement might be to establish the capability to scan a transducer along axes orthogonal to the main tank axis. This capability would be valuable when undertaking panel measurements, and would allow near-field measurement techniques to be used in the APV.

3. IMPROVEMENTS TO ELECTRICAL IMPEDANCE MEASUREMENTS

3.1 INTRODUCTION

The electrical impedance of a device is typically measured in the Acoustic Pressure Vessel (APV) using an Agilent 4294A Precision Impedance Analyser. This instrument steps through the frequency range of interest and measures the electrical impedance by applying a low voltage continuous wave signal to the device under test. While this method produces accurate results for the majority of devices, the measurements can be affected by interference due to reflections from the APV walls when the device under test is a low frequency, omni directional transducer [9]. A method of measuring the electrical impedance of a device using tone burst rather than continuous wave signals would enable reflections to be gated out and thereby improve the accuracy of the measurements made.

3.2 METHOD

3.2.1 Theory

The complex impedance is given by

$$Z_0 \cdot e^{i\theta_Z} = \frac{V_0 e^{i\theta_V}}{I_0 e^{i\theta_I}} \qquad (3.1)$$

or

$$Z_0 \cdot e^{i\theta_Z} = \frac{V_0}{I_0} \cdot e^{i(\theta_V - \theta_I)} \qquad (3.2)$$

so the magnitude and phase of the impedance are given by

$$Z_0 = \frac{V_0}{I_0} \quad \text{and} \quad \theta_Z = \theta_V - \theta_I \qquad (3.3)$$

The electrical impedance of a device can therefore be derived by applying a signal at the frequency of interest and measuring the voltage and current and the phase difference between them. Similarly, the magnitude and phase of the admittance are given by

$$Y_0 = \frac{I_0}{V_0} \quad \text{and} \quad \theta_Y = \theta_I - \theta_V \qquad (3.4)$$

From these values the conductance and susceptance can be obtained as follows

$$G = Y_0 \cos\theta_Y \quad \text{and} \quad B = Y_0 \sin\theta_Y \qquad (3.5)$$

3.2.2 Instrumentation

The HP89410A Vector Signal Analyser used at NPL has two input channels and a frequency response measurement mode which can display both the ratio of the signals appearing at the two inputs and the phase difference between them. Hence, by applying the voltage to channel 1 and the current to channel 2, both the magnitude and phase of the admittance of a device can be measured directly. Two methods of measuring the current have been used: a VIT-13 voltage/current sensor manufactured by Instruments Inc. and a low value resistor. The VIT sensor is connected between the signal source and the device under test and provides both voltage and current outputs. With the resistor method a low value resistor is connected in series with the device and by measuring the voltage drop across the resistor the current flow through it, and hence the device, can be calculated.

3.2.3 VIT voltage/current sensor

Figure 3.1 shows the equipment setup used for gated tone burst measurements of electrical impedance using the VIT sensor to monitor the voltage and current.

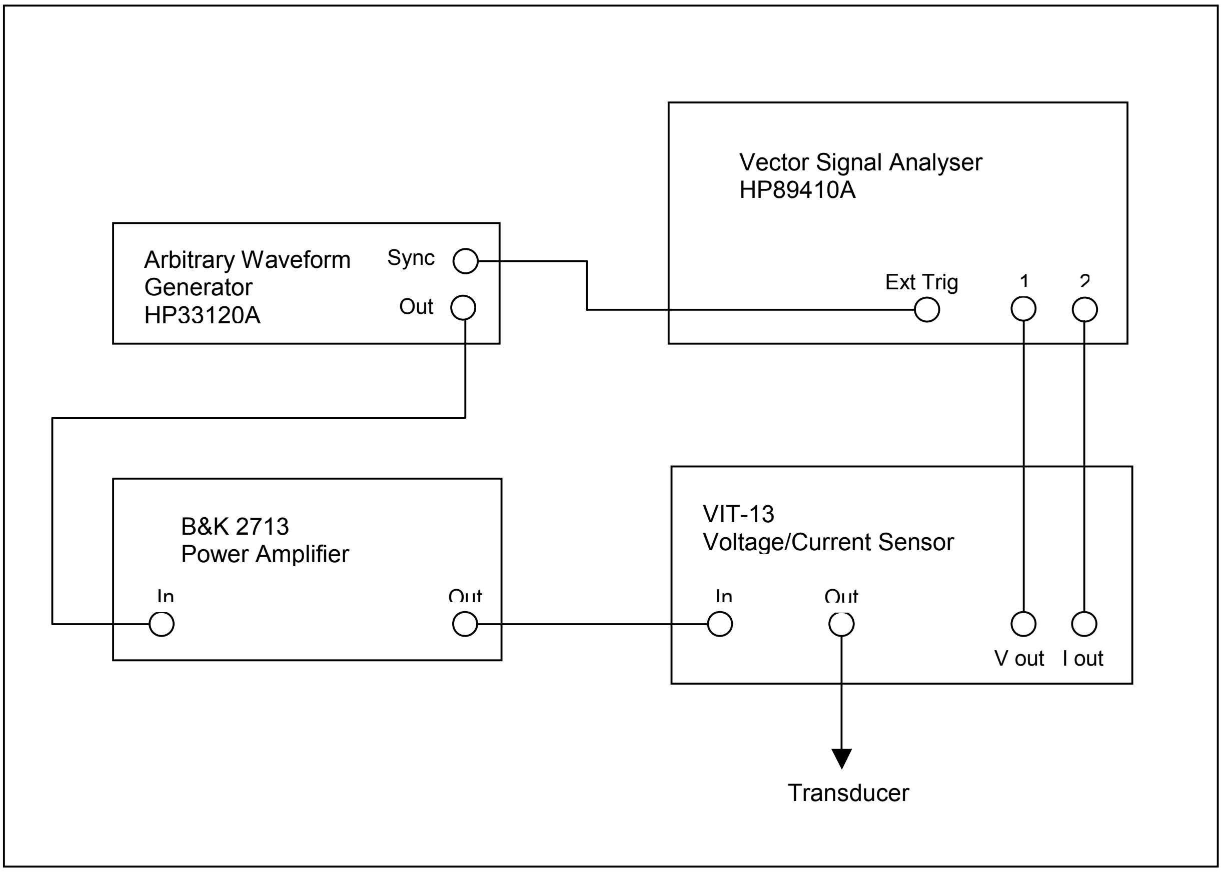

Figure 3.1 Equipment setup for gated tone burst impedance measurements using the VIT voltage/current sensor

A HP33120A arbitrary waveform generator is used to generate a short tone burst at the frequency of interest. This signal is then amplified by a B&K 2713 power amplifier before driving the transducer under test via a VIT-13 voltage/current sensor. The voltage and current outputs from the VIT sensor are then fed into the channel inputs of a HP89410A vector signal analyser, which is externally triggered from the SYNC output of the arbitrary waveform generator. Both the voltage and current channels of the VIT sensor have switchable sensitivity ranges enabling the impedance of a device to be measured using a high drive voltage without overloading the inputs of the HP89410A analyser.

3.2.4 Resistor method

Figure 3.2 shows the equipment and connections for current measurements using a resistor.

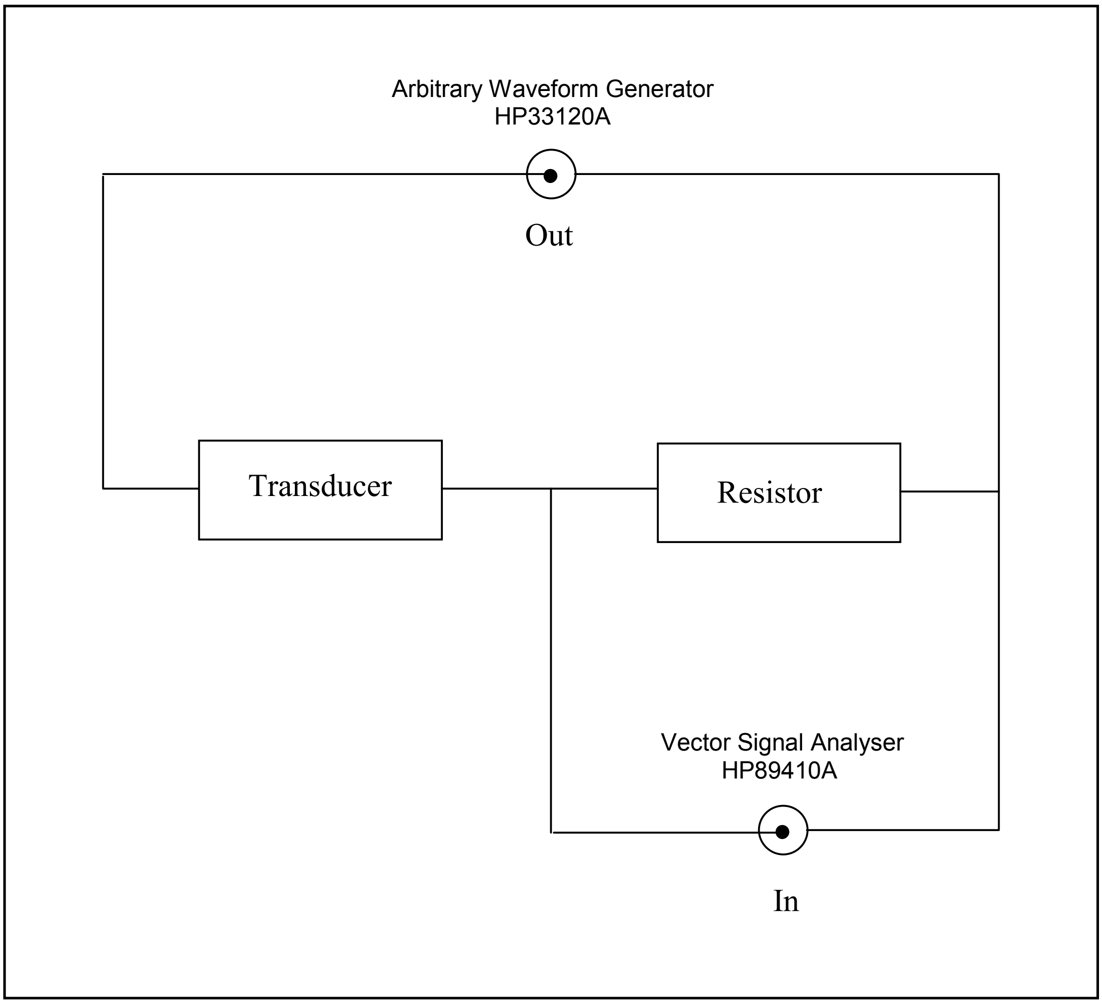

Figure 3.2 Current measurement using a resistor

The HP33120A arbitrary waveform generator is again used to generate a short tone burst at the frequency of interest, and this is applied across the transducer and a low value resistor connected in series. The current is calculated from the voltage drop across the resistor measured using the HP89410A vector signal analyser. For the voltage measurement the positions of the transducer and resistor are reversed and the voltage is measured directly across the transducer. As both the vector signal analyser inputs and the arbitrary waveform generator output are permanently grounded, the voltage and current measurements cannot be made simultaneously. In this case only one channel of the analyser is used and the magnitude and phase of the voltage and current are measured separately.

3.3 MEASUREMENTS

An example of the effect of interference from reflections is shown in Figure 3.3. An ITC 1001 transducer was mounted in the APV and the conductance and susceptance of the device measured over the frequency range 10 kHz – 35 kHz using the HP4294A impedance analyser. The data is displayed as an admittance loop by plotting the susceptance against the conductance for each frequency point. The effect of reflections from the walls of the APV can be seen as smaller re-entrant loops around the main resonance loop.

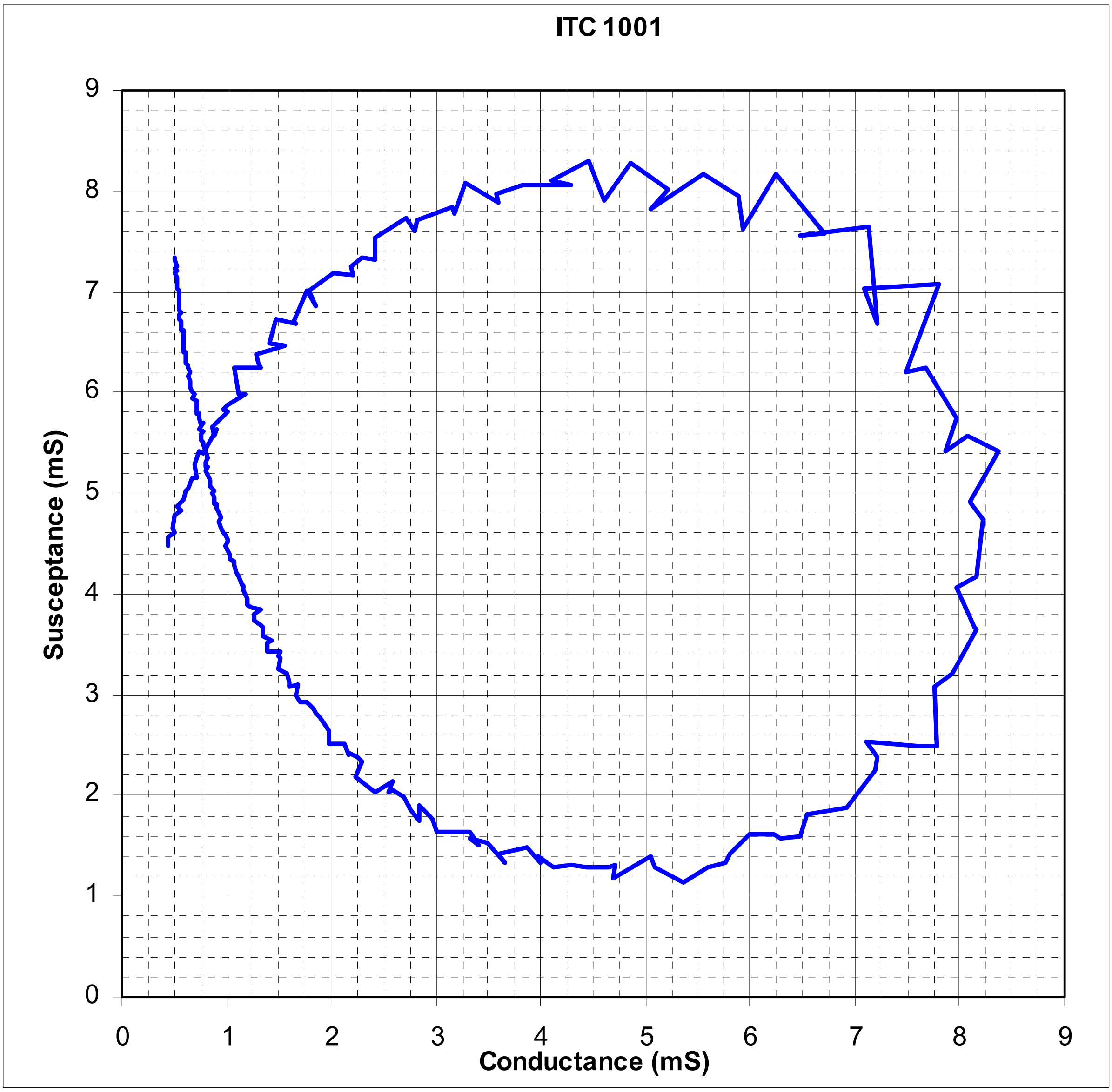

Figure 3.3 Admittance loop of ITC 1001 transducer measured in the APV using the HP4294A analyser

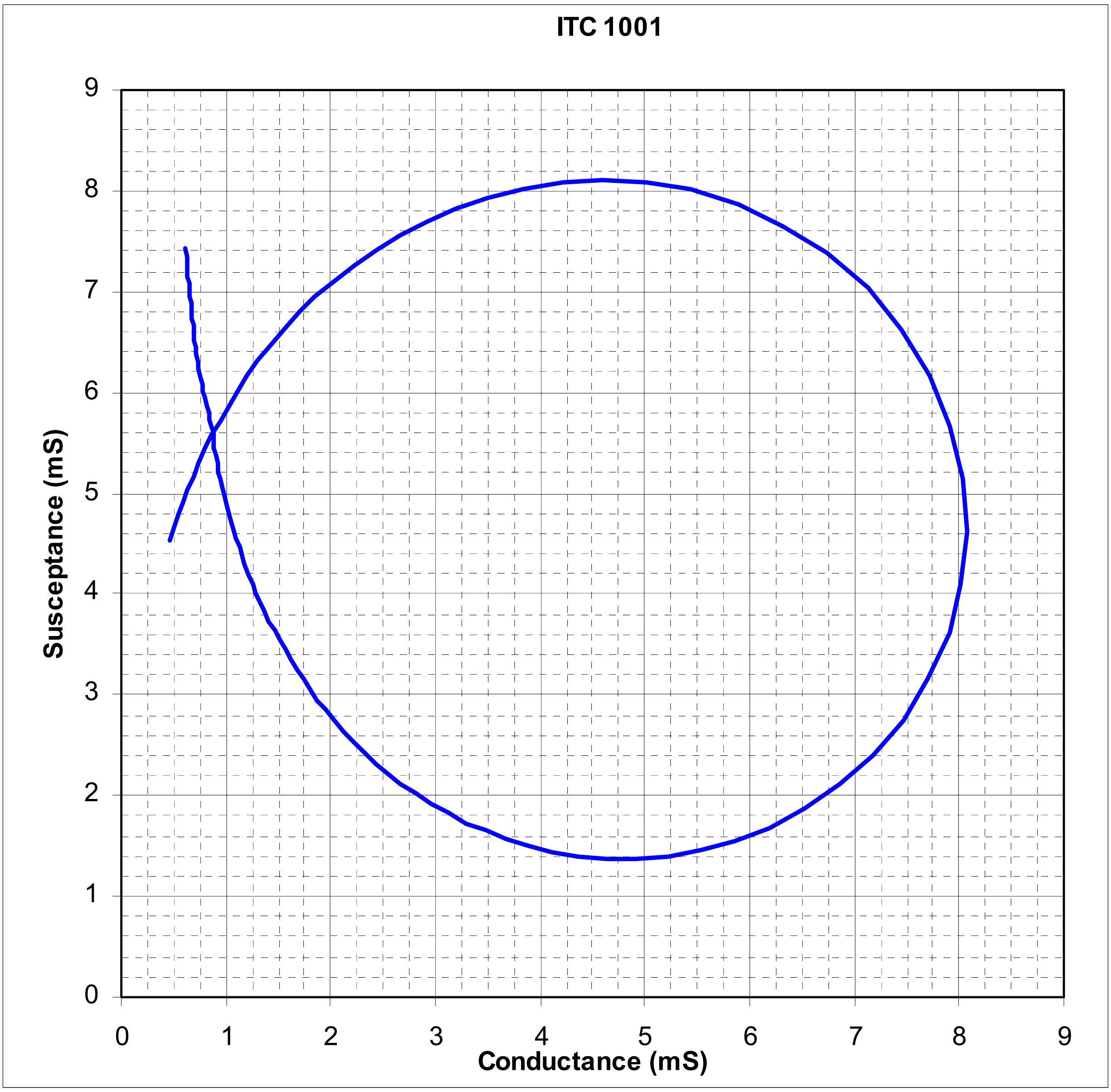

Figure 3.4 Admittance loop of ITC 1001 transducer measured in the APV using the gated tone burst method

By contrast, Figure 3.4 shows the same measurements made using the gated tone burst method. Here the measurement of the magnitude and phase of the voltage and current is completed before any reflections from the walls of the APV arrive back at the device.

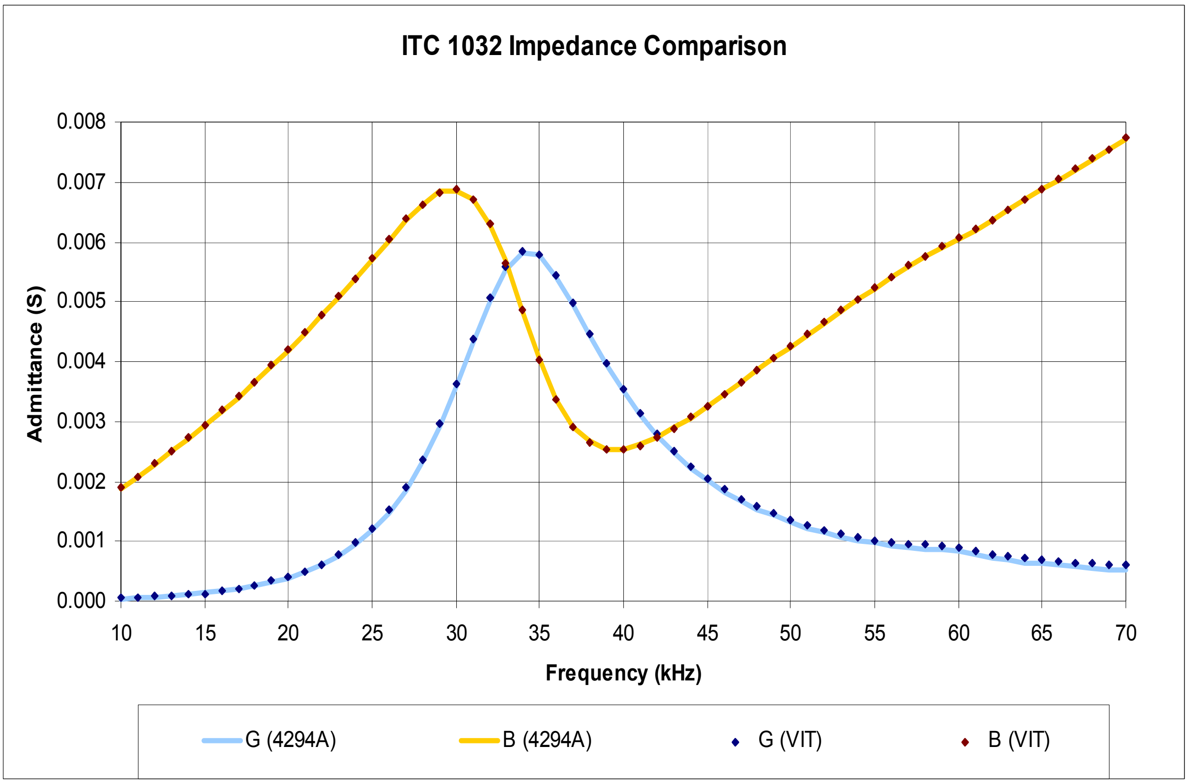

Figure 3.5 Comparison of ITC 1032 hydrophone impedance measurements (VIT method)

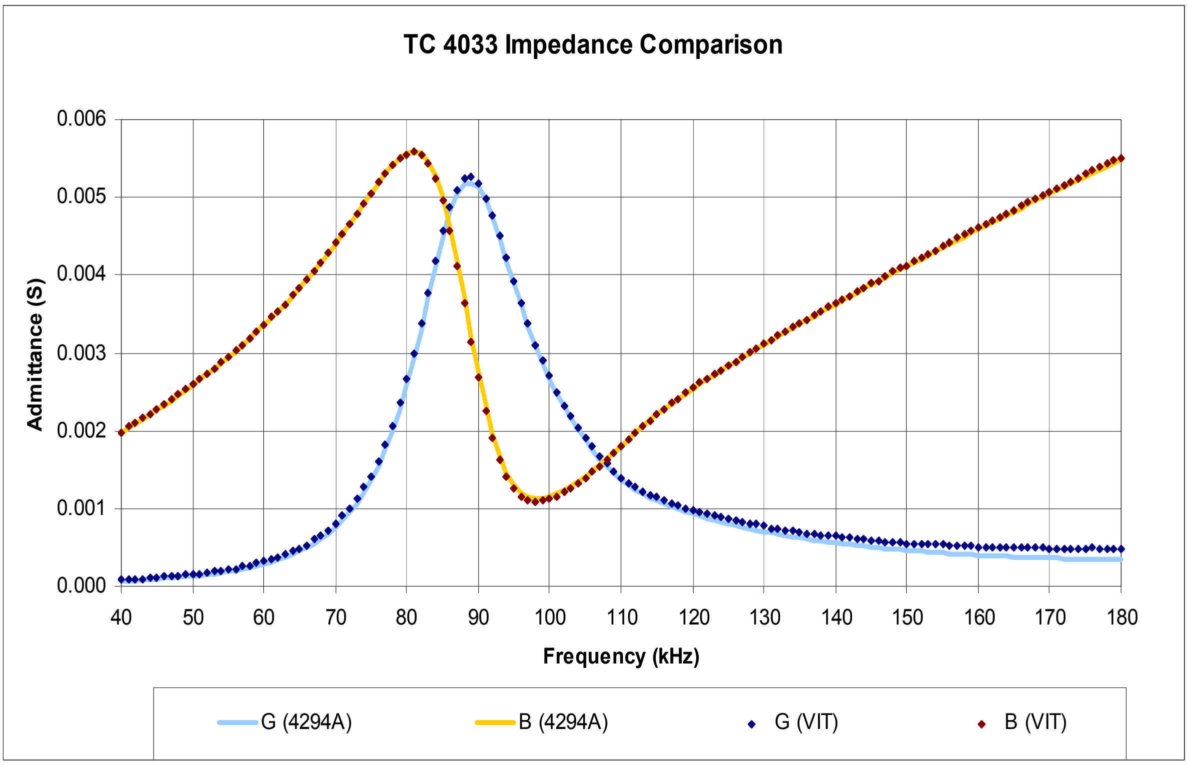

Figure 3.6 Comparison of Reson TC4033 hydrophone impedance measurements (VIT method)

Figures 3.5 and 3.6 show a comparison of measurements made in the NPL large open tank using the 4294A impedance analyser and the VIT sensor with a gated tone burst signal. The hydrophones were hung at approximately half depth in the tank (2.5 metres) and well away from the sides of the vessel to minimise the effect of any reflections on the continuous wave measurements made using the 4294A analyser. Figure 3.5 shows the measurements made on an ITC 1032 hydrophone with a resonant frequency of around 35 kHz. For this hydrophone the susceptance measurements agree to within 1% throughout the frequency range. But while the conductance measurements show a similar agreement around the resonant frequency, the differences increase as the conductance values decrease at either end of the frequency range, up to a maximum of around 15% at the highest frequency. Figure 3.6 shows higher frequency measurements made on a Reson TC4033 hydrophone with a resonant frequency of approximately 90 kHz. The differences show similar characteristics to the ITC 1032 hydrophone, but this time the differences in the susceptance increase to about 3% around the resonant frequency and there is a greater discrepancy in the conductance measurements at the highest frequencies.

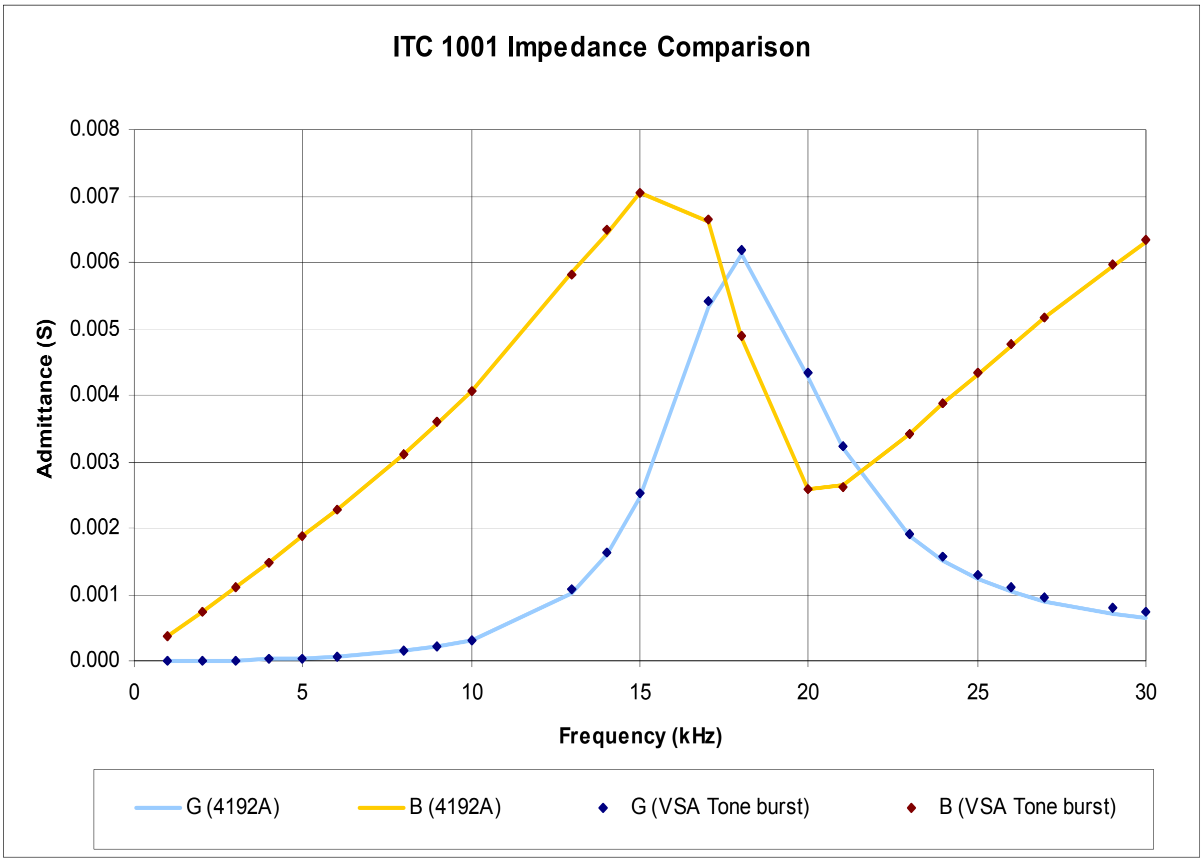

Figure 3.7 Comparison of ITC1001 hydrophone impedance measurements (resistor method)

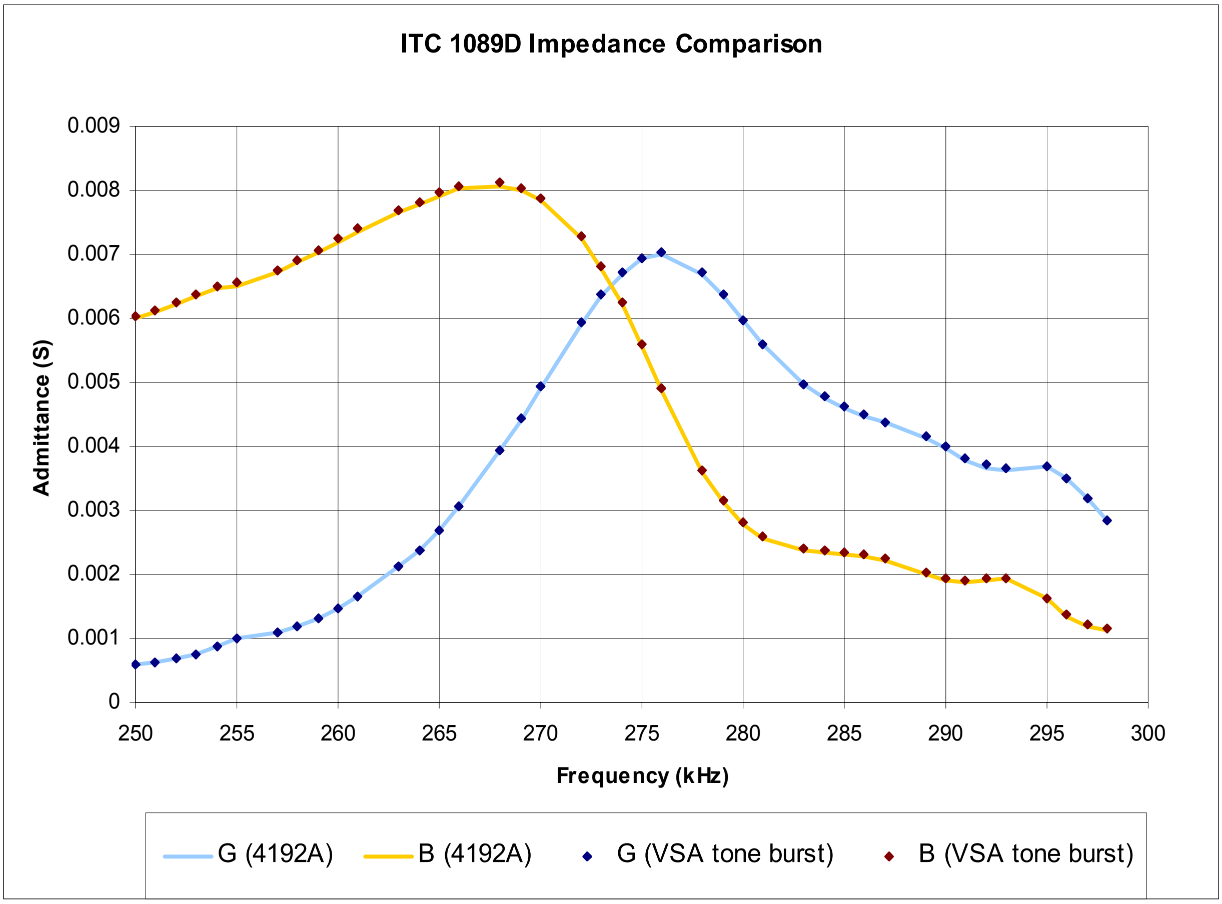

Figure 3.8 Comparison of ITC1089D hydrophone impedance measurements (resistor method)

Similarly, Figures 3.7 and 3.8 show a comparison of measurements made in the NPL large open tank using a 4192A impedance analyser with a gated tone burst method using a resistor to measure the current. Again the hydrophones were positioned in the tank so as to minimise the effect of any reflections on the continuous wave measurements made using the 4192A analyser. Figure 3.7 shows the measurements made on an ITC 1001 hydrophone with a resonant frequency of around 18 kHz, while Figure 3.8 shows the measurements made on a smaller ITC 1089D hydrophone with a resonant frequency of around 275 kHz. For both measurements a nominal 100 Ω resistor was used to measure the current. The actual value was checked using the 4192A impedance analyser and found to be 98.58 Ω, and so this figure was used in the calculation of the conductance and susceptance. The measurements on the ITC 1089D transducer show very good agreement with differences in the conductance of less than 1% throughout the frequency range, while the differences in the susceptance values are generally less than 1% but increase up to around 2% at the upper end of the frequency range where the susceptance values are lower. For the ITC 1001 transducer the differences in the susceptance values are all less than 1%, while the conductance values show differences of about 1% around the resonant frequency but increase towards the ends of the frequency range up to over 20% below 3 kHz where the conductance values are very small.

3.4 UNCERTAINTIES

From the above measurements it can be seen that the errors in the susceptance measurements are generally low throughout the measured frequency range, while the errors in the conductance measurements are generally low around the resonant frequency where the values are high but increase as the values become smaller at the ends of the frequency range. At frequencies where the value of the susceptance is much greater than that of the conductance the phase difference between them will be close to 90°. In this case a small error in the measurement of the phase difference will cause a large error in the calculated conductance due to the cosine term being close to zero. Similarly it can be seen that, although the errors in the susceptance values are small throughout the measured frequency range, the largest errors occur when the susceptance is smaller than the conductance and so the phase difference, and hence the sine term used in the calculation of the susceptance, is small.

4 IMPROVEMENTS TO RECIPROCITY CALIBRATIONS

4.1 INTRODUCTION

4.1.1 Orthodox methods

The primary reason for conducting calibrations in the APV using the primary method of three-transducer spherical-wave reciprocity is to determine the pressure and temperature coefficients of devices that are to be used as reference devices for the APV facility. It is necessary to perform several calibrations across the operational environmental range of the facility to determine the temperature and pressure characteristics of each device that is to be used as a reference device, and this can only be done using an absolute calibration method, such as three-transducer spherical-wave reciprocity. These characterised reference devices are then used for general calibrations conducted in the facility where relative methods are employed. An example of a relative measurement technique employed in the APV facility is one that uses a previously calibrated projector or hydrophone to obtain the absolute sensitivity values for a device under test. This method will be discussed in more detail in the following chapter [9].

The measurement methodology for free-field reciprocity is already established and is currently employed in the NPL open tank facilities [14-16]. However, significant alterations to many aspects of the existing procedure were required to enable this absolute method to be more suitably used within the APV.

4.1.2 Existing methodology and the need to improve

The reciprocity method for absolute calibration requires the use of three transducers, designated as P, T and H, of which at least one must be reciprocal, i.e. its transmitting and receiving sensitivities are related by a constant factor known as the reciprocity factor. The complete calibration requires the devices to be used in pairs during the three measurement stages, each of which requires a device to be used as a transmitter and the other a receiver. The paired measurement sequence is as follows, P⇒T followed by T⇒P, P⇒H and finally T⇒H. The completion of these measurement runs would conclude the measurement cycle and enable the sensitivity to be determined for any one of the three devices used for the calibration.

The three mounting stages available in the large open tank facility enable all the devices to be mounted at the start of the calibration. Each pair of devices is then rotated to face each other to allow all four measurements runs to take place. The small open tank facility only has the capability to hold two devices at any one time and therefore, devices must be changed at the appropriate times to enable the measurement of the correct pairings.

It would be difficult to implement a measurement methodology in the APV comparable to that used in the large open tank as the three original mounting stages in the vessel all share the longitudinal centre line. This would mean that all the devices would be in the same line going down the length of the test chamber, which would lead to complications and in potential inaccuracies in the measurement results. For example, it would not be possible to rotate the device held on the central mount without removing it, which is a time consuming action that needs to be avoided if the measurement cycle is to be completed in an acceptable period of time. This is also an important consideration when calibrations are to be performed at a series of pressures, as the vessel must be de-pressurised prior to re-mounting any devices. In addition, a shadowing effect would be present when measurements are taken between the devices held on the two mounting stages at each end, due to there being a device present on the central mount.

Following the methodology implemented for the small open tank facility is also not totally satisfactory. It has the benefit of only requiring there to be two devices present within the test chamber at any one time, which eliminates the problem of there being any shadowing effect present during the calibration, but would require one of the lids to be removed to facilitate the two remounting processes that would be required to complete the measurement cycle. As previously stated, re-mounting devices during a calibration must be avoided whenever possible if calibration time is to be kept to a minimum, particularly if the calibration is to be repeated at a series of pressures. With re-mounting being a major consideration in any methodology employed in the APV, it was concluded that this method would also not be suitable.

4.2 APV METHODOLOGY AND PROCEDURE

With the existing methods being deemed unsuitable for the APV, the solution was found in the form of a hybrid method that consisted of elements taken from the two existing approaches currently in use in both of the open tank facilities. The main consideration for enabling the calibrations to be completed in a timely manner when calibrations are required at several pressures is to limit the number of de-pressurisations and remounting of transducers that are necessary to complete the measurement cycle. This challenge was met by utilising the dual hydrophone mount shown in Figure 2.3. With the use of this specific mount, it is possible to have all three transducers that are required to conduct the calibration in the test chamber at the same time, and still have the capability to rotate two of the devices out of the way when they are not being used in the measurement pair.

A typical measurement set-up within the vessel is shown below in Figure 4.1. The positions of the three transducers can be clearly seen with transducer P being mounted on the extension cradle and set-up so the transducers alignment mark faces in the direction of the two devices held beneath the large lid. Transducers T and H are mounted coaxially from mounting poles that are attached to the lid rotator via the dual hydrophone mount and they are initially set-up so that their respective alignment marks face towards the transmitting transducer P when they are rotated to the measurement position; with the measurement position being shown for devices P and T in Figure 4.1. It is possible to rotate transducers T and H through ± 180° while the vessel is at full pressure and this ability enables three of the four required measurement runs to take place without any alterations being required to the three devices used in the calibration. Therefore, only one re-alignment of transducers is required to complete the calibration and that is to re-orientate transducers T and H about the vertical axis of their respective mounting poles so their respective alignment marks now face toward each other.

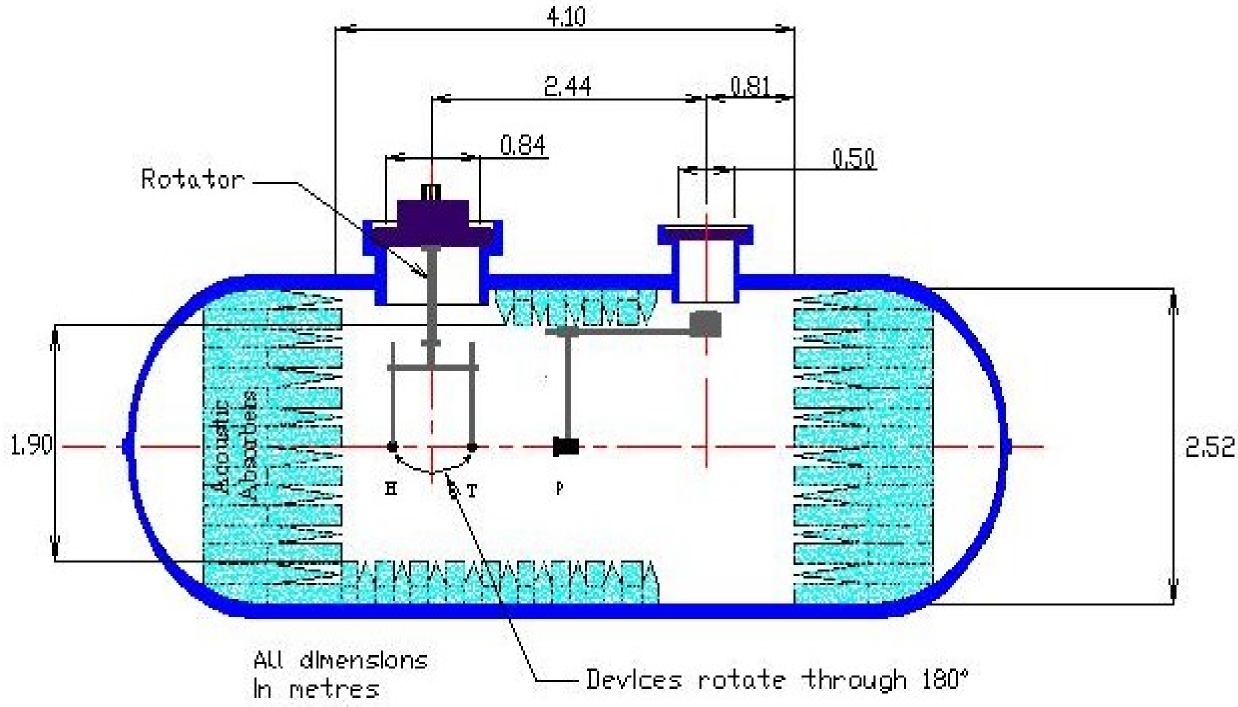

Figure 4.1 Measurement set-up in APV

With the device configuration and orientation considered, the measurement process to fulfil a complete calibration is now as follows:

- Conduct measurement runs P⇒T and T⇒P
- Rotate large lid so that H is in the measurement position
- Conduct measurement run P⇒H
- Lift lid and re-align transducers T and H
- Conduct measurement run T⇒H

This measurement process considerably decreases the time taken to complete a calibration in the APV as all the device mounting is conducted at the start of the calibration and only one lid lift is required to re-align transducers during the suite of four required measurement runs. This becomes an important factor, as there is a common requirement to conduct these calibrations over a series of pressures, particularly when conducting calibrations to determine the pressure and temperature coefficients of devices that are to be used as reference devices for the APV facility.

An additional improvement to this current method would be to have the ability to automatically rotate the transducers that are mounted on the dual hydrophone mount axially about their respective mounting poles centre. If this were possible, it would eliminate the requirement to lift the large lid during the calibration and this would further improve the time needed to perform a calibration.

4.3 SOFTWARE AND DATA ACQUISITION

Some modifications to the existing acoustic measurement software were required to enable this new measurement process to be put in place. The most significant addition to the software was one that gives the ability to save the data gained for the first three measurement runs to a file. This allows the data for those measurement runs to be acquired and saved at each pressure of interest. The transducers are then re-aligned for the final measurement run, with the appropriate saved files being re-called to enable the saving of the data for the final measurement run to the appropriate file. The new file forms the completed measurement file that is used to generate final calibration results.

This method requires care to be taken during the calibration to ensure that the correct part-finished files are re-called at the appropriate time, then to ensure that the data from the final measurement at the corresponding pressure is added to that file. In addition, no indication of the potential calibration results can be gained until the four measurement runs have been completed. Therefore, care must be taken to ensure that the calibration set-up has been performed correctly to eliminate the possibility of conducting a significant amount of work, only to find that calibration results are not what was expected and the work has to be repeated due to an error in the measurement set-up.

4.4 RESULTS

All results shown in this section have been gained by using the primary standard method of three transducer spherical-wave reciprocity. The results for calibrations conducted in the APV facility were obtained by following the methodology previously described.

Shown below in Figure 4.2 is the agreement obtained between measurements carried out in the NPL small open tank and the APV facilities. The transducer used for the example shown is a USRD E27, which is a high frequency directional transducer with an operational frequency range of approximately 80 kHz to 700 kHz. The calibrations cover a frequency range of 100 kHz to 500 kHz, which represents a significant part of the vessels operational frequency range. The error bars for the results gained in the small open tank have been removed for clarity, but these are approximately 0.5 dB. Good agreement can be seen throughout the entire measured frequency range with the largest deviation being approximately 0.5 dB at 150 kHz. The results shown here give confidence that the procedure adopted to perform reciprocity calibrations in the APV can provide suitably accurate results if applied carefully.

The receive sensitivity of various transducers has been determined in the APV facility over a range of temperatures and pressures and example results are shown below for several devices covering an overall frequency range of 3 kHz to 500 kHz, with this frequency range being split into three sections: low frequency range, medium frequency range and high frequency range.

4.4.1 Low frequency range plots

Figure 4.3 shows a calibration of an ITC 1001 spherical transducer conducted at 18 °C and at a total of four pressures: atmospheric pressure and three elevated hydrostatic pressures including 6.8 MPa, the maximum working pressure of the test chamber. The transducer proves to be very stable when subjected to a variation in the test chamber pressure, with very little change in the receive sensitivity being visible from 4 kHz up to 40 kHz.

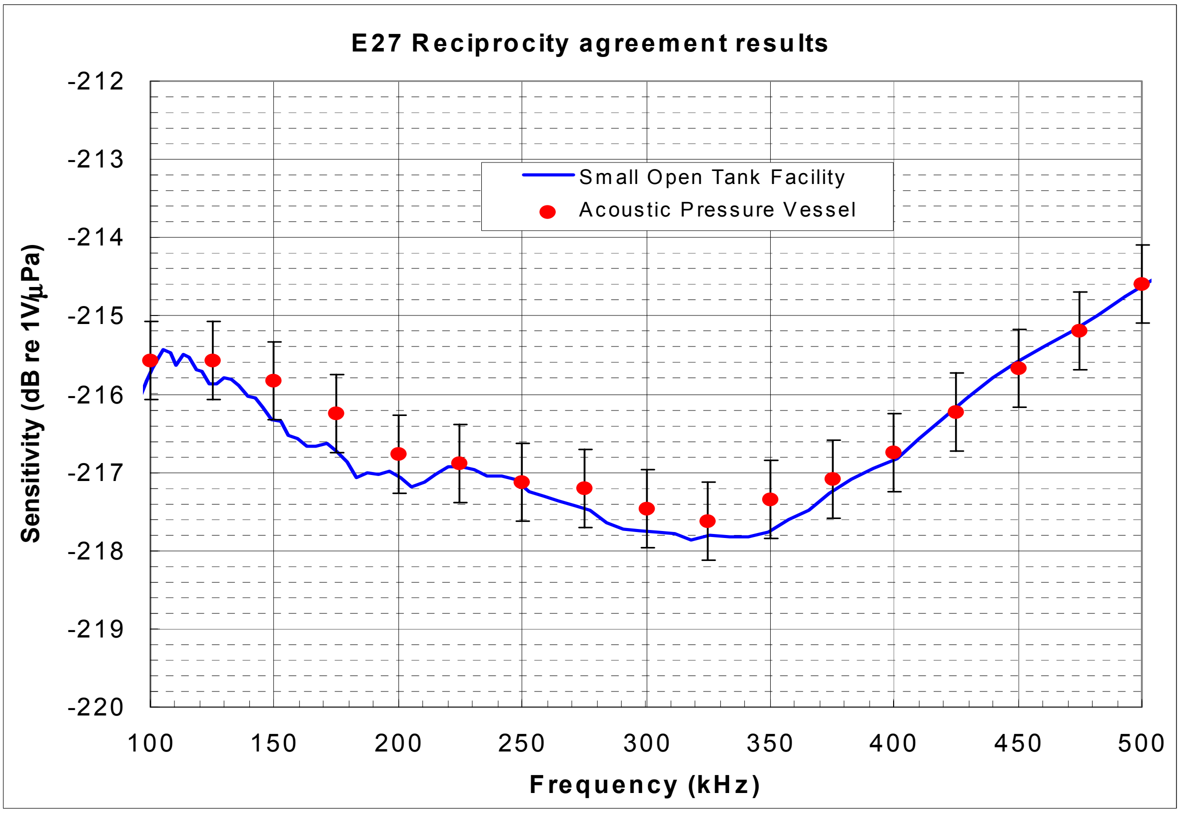

Figure 4.2 Validation of the new reciprocity technique adopted for the APV

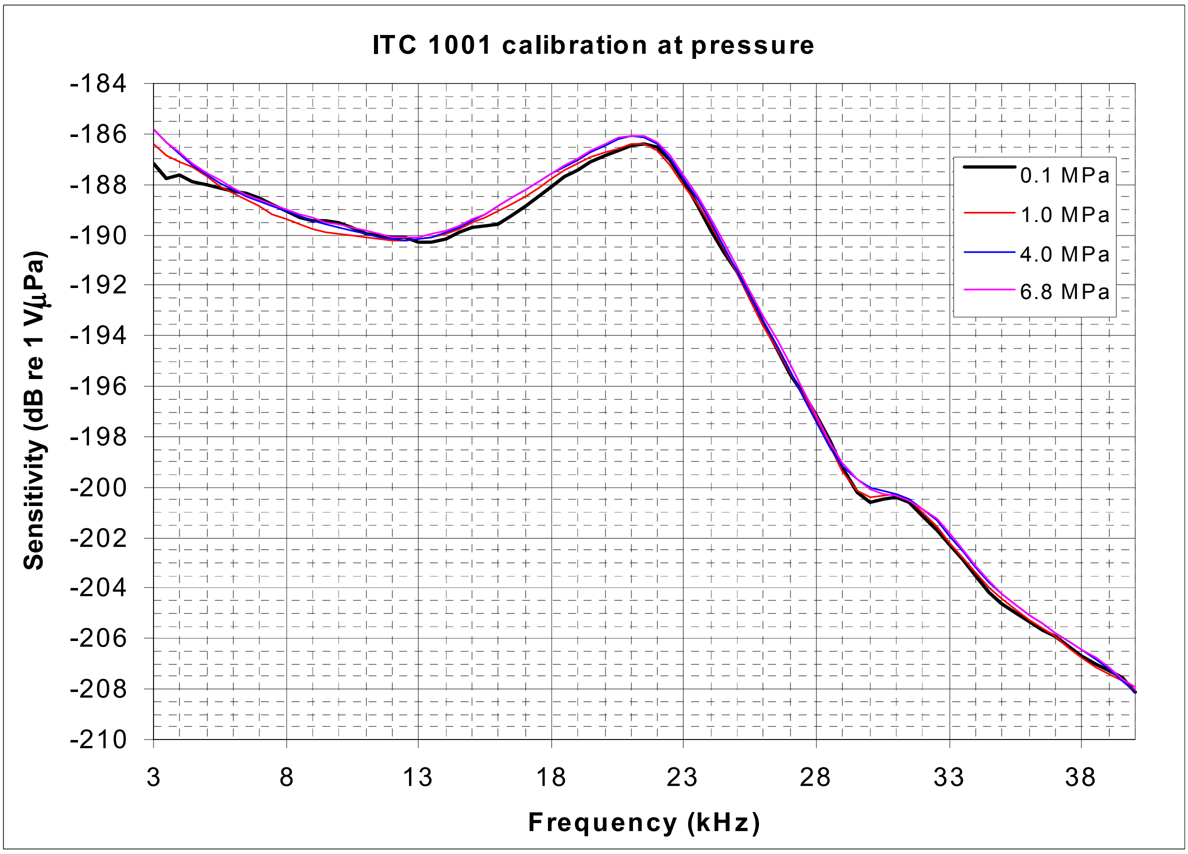

Figure 4.3 Calibration of an ITC 1001 at elevated hydrostatic pressures

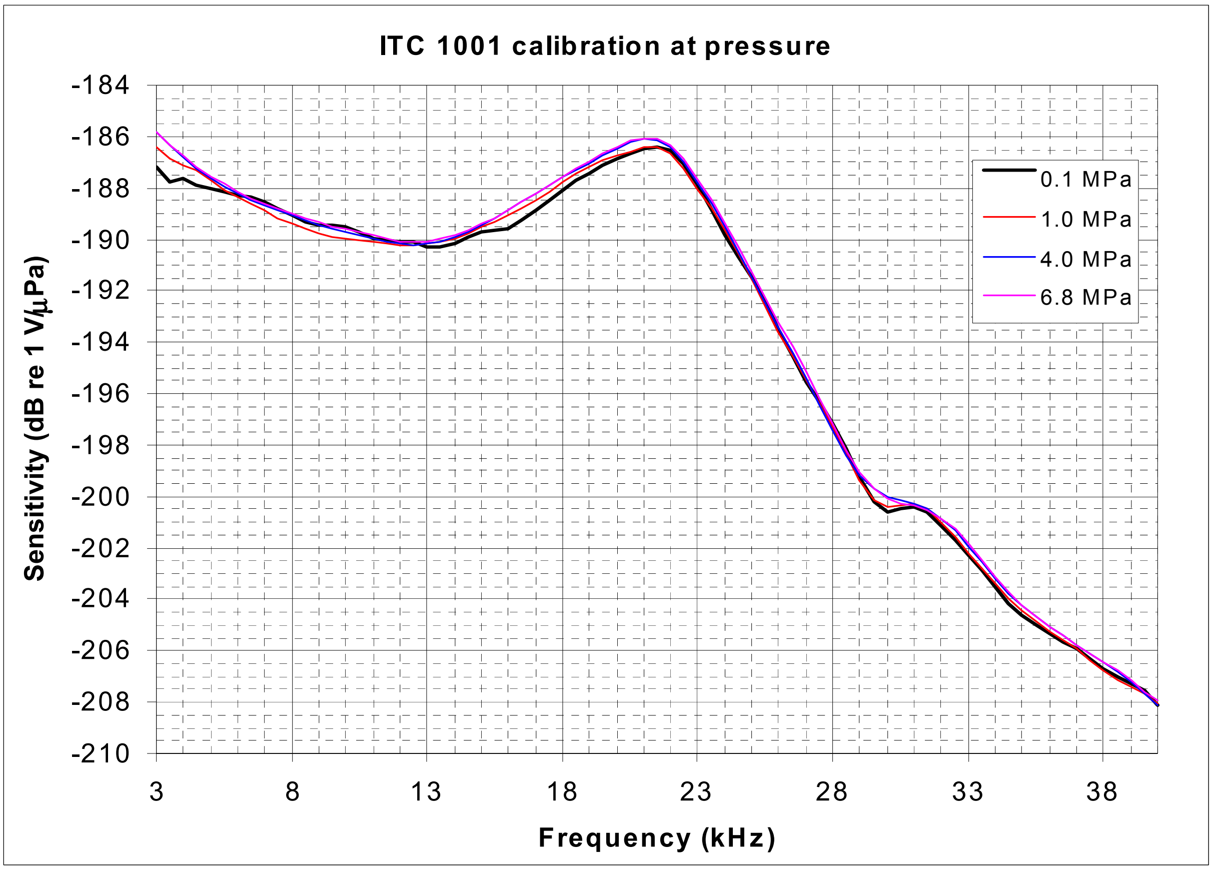

Figure 4.4 ITC 1001 calibrated at various Temperatures

Figure 4.4 shows a calibration of the same ITC 1001 spherical transducer. In this case the calibration was conducted at five temperatures: 4 °C, 11 °C, 18 °C, 25°C and 32 °C with the vessel at atmospheric pressure. As with the calibration conducted at a series of pressures, there is very little change in the devices receive sensitivity when measurements are taken across the operational temperature range of the APV.

4.4.2 Medium frequency range plots

Figure 4.5 shows a calibration of an ITC 1042 spherical transducer conducted at atmospheric pressure and three elevated hydrostatic pressures up to 6.0 MPa, while at 18 °C. The plot shows that there is very little variation between the measurement results gained at the different hydrostatic pressures. The maximum relative difference in receive sensitivity between the calibrations is approximately 0.8 dB at 126 kHz and that is between the calibration conducted at ambient pressure and 6 MPa.

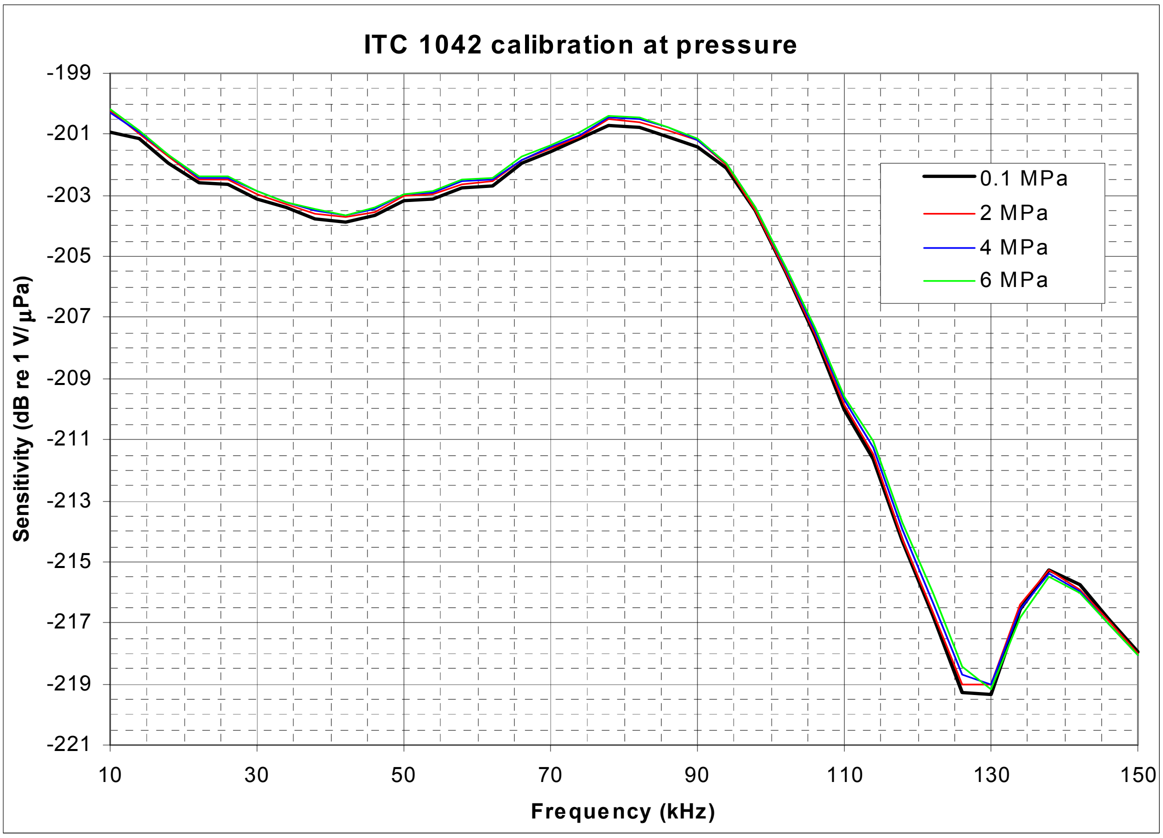

Figure 4.5 Calibration of an ITC 1042 at elevated hydrostatic pressures

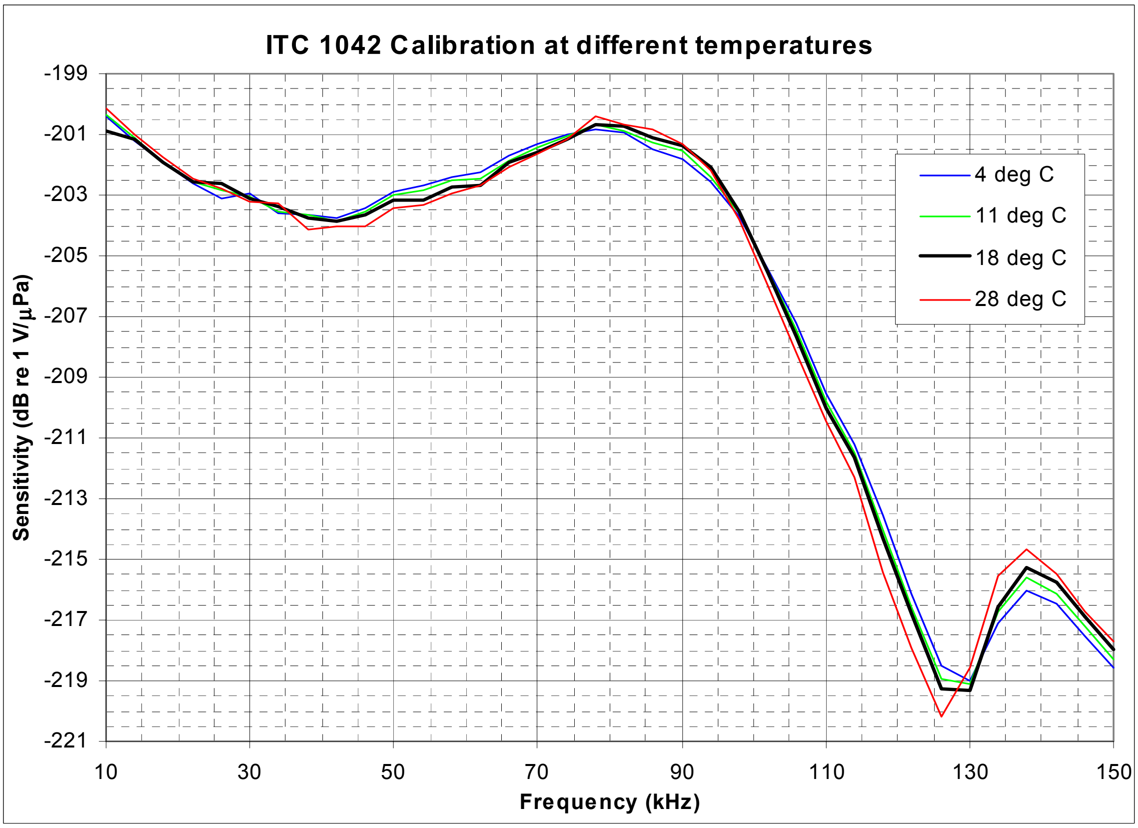

Figure 4.6 ITC 1042 calibrated at various temperatures.

Figure 4.6 shows a calibration, again for the ITC 1042 spherical transducer. In this case the calibration was conducted at four temperatures: 4 °C, 11 °C, 18 °C and 28 °C with the vessel at atmospheric pressure. As with the calibration conducted at a series of pressures, there is only a small relative change in the devices receive sensitivity when measurements are taken at a number of temperatures. It can be seen that the most notable change takes place when the device is subjected to particularly warm water as the results gained at 28 °C show the most variation, particularly in the range from approximately 120 kHz to 145 kHz.

4.4.3 High frequency range plots

Figure 4.7 shows a calibration of an ITC 1089D transducer conducted at atmospheric pressure and six elevated hydrostatic pressures including 6.8 MPa while at 18 °C. The transducer proves to be very stable when subjected to a variation in the test chamber pressure, with very little change in the receive sensitivity being visible across the measured frequency range of 100 kHz to 500 kHz. The maximum relative change in the transducers sensitivity is approximately 0.9 dB at 455 kHz, once again that is for the measurements taken at ambient pressure and at 6.8 MPa and so represents the greatest variation in the environmental conditions that the devices was subjected to.

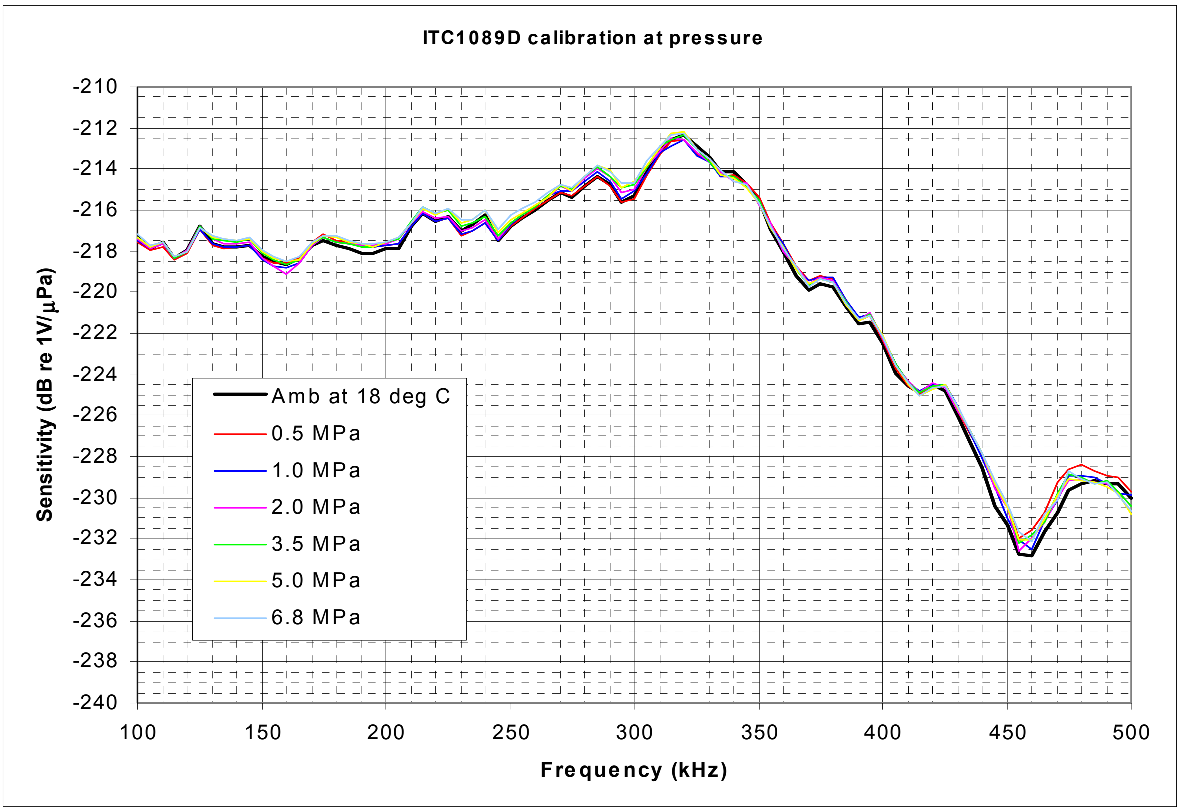

Figure 4.7 Calibration of an ITC 1089D at elevated hydrostatic pressures

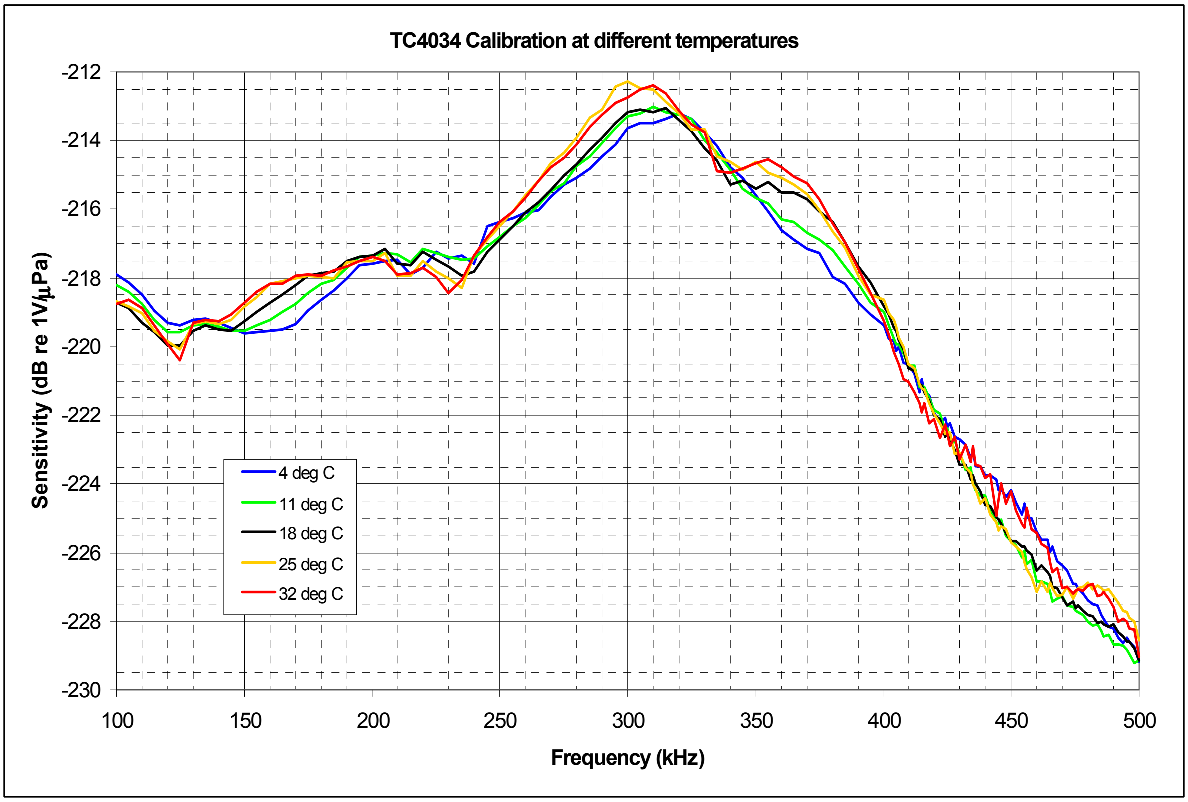

Figure 4.8 Reson TC 4034 calibrated at various Temperatures

Figure 4.8 shows a calibration of a Reson TC 4034 transducer. In this case the calibration was conducted at five temperatures: 4 °C, 11 °C, 18 °C, 25°C and 32 °C with the vessel at atmospheric pressure. Generally, there is little change in the devices receive sensitivity when measurements are taken across the operational temperature range of the APV. The greatest variation in receive sensitivity can be seen at around 350 kHz to 400 kHz where there is a maximum relative change of 1.9 dB at 370 kHz for the measurement gained at 4 °C and 32 °C.

4.5 UNCERTAINTIES

The basic calibration system employed for reciprocity calibrations within the APV is basically the same as that implemented in the NPL open tank facilities [14]. Therefore, the majority of the uncertainty budget for the APV is the same as for the open tanks (already reported in reference [15]). However, there are a few contributing factors that require to be increased for calibrations undertaken in the APV. The current positioning system in the test chamber has greater limitations than that in the open tanks with respect to the degrees of freedom of the transducers and can therefore lead to larger inaccuracies in the alignment of devices, and to subsequently larger uncertainty components.

4.6 APV REFERENCE DEVICES

The transducers and hydrophones currently used as reference devices in the APV facility were identified from a series of calibrations conducted on commonly available commercial devices. Devices that showed a relatively good stable response with temperature and pressure through initial investigative calibration work were then calibrated by the primary standard method of three transducer free-field reciprocity in an NPL open tank facility at ambient pressure and 18 °C. The devices were then thoroughly characterised in the APV by conducting absolute calibrations over the full environmental range of the test chamber to determine the variation of response of the transducers and hydrophones with temperature and depth. The data gained by the calibrations in the NPL open tank facility were used to generate the reference sensitivities that are traceable to the UK primary standards. The coefficient data gained through the APV calibrations are used to correct the reference sensitivities for any slight variations in response that the reference devices have associated with them, due to a change in the environmental conditions of the measurement medium. Of course, it is not acceptable for a reference devices performance to vary greatly with temperature and depth, as large corrections will then required to be applied to the reference sensitivities and this may introduce large uncertainties into the calibration process.

The plots shown above in Figure 4.3 to Figure 4.8 show some of the transducers that have been selected for APV reference devices because they demonstrate reasonably good stability when they are subjected to variations in the environmental conditions across the operational specification of the APV facility. All the transducers currently selected for reference devices are listed in Appendix 2.

5. IMPROVED RELATIVE CALIBRATION METHODS

5.1 INTRODUCTION

Although the time taken to perform a three-transducer spherical-wave reciprocity calibration in the Acoustic Pressure Vessel (APV) has been reduced significantly (see Section 4), it is still a relatively time-consuming method when used to characterise a device as a function of pressure and/or temperature. Where a reference transducer is available, which has been calibrated and characterised as a function of temperature and pressure by an absolute method, this can be used to calibrate and characterise an unknown device using a relative calibration method. Such methods are between 2 and 5 times faster and better suited to performing multiple measurements at various temperatures and pressures in a time-efficient manner.

5.2 METHODS

Three relative calibration methods are used in the APV and these are described below.

5.2.1 Calibrated reference projector method

In this method, a reference projector is used to calibrate an unknown hydrophone [14]. The transmitting current response (TCR) of the projector has previously been determined by an absolute calibration by three-transducer spherical-wave reciprocity. By monitoring the drive current and knowing the separation between the projector and hydrophone, the sound pressure level at the hydrophone can be determined. A measurement of the electrical signal produced by the hydrophone will then enable the calculation of the receive sensitivity as follows:

$$M_H = \frac{V_H}{I_P}\frac{D}{S_P} \qquad (5.1)$$

where M_H is the hydrophone receive sensitivity, V_H is the receive voltage from the hydrophone under test, I_P is the projector drive current, D is the projector-hydrophone separation, and S_P is the transmitting current response of calibrated projector.

5.2.2 Calibrated reference hydrophone method

Here, a reference hydrophone is used to calibrate a projector under test [14]. This is effectively the reverse of the calibrated projector method described above. The measurement setup is the same except that this time the receive sensitivity of the reference hydrophone has previously been determined by an absolute calibration by three-transducer spherical-wave reciprocity. The sound pressure level produced by the projector under test can be calculated from the signal received by the reference hydrophone, the drive current and the transducer separation as follows:

$$S_P = \frac{V_H}{I_P}\frac{D}{M_H} \qquad (5.2)$$

A measurement of the impedance of the projector will also enable its transmitting voltage response (TVR) to be calculated.

$$TVR_P = \frac{S_P}{Z_P} \qquad (5.3)$$

where Z_P is the projector impedance.

5.2.3 Comparison calibration against a reference hydrophone

Here, a reference hydrophone is used to calibrate a hydrophone under test by a substitution method [14]. In the APV, this method may be used in combination with the dual bracket described in Section 4 so that three devices are mounted in the APV at the same time. A projector, which may be an uncalibrated device, is mounted on the small port cradle, the reference hydrophone and the hydrophone under test are mounted on the large lid on each arm of the dual bracket. The hydrophones are mounted such that their reference directions are pointing away from the centre of the large lid. Initially, a measurement is made with the reference hydrophone facing the projector. The dual bracket is then rotated so that the hydrophone under test is in exactly the same position as the reference hydrophone was previously. A second measurement is made, and from these two measurements the receive sensitivity of the unknown hydrophone can be calculated.

$$M_H = \frac{V_H}{V_{REF}} M_{REF} \qquad (5.4)$$

where V_H is the receive voltage from hydrophone under test, V_{REF} is the receive voltage from reference hydrophone, M_{REF} is the reference hydrophone sensitivity.

If the projector is also a calibrated device, the hydrophone under test stage of the calibration can be performed as a calibrated projector measurement described above, thereby giving two independent values for the receive sensitivity of the hydrophone. This provides a useful check of the method.

5.2.4 Relative merits of the calibration methods

Both the calibrated reference projector and calibrated reference hydrophone methods have the advantage of being very quick methods in that they produce the final sensitivity values as the measurements are made. This is very useful when there is a requirement to maximise the number of measurements made so that best use is made of the available time (this is frequently the case with the APV where the logistics of the operation of the vessel can place limitations on the available measurement time). However, the calibrated projector-hydrophone methods are subject to more sources of uncertainty because they are more sensitive to errors from lack of free-field conditions and lack of far-field conditions. For example, the methods assume spherically spreading waves exist in the acoustic far-field of the projector, and that the measured signal is free from interference from reflections. The calibrated projector is also often assumed to be linear, important since it may not be driven at the same level during the calibration as it was during its own calibration by the reciprocity method. The linearity can be checked by performing and comparing measurements using different drive levels, but then the advantage of a speedy calibration is lost. The alignment requirements for the calibrated projector methods are also more stringent, since the projector must be accurately aligned along the reference direction used during its own absolute calibration.

The hydrophone comparison method requires two measurement stages (for the reference hydrophone and hydrophone under test) to be completed before the sensitivity values can be calculated, and this can lead to more time-consuming measurements. However, the method has the potential for greater accuracy. The projector used for a comparison calibration does not need to be a calibrated device nor particularly accurately aligned, and is merely used to provide a stable acoustic field in which to undertake the calibration. Any lack of ideal conditions in a comparison calibration (for example, caused by small acoustic reflections from boundaries or mounting fixtures) will tend to cancel if they are the present to the same degree for both devices.

5.2.5 Reference transducer data

The absolute sensitivity values for the reference projectors/hydrophones used in the above methods are determined by an absolute calibration by three-transducer spherical-wave reciprocity in the NPL open-tank facilities. Calibrations by the same method at various pressures and temperatures are also performed in the APV to determine the pressure and temperature coefficients for the devices. These coefficients are stored in an electronic file which is used by the measurement software to apply appropriate corrections to the absolute sensitivity of the reference transducer used in the calibration methods described above.

To achieve calibrations with the lowest possible uncertainties, it is preferable that the reference transducers used in the APV show little variation with both temperature and pressure. The hydrophones and transducers chosen as reference devices are listed in Appendix 1. The temperature and pressure coefficients for some of the reference transducers and hydrophones used in the APV are also given in Appendix 2. Two of the reference transducers used are maintained on loan from USRD-NUWC in the USA, namely the H52 and F30 [17]. The remainder are supplied by commercial producers of hydrophones. Taking the H52 reference hydrophone as an example, the results show that, for the frequency range up to 120 kHz over which this hydrophone is primarily used, the sensitivity of the hydrophone varies by less than 0.03 dB for each degree Celsius change in temperature. These results are in good general agreement with those already published by USRD-NUWC [18]. Similarly, the pressure coefficients also show excellent stability over the same frequency range with a variation of less than 0.03 dB for each MPa change in pressure.

5.3 RESULTS

To verify the relative calibration methods used in the APV, transducers calibrated by these methods were also calibrated in the NPL open tank facilities by three-transducer spherical-wave reciprocity and the results compared.

Figure 5.1 shows a comparison of calibrations of the H52 reference hydrophone by the calibrated projector method in the APV and three-transducer reciprocity in the open tank. It can be seen that the two calibrations show very good agreement with differences of less than 0.25 dB throughout the entire frequency range. This is well within the uncertainties of the two calibrations, these being 0.5 dB for three-transducer reciprocity and 0.9 dB for the calibrated projector method.

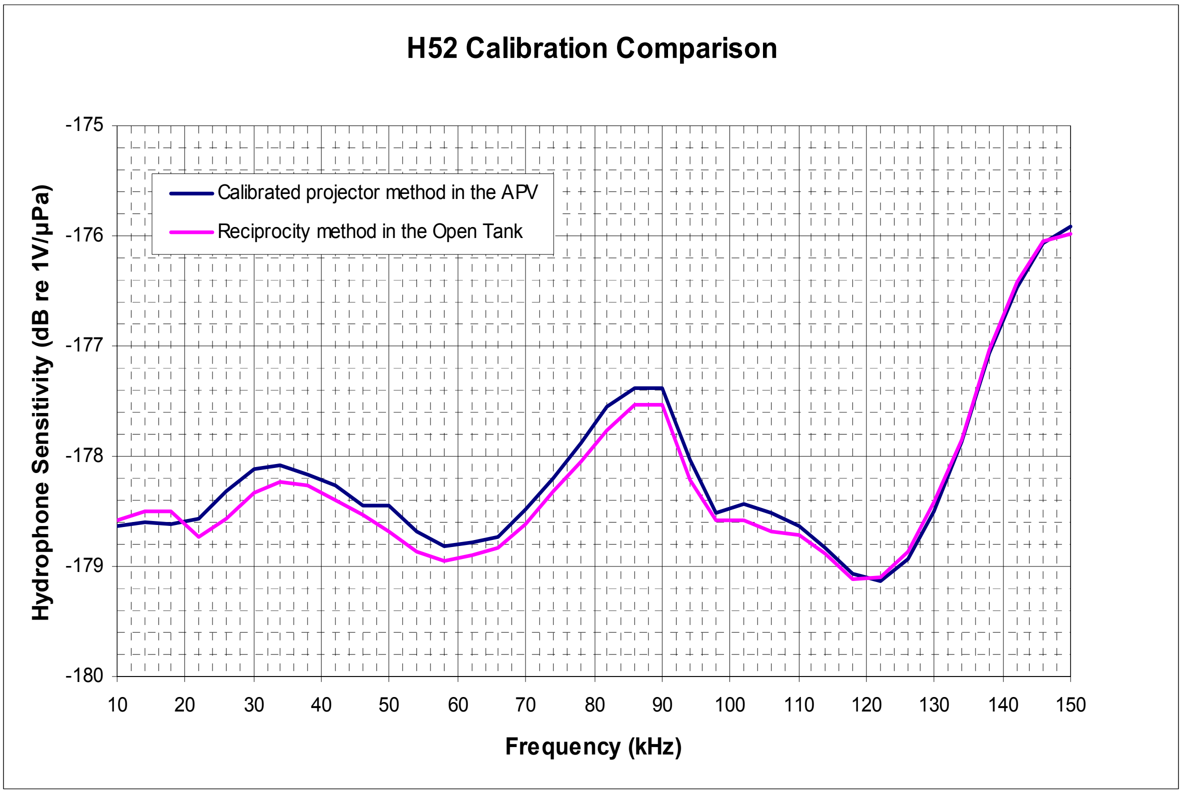

Figure 5.1 Comparison of calibration methods

Examples of how relative calibration methods have been used in the APV to characterise transducers for their variation with pressure and temperature are shown in Figures 5.2 and 5.3. The transducer shown in Figure 5.2 is a B&K 8105 hydrophone and it can be seen that the sensitivity of this device exhibits a marked change of up to over 2 dB as the pressure is increased from ambient to 1 MPa. It is important that the time between measurements at the different pressures be as short as possible so that any changes can be attributed purely to the change in pressure and not other environmental factors such as temperature drift or the soaking characteristics of the device.

Similarly, Figure 5.3 shows the results of a set of measurements to characterise a B&K 8103 hydrophone for temperature. It can be seen that the sensitivity of the device changes by as much as 7 dB as the temperature increases from 5 °C up to 32 °C, and while the gradient of the variation is negative at frequencies around 200 kHz (sensitivity decreases as the temperature increases), it become positive around 270 kHz (sensitivity increases with increasing temperature).

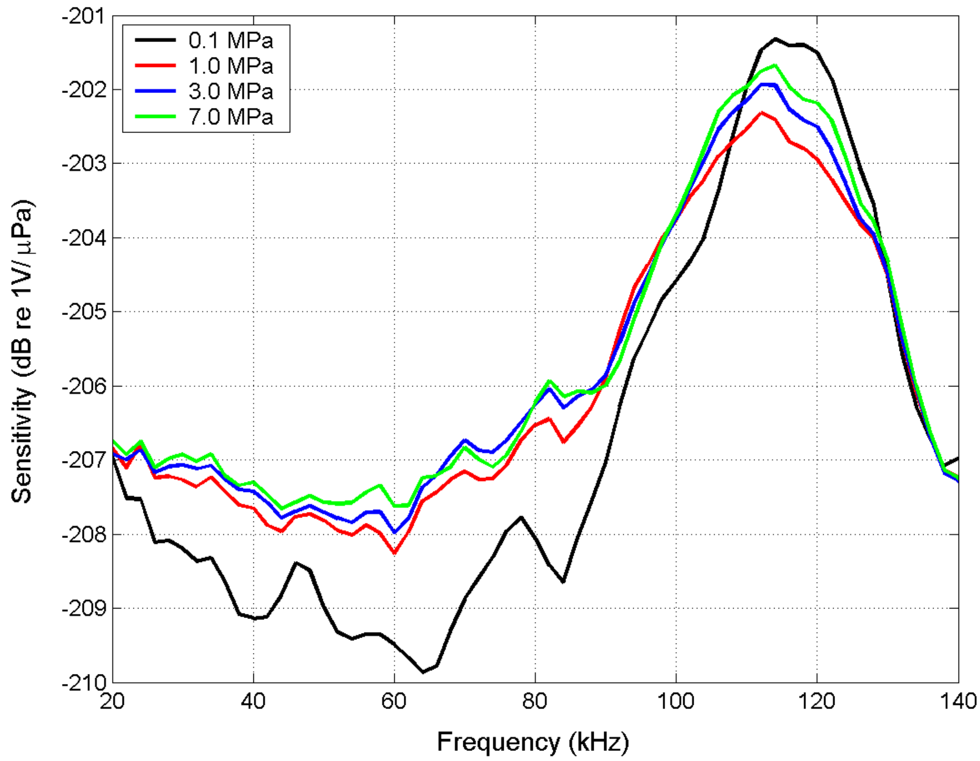

Figure 5.2 B&K 8105 hydrophone sensitivity variation with pressure.

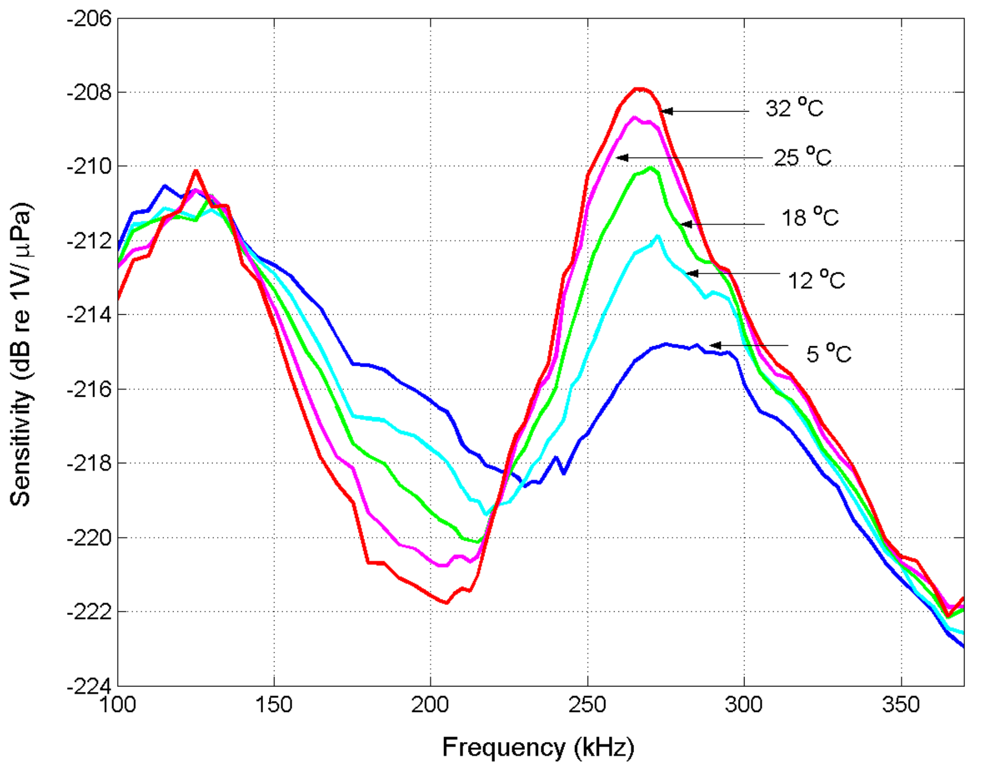

Figure 5.3 B&K 8103 hydrophone sensitivity variation with temperature.

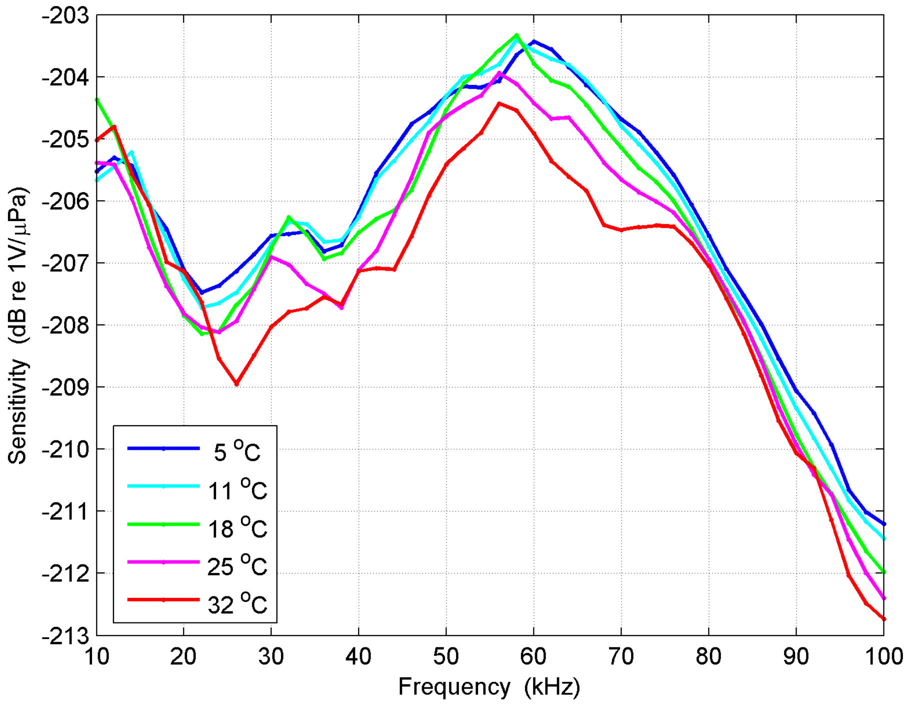

Figure 5.4 B&K 8104 hydrophone sensitivity variation with temperature for frequencies in the range 10 kHz to 100 kHz.

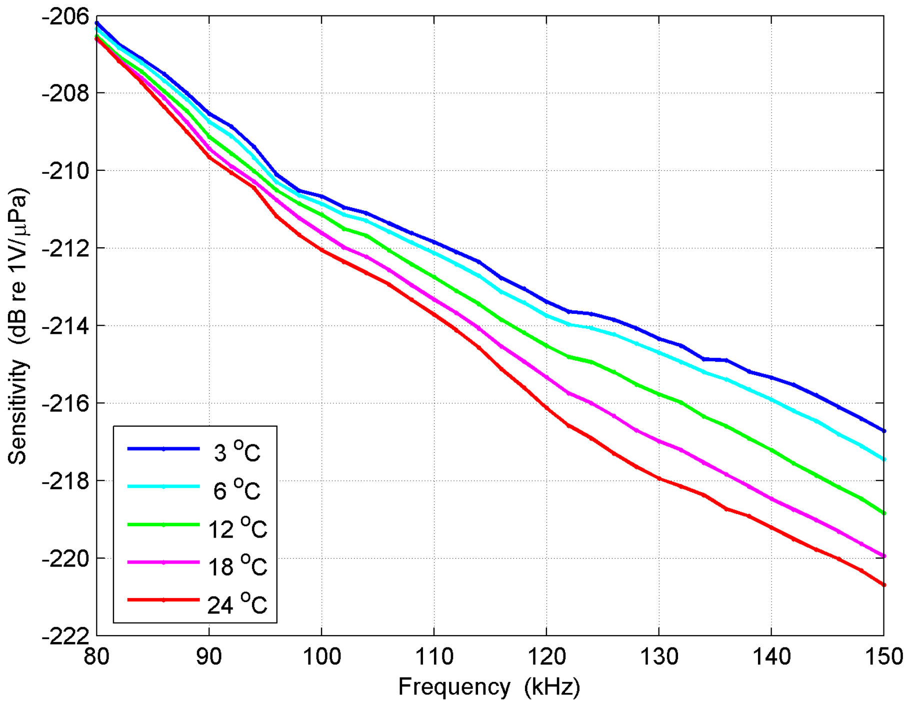

Figure 5.5 B&K 8104 hydrophone sensitivity variation with temperature for frequencies in the range 80 kHz to 150 kHz.

Figures 5.4 and 5.5 show the variation in sensitivity with temperature for the B&K8104 hydrophone. The figures show the results of two separate sets of measurements covering slightly different values of temperature and different frequency ranges. In Figure 5.4, it can be seen that for the range of frequencies above 25 kHz, the gradient of the variation is negative (sensitivity decreases as the temperature increases). Figure 5.5 shows that this trend is maintained for frequencies up to 150 kHz, with a maximum variation of about 4 dB observed at 150 kHz between temperatures of 3 ºC and 24 ºC. The variation observed in Figure 5.4 for the range 10 kHz to 25 kHz is clearly more complex.

5.4 UNCERTAINTIES

The total uncertainty in the calibration methods was determined by following the guidance given in the ISO *Guide to the Expression of Uncertainty in Measurement* [19]. The overall uncertainty is then expressed for a confidence level of 95%. The various Type B uncertainty components for a calibration using the calibrated reference projector or calibrated reference hydrophone method are listed in Table 5.1, and those for comparison calibrations in Table 5.2. The Type A (random) uncertainty value quoted is a typical figure derived from previous measurements. The values in the tables are minimum values and relate to the frequency range 3 kHz – 200 kHz. Below 3 kHz, the components due to non-steady state conditions and reflections will increase, and above 200 kHz the orientation and alignment component must be increased.

					Est.	Std. Unc
Source of uncertainty	Probability distribution	Divisor	c_i	v_i or v_{eff}	value ± %	u_i ± %
Reference transducer calibration	normal	2.00	1.0	infinity	7.00	3.50
Calibrated attenuator accuracy	normal	2.00	1.0	infinity	0.50	0.25
Current probe accuracy	normal	2.00	1.0	infinity	2.00	1.00
Separation distance	rectangular	1.73	1.0	infinity	1.00	0.58
Non-spherical field	rectangular	1.73	1.0	infinity	2.00	1.15
Non-steady state conditions	rectangular	1.73	1.0	infinity	2.00	1.15
Orientation & alignment	rectangular	1.73	1.0	infinity	3.00	1.73
Reflections	rectangular	1.73	1.0	infinity	1.00	0.58
Noise/electrical effects	rectangular	1.73	1.0	infinity	0.50	0.29
Wetting	rectangular	1.73	1.0	infinity	0.50	0.29
Reference transducer impedance	rectangular	1.73	1.0	infinity	2.00	1.16
Amplifier loading correction	rectangular	1.73	1.0	infinity	1.20	0.69
Pressure coefficient of reference	normal	2.00	1.0	infinity	2.00	1.00
Temperature coefficient of reference	normal	2.00	1.0	infinity	2.20	1.10
Total systematic uncertainty	normal	1.00	1.0	infinity		4.88
Random uncertainty	normal	1.00	1.0	3 (n-1)	2.00	2.00
Combined uncertainty	normal					5.28
Expanded uncertainty	normal (k=2)					10.55
Expanded uncertainty (dB)	normal (k=2)					0.87

Table 5.1: Uncertainty budget for calibrated projector/hydrophone calibrations

From the tables it can be seen that the typical overall uncertainty for a calibrated projector or calibrated hydrophone calibration is around 0.9 dB, and for a comparison calibration around 0.8 dB. Although these values are higher than the typical 0.5 dB overall uncertainty of a three-transducer spherical-wave reciprocity calibration, it is the relative uncertainty between calibrations at various pressures/temperatures which has to be considered when characterising a device for pressure or temperature. For these measurements, many of the Type B uncertainty components will be the same, and so will cancel when looking at the differences between measurements. Consideration will have to be given as to whether the random uncertainty components are significant in relation to any differences seen in the measurements of the sensitivity of a device at different pressures or temperatures. If lower overall uncertainty values are required, then this may be achieved by performing a single absolute calibration by three-transducer spherical-wave reciprocity at one pressure and temperature.

					Est.	Std. Unc
Source of uncertainty	Probability distribution	Divisor	c_i	v_i or v_{eff}	value ± %	u_i ± %
Reference hydrophone	normal	2.00	1.0	infinity	6.00	3.00
Linearity of preamplifier	rectangular	1.73	1.0	infinity	1.00	0.58
Linearity of digitiser	rectangular	1.73	1.0	infinity	1.00	0.58
Agreement versus each reference	rectangular	1.73	1.0	infinity	2.50	1.44
Orientation & alignment	rectangular	1.73	1.0	infinity	2.50	1.44
Error from curve fitting reference data	rectangular	1.73	1.0	infinity	1.00	0.58
Stability of source transducer/drive	rectangular	1.73	1.0	infinity	1.00	0.58
Mounting/remounting references	rectangular	1.73	1.0	infinity	2.00	1.15
Wetting	rectangular	1.73	1.0	infinity	1.00	0.58
Stability of references (thermal)	rectangular	1.73	1.0	infinity	1.00	0.58
Non-steady state conditions	rectangular	1.73	1.0	infinity	1.00	0.58
Spatial-averaging	rectangular	1.73	1.0	infinity	0.50	0.29
Amplifier loading correction	rectangular	1.73	1.0	infinity	1.20	0.69
Pressure coefficient of hydrophone	normal	2.00	1.0	infinity	2.00	1.00
Temperature coefficient of hydrophone	normal	2.00	1.0	infinity	2.20	1.10
Total systematic uncertainty	normal	1.00	1.0	infinity		4.43
Random uncertainty	normal	1.00	1.0	3 (n-1)	2.00	2.00
Combined uncertainty	normal					4.86
Expanded uncertainty	normal (k=2)					9.72
Expanded uncertainty (dB)	normal (k=2)					0.81

Table 5.2 Uncertainty budget for comparison calibrations

6 ACOUSTIC PROPERTIES OF THE APV

6.1 ECHO FREE TIME AND SOURCES OF BOUNDARY REFLECTIONS

The echo-free time is an important parameter when undertaking measurements in a laboratory tank if free-field conditions are to be simulated using time-gating techniques [20]. Echo-free time can be defined as the time delay between the arrival of the direct signal and the arrival of the first boundary reflection, and is a function of position within the tank. Free-field conditions can be achieved by the use of tone-burst signals with time-gating techniques used to isolate the direct signal before reflections from boundaries arrive. To make best use of the APV for free-field measurements, it is useful to analyse how the echo-free time varies with position of transducers in the tank, and what are the main sources of boundary reflection within the vessel.

The echo-free time and the origin of the primary reflections within the APV have been investigated experimentally and a comparison made with theory based on simple geometrical considerations. In order to determine the echo free time available in the APV experimentally, two transducers were mounted as shown in Figure 6.1. The acoustic projector was mounted on the small extension cradle of the APV and the hydrophone was fixed under the large lid. The separation distance between the transducers was varied by moving the projector along the axis of the vessel by use of the traversing system under computer control. The separation was varied from 0.85 m to 2.4 m in increments of 10 mm.

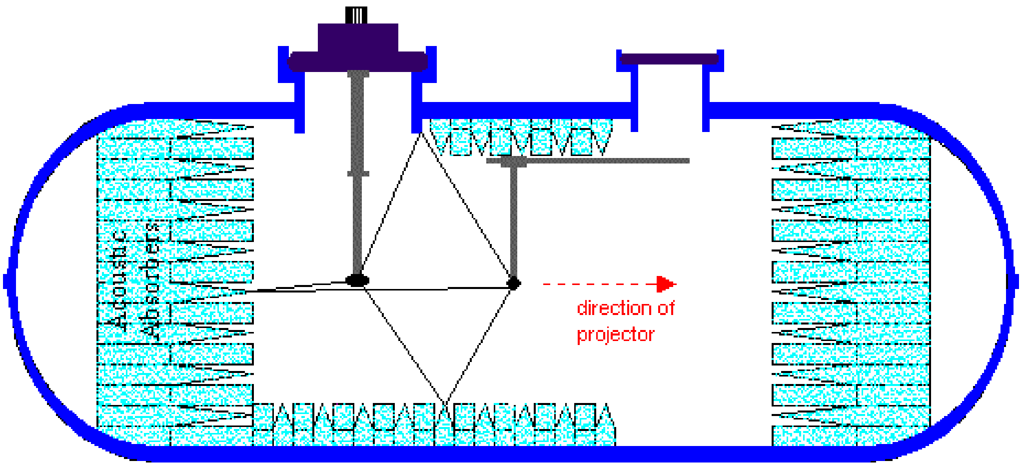

Figure 6.1 Arrangement for measurement of echo free time, showing three examples of possible internal reflections

The receive hydrophone used in the measurements was the USRD H52. Three different nominally omnidirectional acoustic projectors were used to cover a range of frequencies; the ITC1042, ITC1032 and ITC1001. Each acoustic projector was driven with a pulse consisting of a few cycles of a discrete frequency, with centre frequencies of 20 kHz, 30 kHz and 75 kHz used. Initial measurements were taken with the hydrophone mounted directly under the large lid of the APV as shown in Figure 6.1. For other measurements, the hydrophone was mounted in the dual hydrophone mount (described in Section 2.6) to investigate the effect of this mounting bracket on the echo free time.

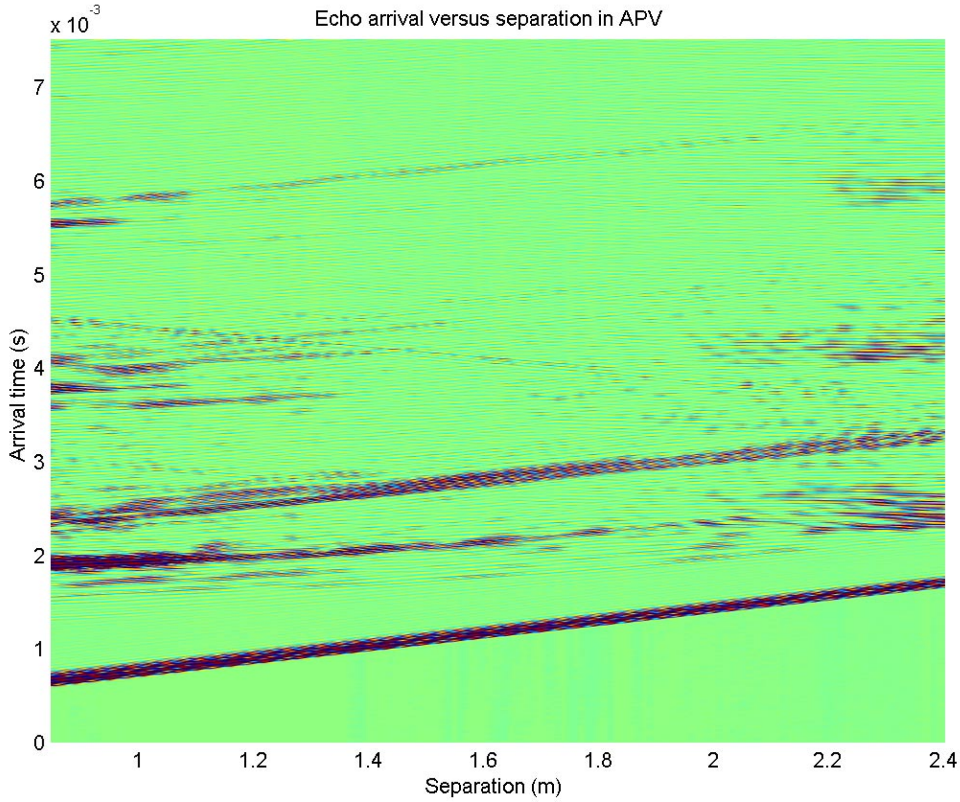

Figure 6.2 Signal arrival time plotted against separation for a pulse frequency of 30 kHz, hydrophone held centrally beneath the large port lid.

Figure 6.2 shows a plot of the results of the measurements made with a 30 kHz pulse and with the hydrophone held centrally beneath the large port lid. The figure is formed by plotting each waveform vertically against separation distance on the horizontal axis with the amplitude of the signal colour mapped such that green corresponds to zero volts (no signal present). A number of features are evident in the plot. The direct arrival is clearly seen at 0.6 ms at a separation distance of 0.8 m, increasing to 1.6 ms at 2.4 m. The time before the arrival of the first reflection (the echo-free time) is about 0.7 ms at 0.8 m, decreasing to about 0.5 ms at 2.4 m, this time diminishing as the separation distance between the projector and hydrophone is increased. At times greater then this, a number of other reflections arrive, including multi-path signals that reflect of several structures in the vessel.

Any theoretical investigation of the origin of the reflected signals requires knowledge of the internal structure and geometry of the vessel. The region around the large port is shown in the photograph in Figure 6.3, which has been taken looking toward the large port end from the small port. Clearly visible are the wedges on the side-wall, the wedges at the end of the tank (large port end), and the bottom of the large port which protrudes downward beyond the end of the wedges. With knowledge of the vessel internal dimensions and the speed of sound, the echo arrival times can be estimated a function of separation distance between the acoustic projector and the hydrophone. It is possible to postulate which internal structures are likely to cause reflections, for example: the protruding internal rim of the large port, the walls of the vessel, and the front of the absorbent wedges lining the vessel. In the case of the wedges, although they are designed to absorb sound energy, a certain amount of energy will be reflected by the tips of the wedges. It is not a simple matter to calculate the strength of the reflected signals, but it is possible to estimate the time of arrival of the signals reflected from each structure within the vessel. A simple model of this kind was developed using the Matlab programming language, and some of the results are plotted in shown in Figure 6.4.

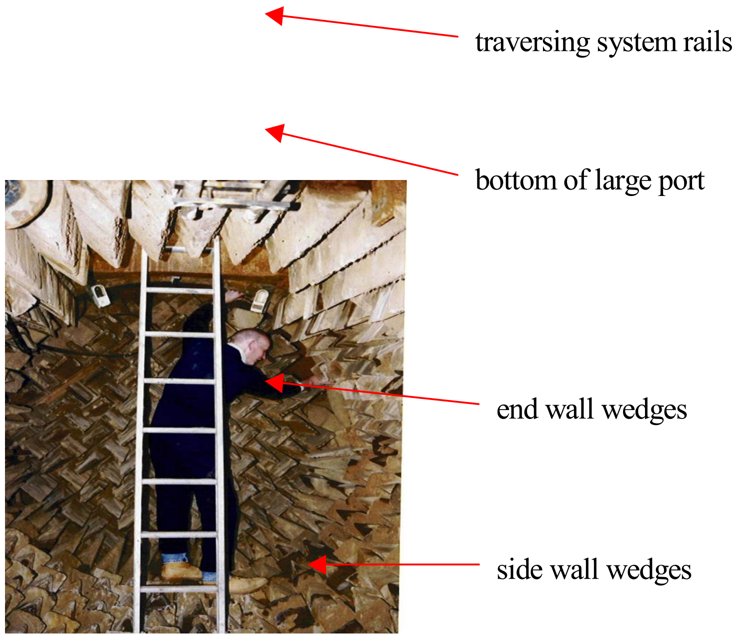

Figure 6.3 Internal structures of APV looking toward the large port.

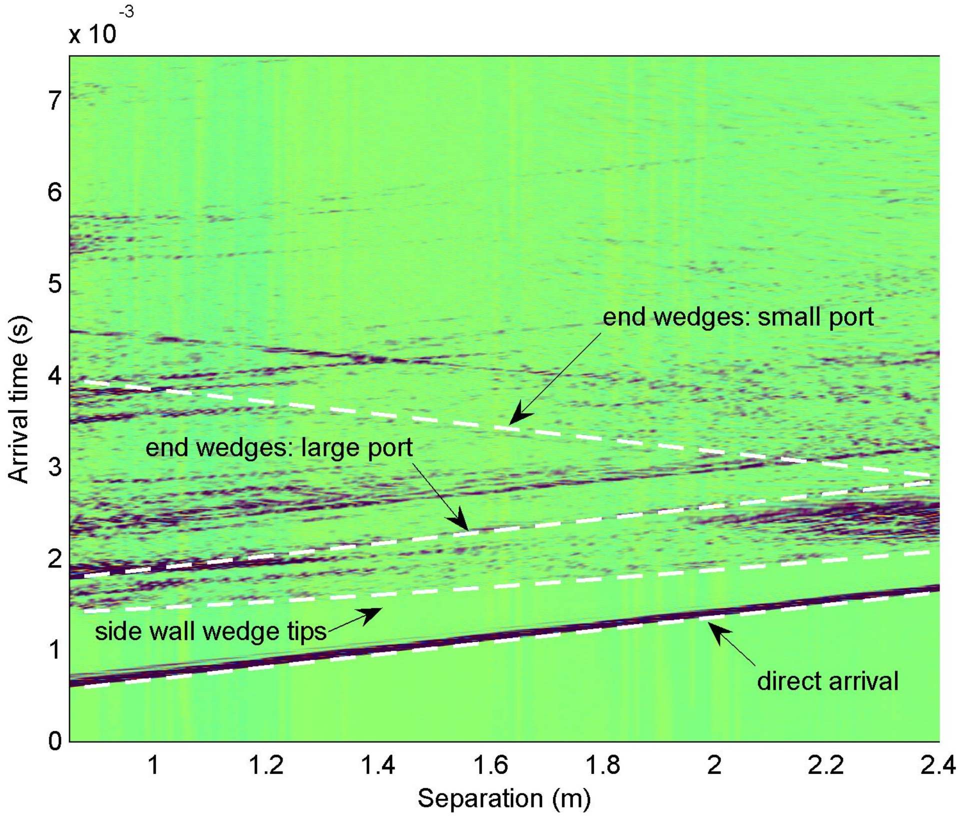

Figure 6.4 Signal arrival time plotted against separation for a pulse frequency of 75 kHz, hydrophone held centrally beneath the large port lid. Also plotted are the theoretical arrival times of the reflections from certain of the internal structures within the vessel.

Figure 6.4 shows the results of measurements made with a 75 kHz pulse and with the hydrophone held centrally beneath the large port lid, with the plot formed in the same way as for the 30 kHz data of Figure 6.2. In this case, the duration of the signals is reduced due to the higher frequency used. Also shown are the theoretical arrivals of reflected signals from the tips of the side-wall wedges, and the tips of the end-wall wedges at the large and small port ends. It was difficult to measure the internal geometry of the vessel with great accuracy, but the agreement with the actual measured data is nevertheless reasonably good.

The curves shown in Figure 6.4 have both positive and negative slopes. The direction of the slope and the type of curve provides information about the location of the reflective surface within the vessel. A straight line with a positive slope implies the reflective surface lies behind the hydrophone, examples being the end wall and wedges at the large port end. A straight line with a negative slope indicates the reflective surface is positioned behind the projector, examples being the end wall and wedges at the small port end. A curved line with a positive slope indicates that the reflecting surface is adjacent to the transducers, examples being the side-walls and side-wall wedges. The strong reflection present at 2 ms and 0.8 m is due to the protruding lower rim of the large port. The strength of this signal is reduced at increased separations due to the change in angle of incidence (at short separations, the bottom of the rim provides an extended edge which can produce more scattered sound).

In general, the sound reflected from the wedge tips has been accurately predicted. However, it is clear that there is some scattered sound arriving at later times which is produced by the internal structure of the wedges. In addition, some of the sound transmitted through the wedges will be reflected by the vessel walls. However, it is more difficult to model these arrivals since the effective sound speed in the wedges is not known, and in any case they do not affect the echo-free time. In addition, the end walls are not planar but curved, leading to multi-path signals bouncing through the wedges at the vessel ends. In general, at greater times it is clear that multi-path signals are present, with a certain periodic structure with time evident in the plots (perhaps most clearly seen in Figure 6.2).

The measurements at 75 kHz were repeated with the hydrophone mounted forward of the centre of the large lid, the hydrophone being mounted on the forward arm of the dual hydrophone mount. This determined the effect of this alternative mounting scheme on echo free time. Figure 6.5 shows the results and demonstrates that the echo-free time for transducers in this configuration is nominally the same as for the hydrophone mounted centrally beneath the large port lid. Interestingly, the reflection from the lower rim of the port is slightly suppressed with this arrangement. In these measurements, the source was still suspended from the extension cradle. If both devices are suspended from the dual-hydrophone mount with a separation of 0.75 ms, the echo-free time is approximately 0.95 ms.

Measurements were also conducted using a 20 kHz pulse and the results of these measurements are shown in Figure 6.6 with the hydrophone this time held centrally beneath the large port lid once again. The echo free time is unchanged but the individual reflections are less easily distinguished due to the increased duration of the signals. Some of the reflected signals are also stronger in amplitude compared to the higher frequencies due to the less effective performance of the anechoic wedges.

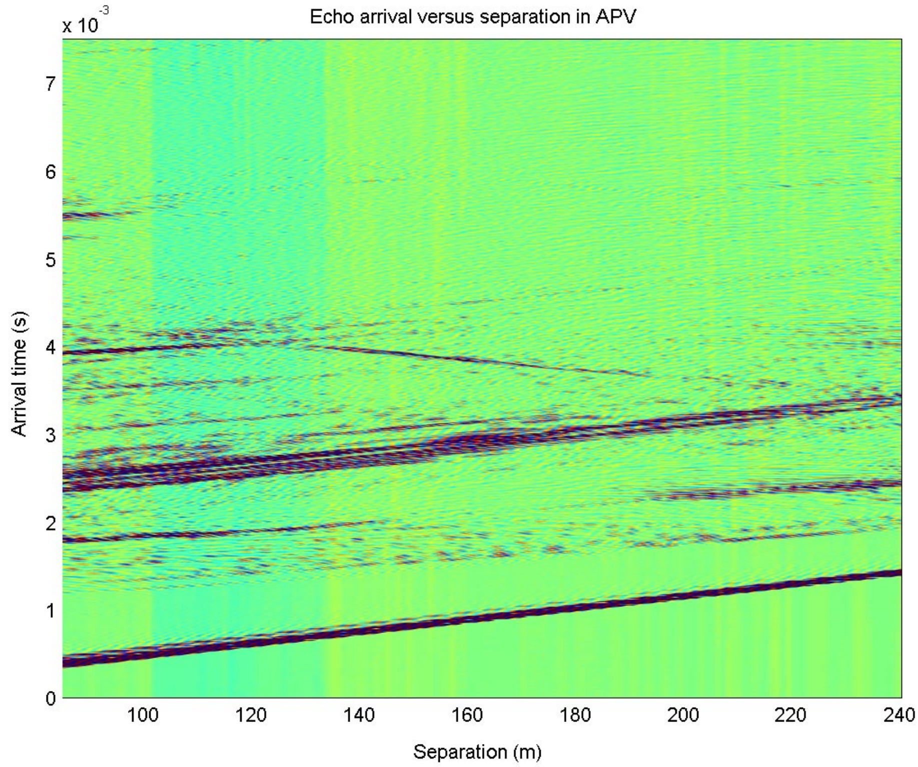

Figure 6.5 Signal **a**rrival time plotted against separation for a pulse frequency of 75 kHz, hydrophone held in the dual hydrophone mount beneath the large port lid.

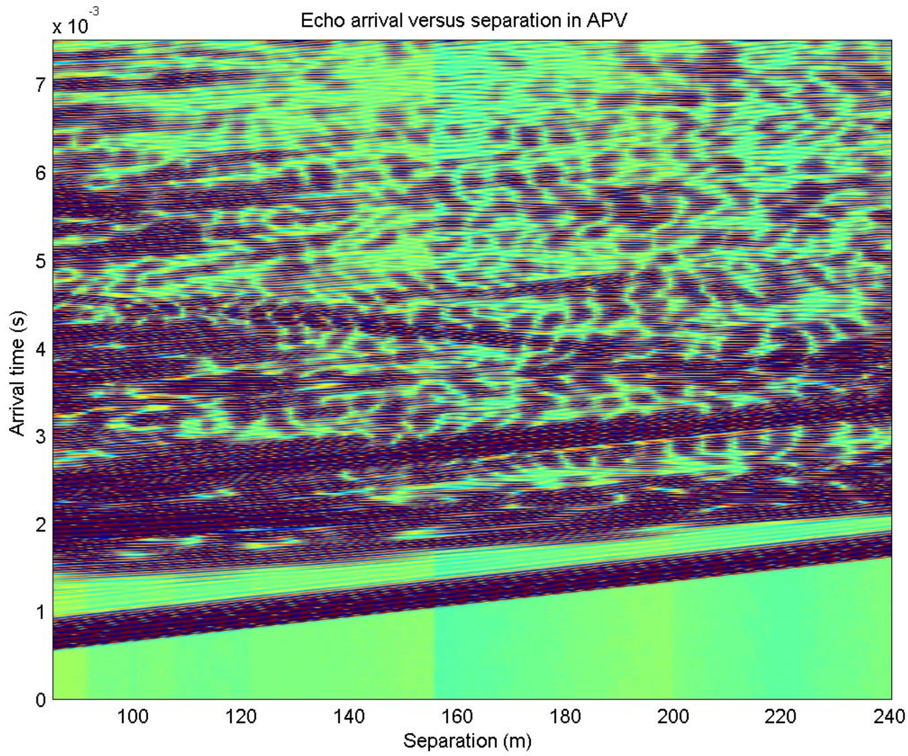

Figure 6.6 Signal arrival time plotted against separation for a pulse frequency of 20 kHz, hydrophone held centrally beneath the large port lid

6.2 REVERBERATION TIME.

The majority of acoustic measurements that take place in the APV are undertaken using discrete frequency tone-bursts, in order to utilise the echo free time within the vessel (see Section 6.1) and simulate a free field environment. In addition, knowledge of the reverberation time may be useful if the APV is used for measurements in a reverberant field.

The reverberation-time measurements were made using an ITC 1007 spherical transducer as a source, driven with white noise from a B&K 1405 noise generator. The received signal was measured using a Reson TC4032 Hydrophone. Measurements were made in accordance with BS EN ISO 3382 – *Measurement of reverberation time of rooms* [21]. The reverberation time, T, my be defined as the time for a signal to fall to a level 60 dB below the steady-state level. It is given by:

$$T = 55.2\frac{V}{cA} \tag{6.1}$$

where V is the volume, c is the sound speed and A is the overall absorption of the tank, the 55.2 constant being derived from the –60 dB definition.

The measurement began with the reverberant noise generated within the vessel and being allowed to reach steady-state levels over a number of seconds. The noise source was then stopped and the decay of sound level in the tank was measured, the signal being captured on an HP89410A vector signal analyser. The stable noise signal level and decay can be seen in Figure 6.7.

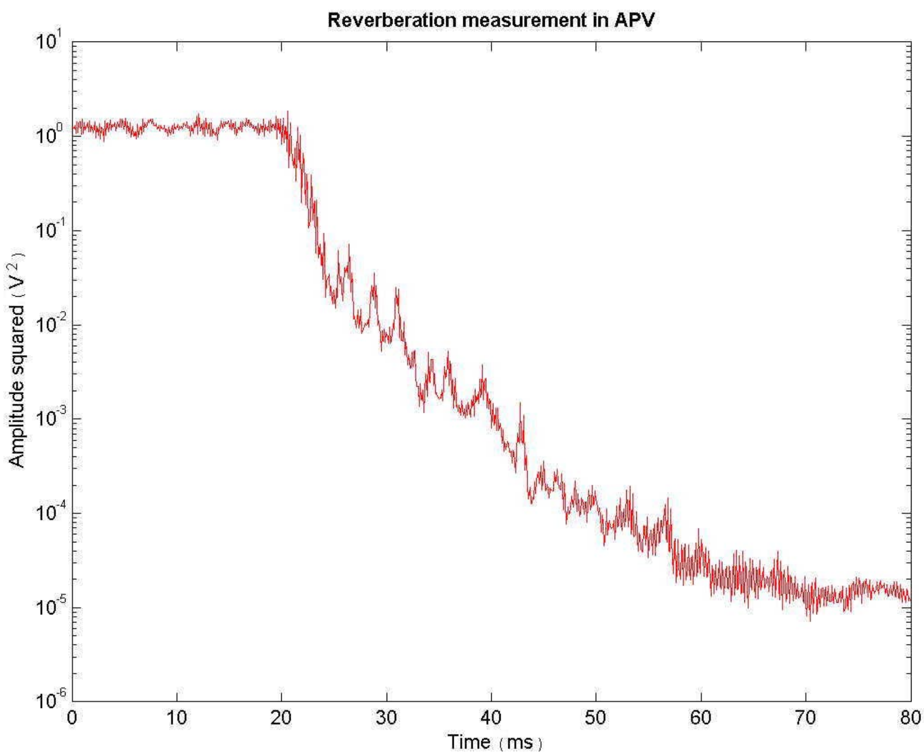

Figure 6.7 Reverberation time measurements, received voltage squared against time.

The decay of the reverberant field after the noise source has been switched off has been shown to be exponential [22]. In Figure 6.8, the exponential decay has been plotted on a decibel scale in to give a linear regression from which the reverberation time can then be calculated.

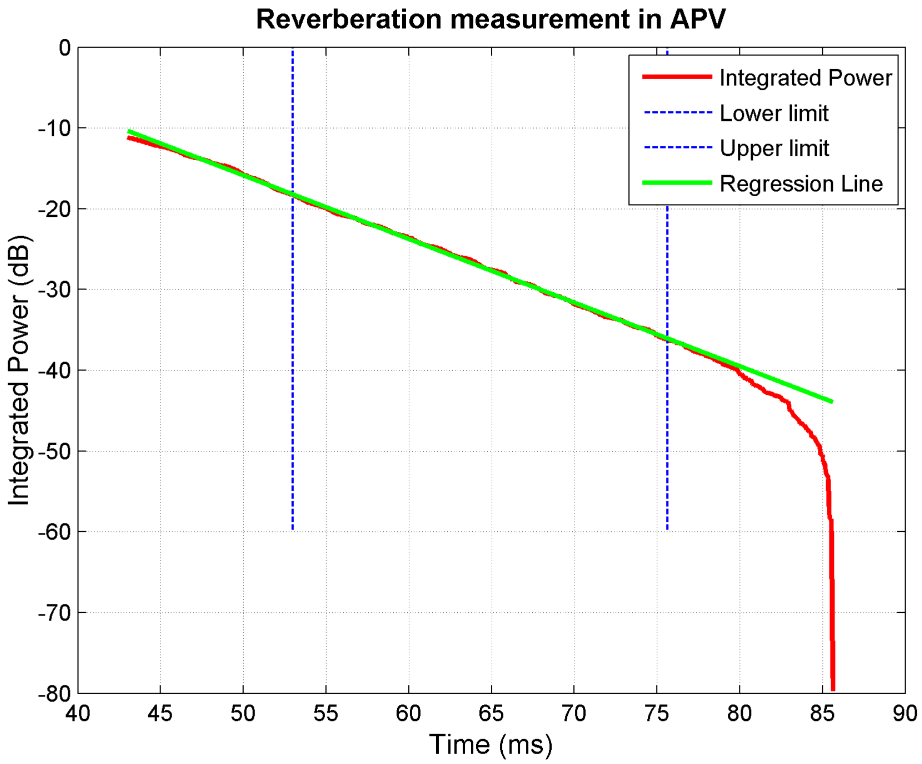

Figure 6.8 Integrated Power in dB versus time, representing decay time of reverberant field.

A band-pass filter was used to control the frequency content of the noise projected during the reverberation time measurements. A number of repeated measurements were made with the data processed as shown above, and the data was averaged to provide a value of reverberation time. The calculated reverberation time for filtered white-noise with a bandwidth of between 10 kHz and 300 kHz was 80.7 ms with a standard deviation of 7.6 ms. The calculated reverberation time for white-noise filtered around 2 kHz was 82.5 ms with a standard deviation of 5.7 ms.

6.3 AMBIENT NOISE

The APV is designed to be a low-noise environment where measurements may be undertaken at ambient noise levels of better than sea-state zero, the ambient noise in the ocean for a sea-state of zero. In order to determine levels of ambient noise, a Reson TC4032 hydrophone was placed into the APV and used to measure noise spectra at frequencies up to 2 kHz. To ensure there was no electrical pick-up from mains supply to the DC power supply to the hydrophone preamplifier, it was powered with a DC 12 V battery source. A number of measurements were made to investigate the ambient noise levels under different conditions including: with and without the pneumatically-activated anti-vibration mounts inflated; with and without the building heating system enabled. Measurements were also made at different times of the day. For all measurements, the voltage output from the hydrophone was converted to sound pressure level using hydrophone sensitivity data. Figure 9 and Figure 10 show the results of the measurements.

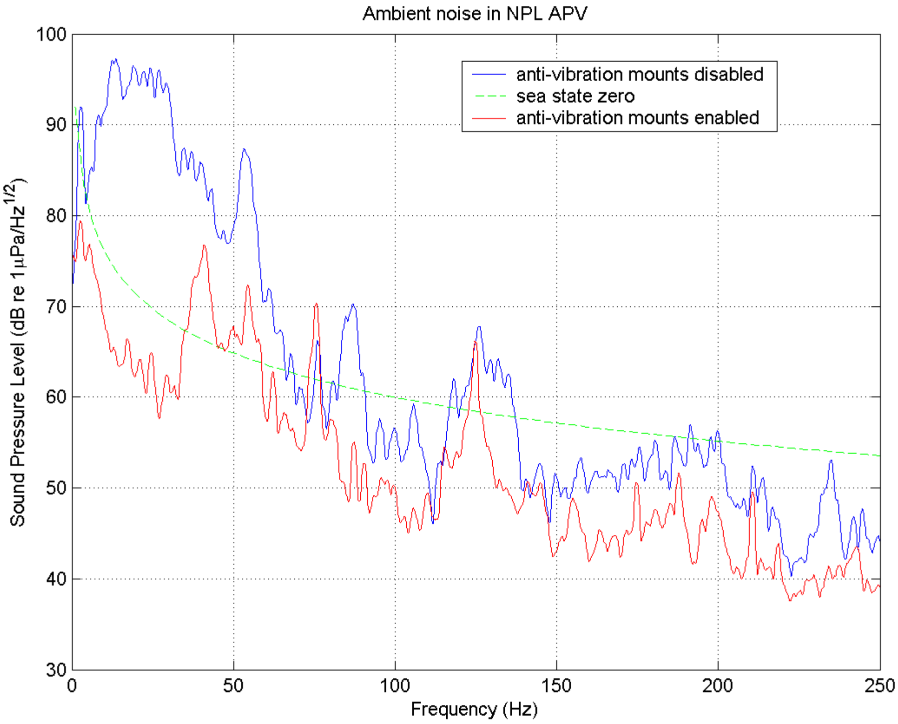

Figure 6.9 Ambient noise measurements in the APV with the air filled anti-vibration mounts inflated and deflated.

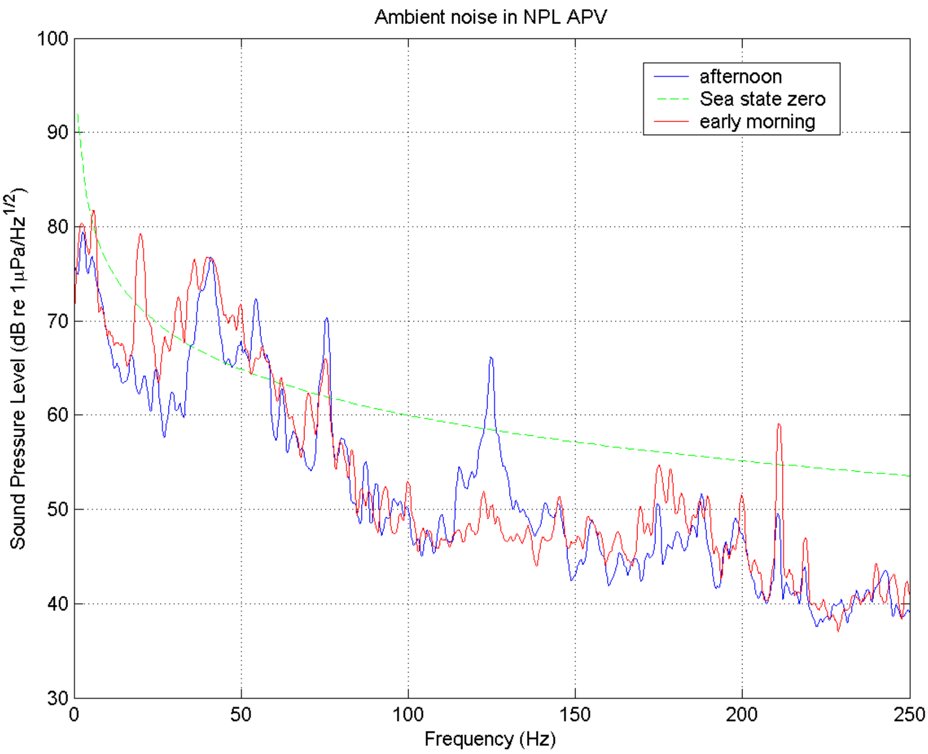

Figure 6.10 Ambient noise measurements in the APV at different times of the day.

The difference in the ambient noise spectra for the inflated and deflated anti-vibration mounts is most pronounced at frequencies below 70 Hz, as shown in Figure 6.9. At frequencies above 70 Hz, the anti-vibration mounts have less effect. The noise spectra with the anti-vibration mounts inflated was consistently below sea state zero, rising above this level for only a few tonal components of the noise spectrum.

Figure 6.10 shows noise spectra made during the afternoon and early morning (about 7 am). The time of day at which the noise spectra is measured does not appear to have a significant effect on the overall level of noise. However, there are certain tonal components in the noise which appear to be more prevalent at certain times of the day. This may be due to fans on building heating plant, or other activity. It was not possible to measure during the night, but this may have improved the noise level even further.

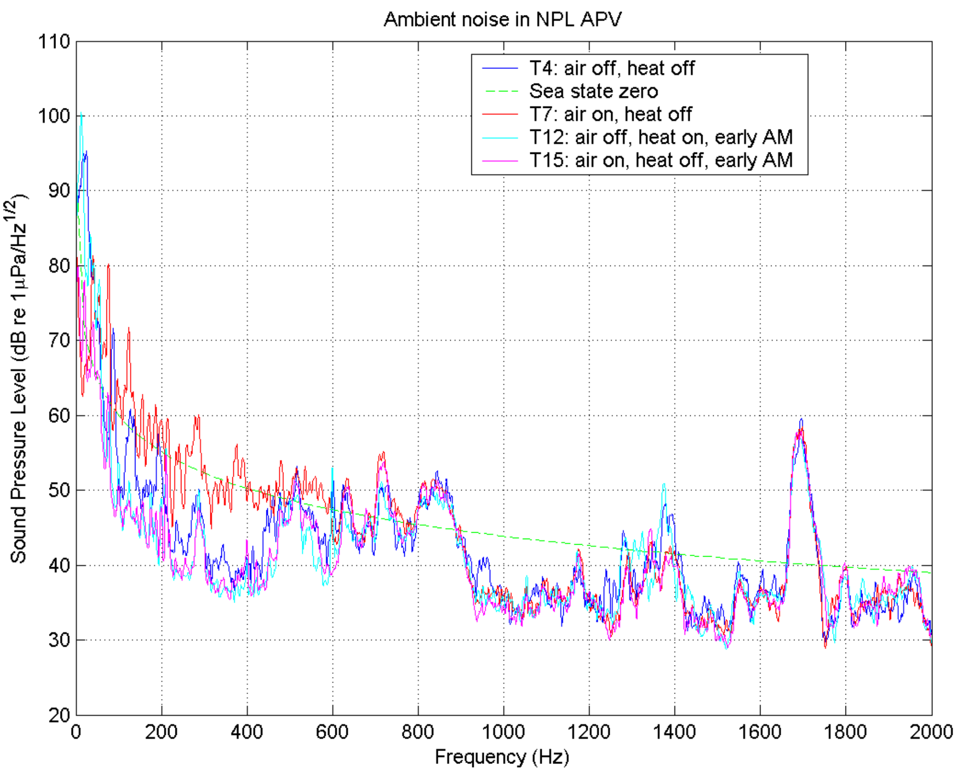

Figure 6.11 Ambient noise spectra in the APV with heating on and off and anti-vibration mounts inflated and deflated at different times in the day.

Figure 6.11 shows ambient noise spectra with the APV heating system on and off combined with the anti-vibration mounts being enabled and disabled. Also shown are measurements made at different times in the day. The effect of having the heating system on was most noticeable at low frequencies, this coupled with the deflation of the anti-vibration mounts gave a high ambient noise level at low frequency. When the heating system was turned off and the anti-vibration mounts were inflated, the ambient noise level dropped below sea state zero at low frequencies. When these measurements were performed in the early morning, the ambient noise spectra was below sea state zero for the majority of the frequency range.

6.4 ECHO REDUCTION DUE TO WEDGES IN THE APV.

The performance of the wedges lining the inside of APV has been investigated experimentally. Measurements of the echo-reduction were made using a USRD F30 acoustic projector and a USRD H52 hydrophone. Both transducers were mounted on the dual hydrophone mount below the large lid of the APV. The acoustic projector was driven with discrete frequency tone-bursts in the range 25 kHz to 100 kHz. The hydrophone was then used to measure the incident wave from the acoustic projector and the reflected wave from the wedges on the end wall of the APV, with the time window for the analysis set to include the reflections from the wedges but to exclude multi-path reflections from the vessel interior (Figure 6.12).

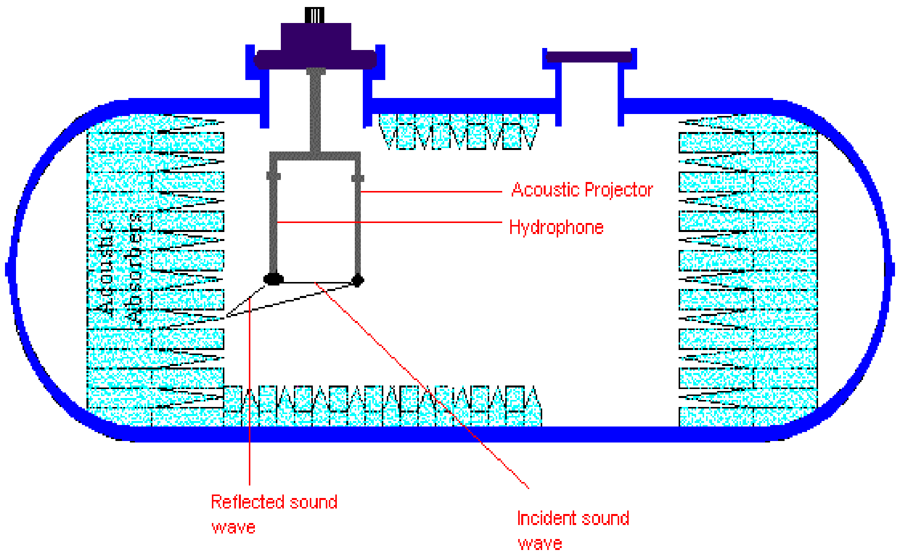

Figure 6.12: Experimental set-up for echo reduction of acoustic wedges.

The incident and reflected waves received by the hydrophone were then used to calculate the echo reduction by the acoustic wedges at the end of the APV. Measurements were made at 2 °C, 20 °C and 35 °C at ambient hydrostatic pressure of 0.1 MPa to investigate the effect of temperature on the performance of the wedges. Further measurements were made at pressures of 0.1 MPa, 3.5 MPa and 6.8 MPa at a temperature of 20 °C to investigate the effect of hydrostatic pressure on the performance of the wedges. Corrections were made during the measurements in order to account for the effect of spherical spreading losses.

From the results shown in Figure 6.13, it is clear that temperature has very little effect on echo reduction at ambient pressure. The wedges by no means render the vessel completely anechoic, with the echo reduction varying with frequency from values of only a few decibels at low frequencies, to between 25 dB and 35 dB at frequencies from 75 kHz to 90 kHz. There are peaks of echo reduction present at certain frequencies, but there are peaks in the general trend at both 40 kHz and 80 kHz, indicating that the acoustic wedges are most effective at these frequencies.

Hydrostatic pressure is seen to have even less of an effect on echo reduction than temperature, as is shown in Figure 6.14. This shows that the change in hydrostatic pressure has little effect on the performance of the wedges, a good characteristic for use in the APV.

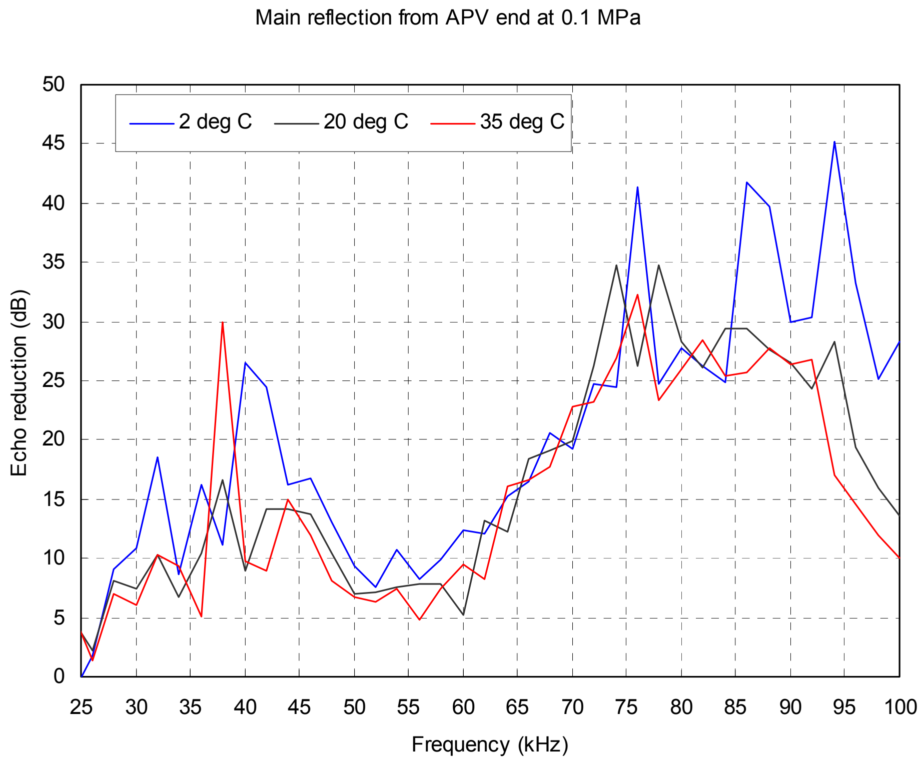

Figure 6.13 Echo reduction for the wedges at different temperatures at 0.1 MPa.

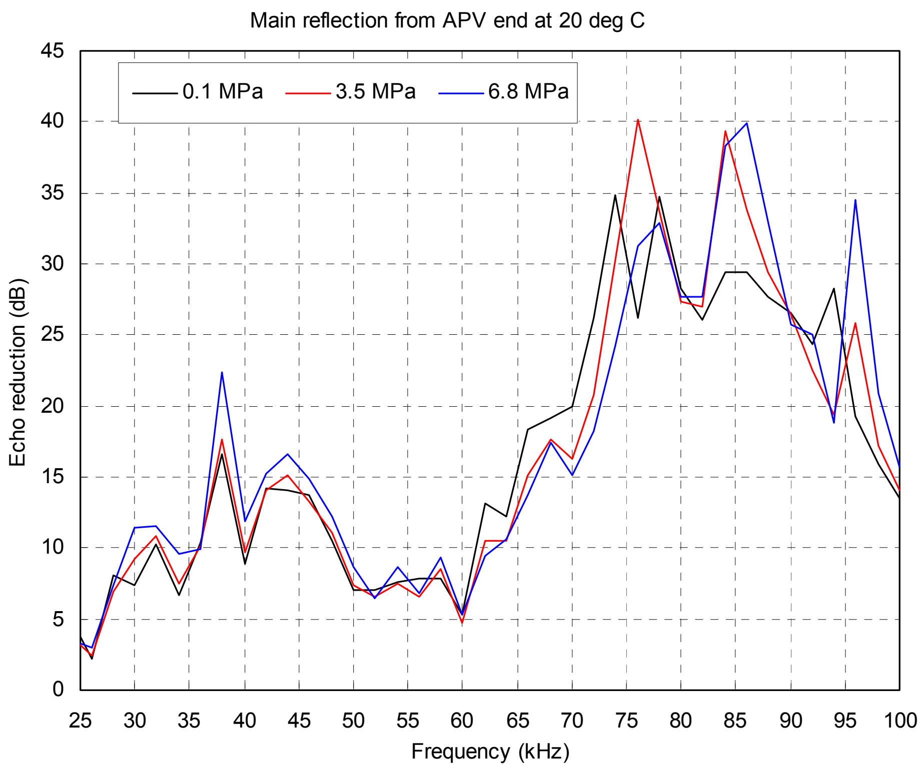

Figure 6.14 Echo reduction for the wedges at different pressures at 20 °C.

7 EXTENDING THE FREQUENCY RANGE USING SIGNAL MODELLING

7.1 BACKGROUND

In reverberant laboratory tanks, free-field measurements are limited by the finite size of the tanks. Although time-gating techniques and tone-burst signals may be used, the signal available for analysis is limited by the arrival of boundary reflections. If the signal does not reach steady-state conditions during this echo-free time, it is not possible to make measurements by conventional means. In particular, this hinders the calibration of high *Q* projectors at frequencies of a few kilohertz or less in laboratory tanks [15,20].

In spite of the presence of the anechoic coating used in the APV, the vessel is not truly anechoic in any meaningful sense at low kilohertz frequencies, and the wedges merely assist in reducing the reverberation time. Results have been presented in Section 6.4 of the performance of the wedges, demonstrating that they have limited effect at low kilohertz frequencies. In Section 6.1, a description has been given of the echo-free time available in the APV along with a discussion of the major sources of boundary reflections. At a separation of 1 m, for a typical configuration with one transducer mounted below the large lid and one on the extension cradle, an echo-free time of only 0.65 ms is available (equivalent to less than 2 cycles of a 2 kHz signal). This may be increased to nearly 1 ms with the transducers attached to the dual-hydrophone mount described in Section 2 (the separation now being 0.75 m). This is not sufficient to allow steady-state to be reached for many low frequency projectors. For example, a projector of resonance frequency 3 kHz and *Q*-factor of 10, steady-state will not be reached for at least 3.3 ms (approximately *Q* cycles of the resonance frequency). Therefore, alternative methods must be used if such projectors are to be calibrated in the APV.

One technique that may be used to overcome these difficulties is signal modelling [23-24]. The efficacy of this technique has been demonstrated previously using measurements undertaken in the NPL open tank facilities [25-26]. In this report, results are presented of applying the method to calibrations undertaken in the APV. To demonstrate the technique, the method is used to calibrate two high *Q* projectors with resonance frequencies of only a few kilohertz. Measurements are undertaken in the APV, and the results are validated by comparison with measurements made under the same conditions at the NPL open water facility at Wraysbury, where it is possible to undertake measurements under steady-state conditions.

7.2 SIGNAL MODELLING METHOD

7.2.1 The model

The difficulties described above may be at least partly overcome if greater use can be made of the initial transient-dominated part of the waveform, in particular if the steady-state signal can be predicted by fitting a model to the initial transient-dominated data. If we consider the response of an electroacoustic transducer at frequencies at or below its first resonance frequency, it is reasonable to assume the behaviour is that of a damped harmonic oscillator. This corresponds to the regime where the device may be modelled with a so-called "lumped-parameter" model. The behaviour of a damped harmonic oscillator is governed by a linear constant coefficient differential equation of the kind familiar from the analysis of systems of masses, springs and dampers (or in an electrical analogue, a resonant LCR circuit). The solutions of such a differential equation are also well known to be combinations of damped sinusoids or, expressed in an alternative way, as a sum of complex exponentials.

In order to achieve good *prediction* from the model fitted to the data (which is important when direct measurement of the steady-state is limited), it is necessary to consider *physical* models. We assume that the measured signal $y(t)$ corresponds to the output of a system that behaves as a linear damped harmonic oscillator, and consequently $y(t)$ solves a linear constant coefficient differential equation of the form

$$\sum_{k=1}^{p+1} c_k \frac{d^{k-1}}{dt^{k-1}} y(t) = 0. \tag{7.1}$$

Solutions to this differential equation include damped and undamped sinusoids, as well as real exponential functions. With appropriate initial conditions, equation (7.1) defines completely the output $y(t)$. A model for $y(t)$ may be derived using solutions to equation (7.1). Using *a priori* knowledge about $y(t)$, this model may be written in the particular form

$$y(t) = A_0 \sin\{2\pi f_0 t + \phi_0\} + \sum_{k=1}^{n_r} A_k e^{d_k t} \sin\{2\pi f_k t + \phi_k\}, \tag{7.2}$$

where the first term is used to describe the steady-state behaviour of the device, and the remaining terms its resonant behaviour. The solution to equation (7.1) is also given by

$$y(t) = \sum_{k=1}^{p} \alpha_k e^{\beta_k t}. \tag{7.3}$$

Equation (7.3) defines the *complex exponential* parametrisation for the output $y(t)$. The variables β_k, $k = 1, \ldots, p$, are known as *poles*, and are the roots of the characteristic polynomial defined by $\{c_k\}$. The variables α_k, $k = 1, \ldots, p$, are known as *residues*, and are determined by the initial conditions for $y(t)$. Notice that the parameters in this model are divided into those (the residues) that appear *linearly* in the model, and those (the poles) that appear *nonlinearly*. This has important implications for algorithms for fitting the model to measured data.

7.2.2 Fitting the model to the data

The models of this form are fitted to waveform data $\{(t_i, y_i): i = 1, \ldots, m\}$ measured at equally spaced times t_i. If ε_i is the measurement error for the ith data value y_i, and the values t_i are known accurately, the function $y(t)$ satisfies the *observation equations*

$$y_i = y(t_i) + \varepsilon_i, \qquad i = 1, \ldots, m. \tag{7.4}$$

Assuming the errors ε_i are uncorrelated samples from a Gaussian probability distribution with mean zero and standard deviation σ, unbiased and efficient estimates of the parameters defining $y(t)$ are obtained by solving

$$\text{minimise} \quad \sum_{i=1}^{m} \{y_i - y(t_i)\}^2 \tag{7.5}$$

with respect to the parameters of $y(t)$. The residuals $e_i = y_i - y(t_i)$ evaluated at the solution provide estimates of the errors ε_i, and an estimate of σ is given by the root-mean-square error s where

$$s = \sqrt{\frac{1}{m-n}\sum_{i=1}^{m} e_i^2}\,, \tag{7.6}$$

and n is the number of parameters defining $y(t)$. If *a priori* knowledge of any of the model parameters is available (for example, the resonance frequency and Q-factor may be known from measurements of electrical impedance), this information can be represented by additional observation equations, and the estimation problem is modified accordingly. For example, if f_r and d_r are the frequency and damping factor for a resonance of the system, the estimation problem becomes

$$\text{minimise} \quad \sum_{i=1}^{m} \{y_i - y(t_i)\}^2 + u^2\{f_r - f_1\}^2 + v^2\{d_r - d_1\}^2, \tag{7.7}$$

where u and v are "weights" that are used to reflect the relative accuracy between the measured data and the *a priori* knowledge.

Since the signal *model* is not linear (it is composed of exponential functions), the fit is performed by use of a nonlinear least squares algorithm to achieve a best fit in a maximum-likelihood sense. This has significant advantages over linear estimators such as the classic method of Prony. However, since a reasonable initial estimate is required for the nonlinear least squares method to be accurate, a modified form of Prony's method has been used to provide this.

In the NPL implementation, the so-called *least-squares Prony method* has been used to provide the initial estimates of the model parameters. However, in the presence of noise, the method gives estimates that do not converge to the true solution as the number of sampled points increases, rendering the basic method difficult to use for poor signal-to-noise ratios. A number of variations have therefore been used to improve the method. For example: (i) the *modified least-squares Prony method* in which, instead of adjacent samples, every lth sample is used to satisfy the recurrence equations; (ii) the use of a large number of poles with so-called *forward* and *backward prediction* to help in distinguishing between "true" system poles and poles associated with measurement noise; (iii) the *Prony-SVD* method in which a large number of poles is used with the singular value decomposition to filter the signal; (iv) a *weighted* version of the least-squares Prony method that correctly accounts for the error structure in the original measured data.

Once the initial estimate has been made using the Prony methods, a nonlinear least-squares method is employed to find the final solution. For this, a Gauss-Newton algorithm is used, safe-guarded with a line search algorithm with *a priori* information incorporated as described in equation 7.7. Furthermore, if additional damped sinusoidal components are used to define the initial model fit, these are either explicitly removed prior to applying the Gauss-Newton algorithm or *regularisation* is used to replace the estimation problem to be solved by one that is better conditioned. A full description of the signal-modelling method as implemented at NPL is given in references [25-26].

7.3 EXPERIMENTAL MEASUREMENTS

To exercise the method using the APV, two projectors were chosen for calibration in terms of their transmitting voltage response (TVR). These were flexural disc transducers with nominal resonance frequencies of 2 kHz and 4 kHz, both of the devices having a *Q*-factor of about 10 (and therefore requiring at least 5 ms and 2.5 ms respectively before steady-state conditions are reached).

7.3.1 Measurements made at the NPL open water facility at Wraysbury

The transducers were first calibrated in a free-field environment at the NPL open water facility located at Wraysbury reservoir. Measurements were made at discrete frequencies at intervals of 50 Hz in the range 1.0 kHz to 3.0 kHz for the 2 kHz device, and in the range 2.5 kHz to 5.5 kHz for the 4 kHz device. At each frequency, measurements were made on the steady-state portion of a tone-burst signal, with the echo-free time being sufficient to allow steady-state conditions to be reached. A measurement was made of the acoustic pressure at a known distance from the projector using a calibrated hydrophone, while simultaneously measuring the drive voltage applied to the projector, the TVR being calculated from the expressions given in Section 5.2.2. The hydrophone receive voltage and the projector drive voltage were measured using an HP89410A vector signal analyser, with the drive voltage first attenuated using a calibrated attenuator. To drive the projectors, an HP33120A signal source was used along with a B&K2713 power amplifier. Measurements were also made of the electrical impedance of the projectors using an HP4192A impedance analyser.

The projectors contain small holes on the rim that can be used for mounting. Thin wire was passed through the holes and the length of the wire was then adjusted to allow the transducer to be suspended freely, with the transducer balanced so that the plane of the face was horizontal in the water. To mount the transducers for measurements, the dual-hydrophone mount described in Section 2 was used. The projector under test was freely suspended 3 m beneath one arm of the cross-bar of the mount using the thin wire, with the cross bar attached to the bottom of the calibration station, the station being lowered to its full depth of 5 m for the calibrations. The total depth at which measurements were conducted was therefore 8 m. The reservoir itself is in excess of 20 m deep, and has lateral dimensions of 1 km by 2 km.

The receiving hydrophone was a USRD H52 hydrophone calibrated over the frequency range of interest. This was suspended from the other arm of the cross-bar of the dual-hydrophone mount, with a free-flooding aluminium pole used to keep the hydrophone vertical in the water. The separation distance between the centres of the transducers was 0.74 m.

The nearest structure to the transducers was the cross-bar of the dual hydrophone mount. Any reflection from this structure would have a total transit distance of about 6 m, equivalent to a transit time of about 4 ms. The echo-free time would therefore be of the order of 3.5 ms (the direct path propagation delay for a separation of 0.75 m being about 0.5 ms). At the frequencies considered here, the cross-bar itself may not be a significant source of reflections, but the mount was attached to the bottom of the station with a metal flange which is likely to cause some sound to be scattered back to the hydrophone. Nevertheless, the reflections from the mount were barely visible on the signal when displayed on the vector signal analyser during measurements. The water surface was a strong source of reflected sound, but the transit time of 11 ms (transit distance of 16 m) allowed this to be easily removed by time-gating techniques.

The results of the measurements undertaken at Wraysbury are shown in Figure 7.1 for the 4 kHz transducer, and Figure 7.2 for the 2 kHz transducer. The small perturbations in the TVR may be due to minor residual reflections from the cross-bar mount. During the measurements, the temperature of the water in the reservoir was 14 ºC.

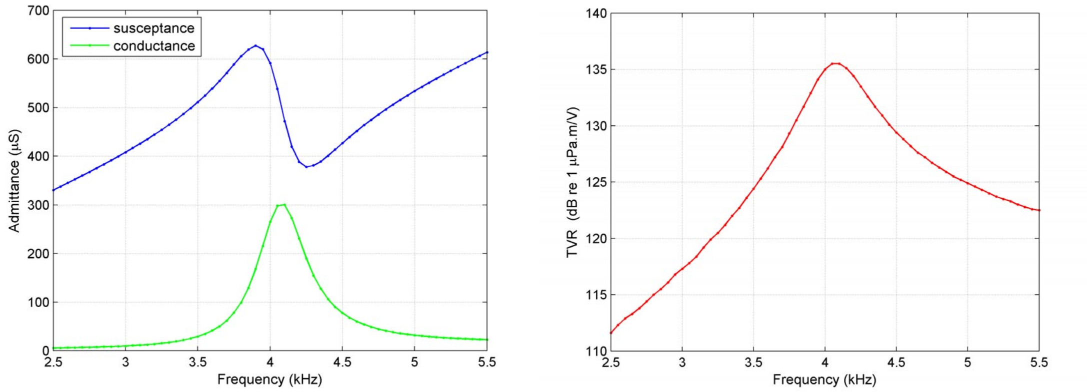

Figure 7.1 Results of measurements undertaken on the 4 kHz transducer at Wraysbury. Left: electrical admittance; right: TVR.

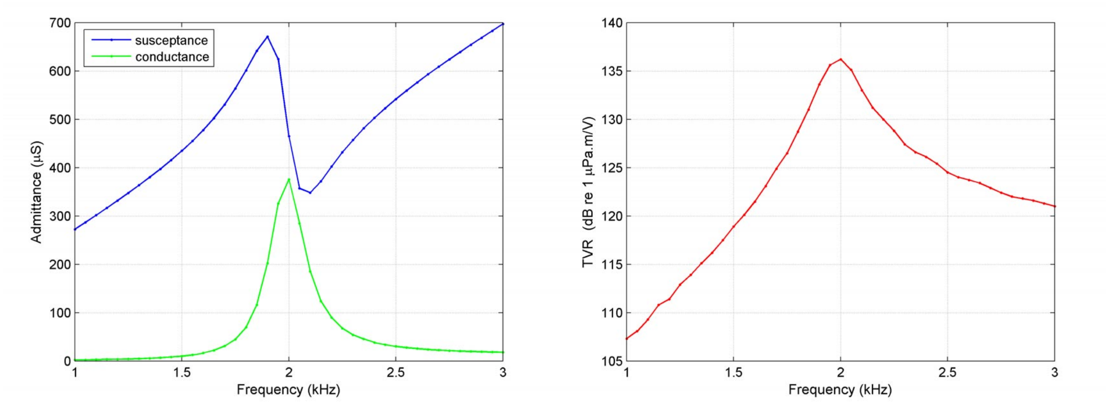

Figure 7.2 Results of measurements undertaken on the 2 kHz transducer at Wraysbury. Left: electrical admittance; right: TVR.

From the measurements of electrical admittance, the resonance frequencies and *Q*-factors for the projectors could be determined. For the 2 kHz transducer, the resonance frequency was found to be 1.99 kHz and the Q-factor was found to be 9.8. The 4 kHz transducer was found to have a resonance frequency of 4.08 kHz and a Q of 9.6.

7.3.2 Measurements made in the NPL APV

Measurements were then undertaken in the NPL APV at the same frequencies used for the calibrations at the NPL Wraysbury facility. The same reference hydrophone and the same models of instrumentation were used as for the measurements at Wraysbury, but in this case the receive waveform captured on the vector signal analyser was saved and analysed using signal modelling method.

The mounting arrangement was as close as possible to the one used at Wraysbury. The dual-hydrophone mount was again used with the projector again suspended by thin wire from one arm of the cross-bar and the H52 hydrophone suspended from the other arm by use of a free-flooding aluminium mounting pole. The separation distance between the centres of the transducers was 0.74 m. However, in the APV it is not possible to suspend the devices 3 m below the dual-hydrophone mount as was achieved at Wraysbury. Here, the transducers were arranged to be on the central axis of the vessel, with the distance from the transducers to the central mounting stem of the dual-hydrophone mount being about 0.95 m. For the measurements in the APV, the temperature of the water was set to 14 ºC, the same as that measured in the reservoir.

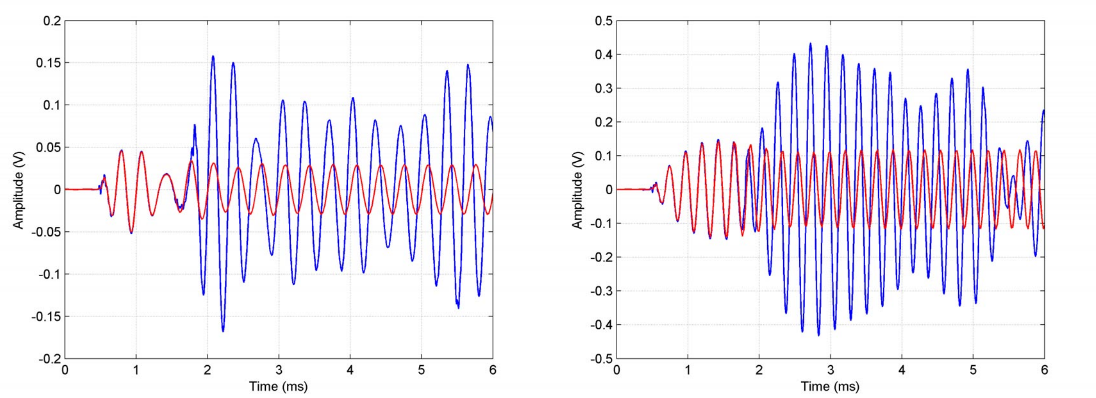

Figure 7.3 An example of waveforms received by the H52 hydrophone for the 4 kHz projector driven at 3.0 kHz (left) and 4.5 kHz (right). The red curve is the waveform from NPL Wraysbury facility, the blue corresponding to the waveform from the NPL APV.

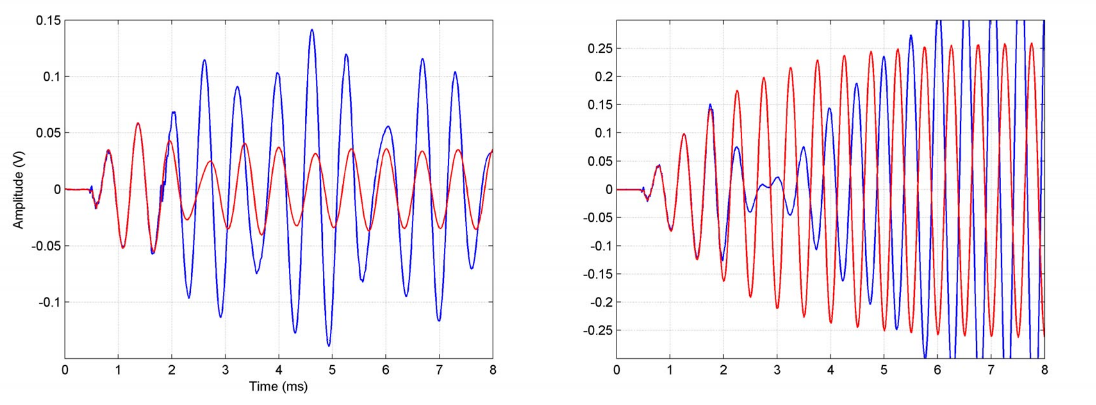

Figure 7.4 An example of waveforms received by the H52 hydrophone for the 2 kHz projector driven at 1.5 kHz (left) and 2.0 kHz (right). The red curve is the waveform from NPL Wraysbury facility, the blue corresponding to the waveform from the NPL APV.

Figure 7.3 and Figure 7.4 show examples of waveforms received by the H52 hydrophone during the measurements at Wraysbury open water facility (red curves) and in the APV (blue curves). Since the projector-hydrophone separations are the same for both the open-water measurements and for the APV, the direct path arrivals coincide. The first reflection arrives in the APV waveforms at approximately 1.6 ms, after which the two waveforms depart from each other. Other reflections arrive later, for example at 1.52 ms, 1.75 ms, and 3.0 ms, though some of these are not so evident without close inspection of the waveform. The reflection arrival times are evident from small high frequency perturbations present in the signal. These occur at the start of the waveform and are due to a higher frequency resonance being excited in the start-up transients of the projector (in the case of the 2 kHz transducer, the higher resonance is at 20 kHz).

It is clear that there is considerable interference present in the APV signal causing rapid fluctuations in amplitude. Since the projector and hydrophone are positioned on the axis of the vessel, the amplitude of the reflections can be greater than the direct signal due to the focusing effect of the curved walls of the vessel (in spite of the greater transit distance of the reflections). This is particularly the case around the large port where some of the anechoic wedges have been removed and the bare vessel walls are exposed.

Note that the steady-state signal is clearly visible in the open-water signal (red curve) after approximately 3 ms for the 4 kHz transducer and 5.5 ms for the 2 kHz transducer. However, there is no possibility of estimating what the steady-state amplitude would be from the APV measurements (blue curve) using conventional methods. However, the signal modelling technique allows extrapolation of the echo-free signal to estimate the steady-state amplitude.

The procedure adopted for the modelling was the same as that described in reference [25]. The echo-free segment of the waveform was identified and this portion alone was used as the input to the model. Some *a priori* information was input to the model, namely the nominal resonance frequency of the projector and the nominal Q-factor. These were known from the design specification of the transducers, and were checked by electrical impedance measurements undertaken within the APV (these were contaminated by boundary reflections but nevertheless provided a cross-check on the approximate values). This information is used to constrain the initial estimates used by the model. Although not essential since the model should converge on the appropriate values anyway, the use of this data helps convergence to occur quickly and militates against lack of convergence for noisy signals. In addition, the impedance data measured in the APV showed higher frequency resonances present in the transducer behaviour. These higher frequency resonances were also specified in the model (the number of resonance frequencies may be specified, or left unspecified for the model to find).

The model runs under the Matlab programming environment and requires the user to specify the time window for analysis. In each case and for each frequency, the decision to accept an estimate of the steady-state response was made as objective as possible. The decision was based on how well the data within the time-window considered was fitted. A fitted model was only accepted if it satisfied the convergence criteria implemented for the nonlinear estimation problem.

7.4 RESULTS

Figure 7.5 shows the result of fitting the model to the echo-free portions of waveforms for the 4 kHz transducer for drive frequencies of 2.5 kHz and 4.0 kHz. As can be seen, the signal conditions were far from steady-state. The effect of the higher frequency resonance can be seen in the small fluctuations at the start of the signals, and is particularly clear in the 2.5 kHz signal. The higher amplitude response close to resonance for the 4 kHz signal means that the higher frequency signal content is not so clear, though it is still discernible. Figure 7.6 shows examples of similar waveforms for the 2 kHz transducer at drive frequencies of 1.0 kHz and 2.0 kHz. The quality of the fit is good in the examples shown, with even the higher frequency resonances being fitted well.

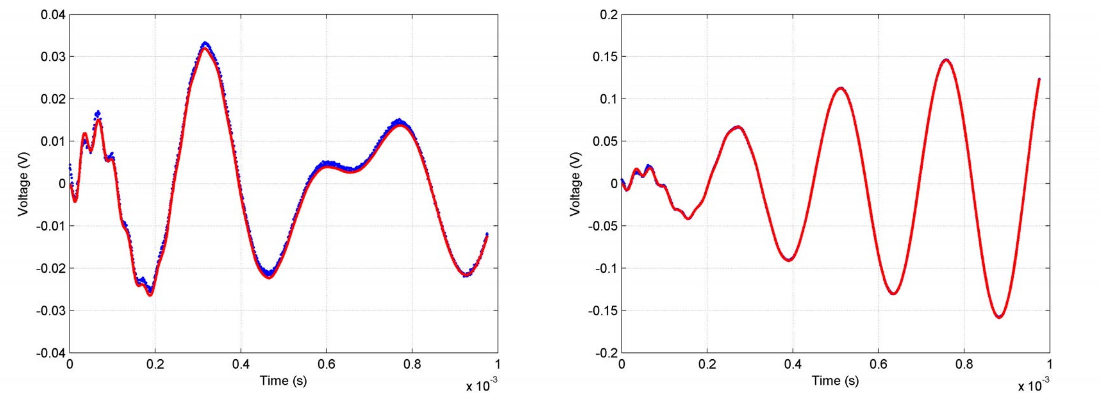

Figure 7.5 Results of fitting model to the echo-free portions of waveforms for the 4 kHz transducer for drive frequencies of 2.5 kHz (left) and 4.0 kHz (right). The blue points are the measured data, the red curve is the fitted data.

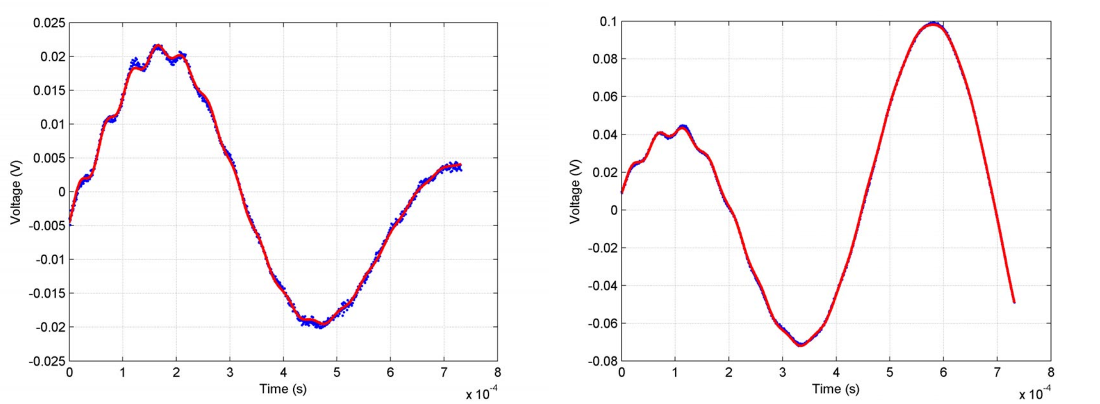

Figure 7.6 Results of fitting model to the echo-free portions of waveforms for the 2 kHz transducer for drive frequencies of 1.0 kHz (left) and 2.0 kHz (right). The blue points are the measured data, the red curve is the fitted data.

The waveforms for each frequency of measurement were separately analysed following the same procedure, and in each case the software provided a value for the steady-state amplitude. In fact, phase information is also provided, but this is not required for the work described here. Measurements were then made of the drive voltage amplitude (a simpler measurement since there are no contaminating reflections). The TVR was then calculated using the formulae described in Section 5.2.2.

The results of the TVR calibration are displayed in Figure 7.7 for the 4 kHz transducer, and Figure 7.8 for the 2 kHz transducer. As can be seen, the agreement is excellent for the 4 kHz transducer, with the maximum difference between the free-field value and the signal modelling value being 0.65 dB, and with a mean difference of +0.29 dB and a root mean square difference 0.33 dB.

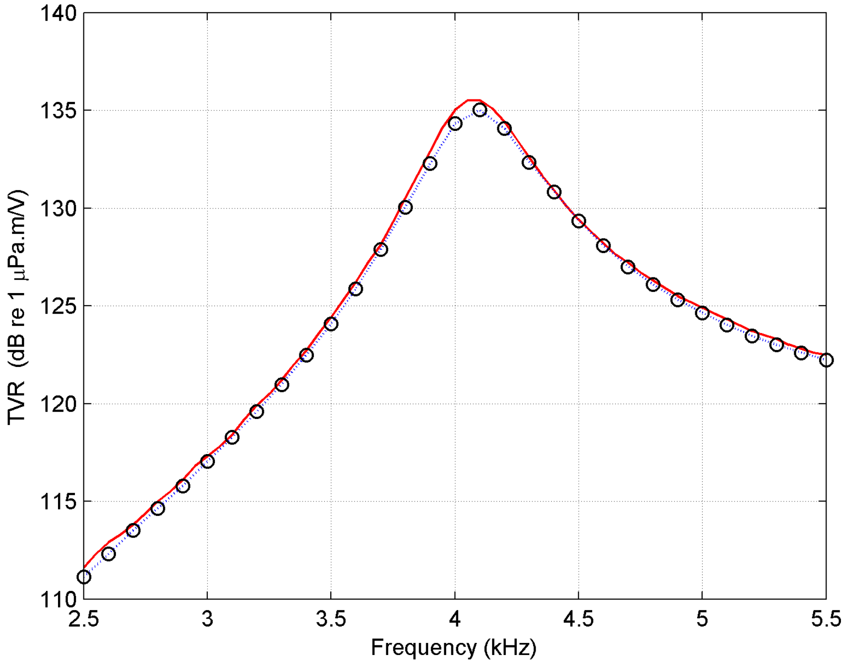

Figure 7.7 Results of measured TVR for the 4 kHz transducer showing the free-field response determined at the NPL Wraysbury facility (red curve), and the results of the signal modelling method (circles with dotted line) applied to the waveforms measured in the APV.

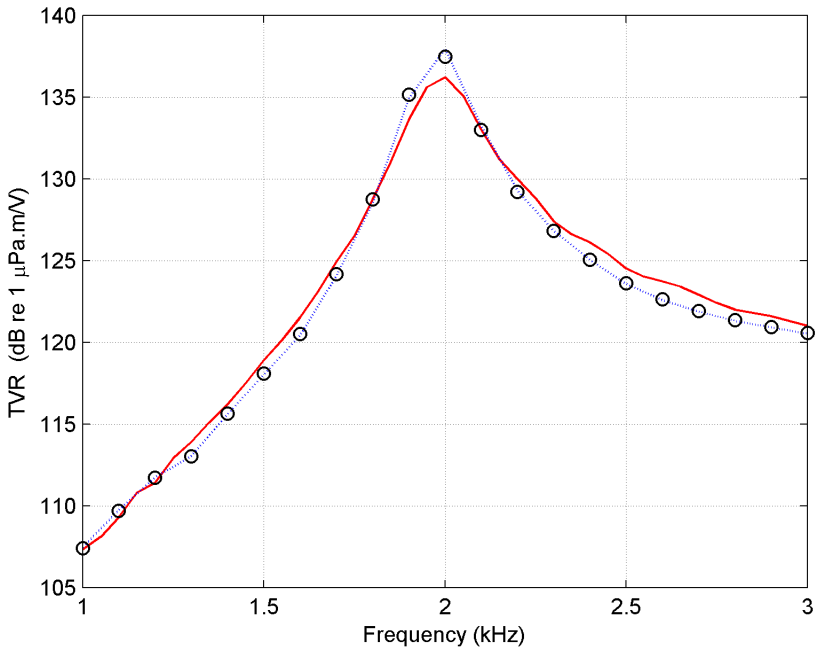

Figure 7.8 Results of measured TVR for the 2 kHz transducer showing the free-field response determined at the NPL Wraysbury facility (red curve), and the results of the signal modelling method (circles and dotted line) applied to the waveforms measured in the APV.

For the 2 kHz transducer, the agreement is not as good, with the maximum difference between the free-field value and the signal modelling value being 1.75 dB, and with a mean difference of +0.36 dB and a root mean square difference 0.85 dB. The agreement is worse close to the resonance frequency of the device. The explanation for this degradation in the results is that for the 2 kHz device there is less information present in the echo-free waveforms than for the 4 kHz device, in particular regarding the behaviour at resonance. As can be seen in Figure 7.6, there is little more than one cycle or so of the signal available for analysis (unlike in Figure 7.5 where several cycles are available for the 4 kHz device). This makes if very difficult to obtain accurate information on the damping factor of the transducer resonance, and this means that the problem can easily become ill-conditioned.

7.5 INCLUDING REFLECTIONS IN THE MODELLING

7.5.1 Theory

In the above, the modelled data is restricted to lie within a time-window containing the echo-free signal. This time-window is delimited by the turn-on of the device and the arrival of the first echo or reflection. However, increasing the information available for analysis would benefit the measurements for the 2 kHz transducers, and one way to achieve this is to extend this time-window into the part of the waveform containing reflections. To do this requires that the signal model be modified to include terms that represent the response of the transducer to the arrival of reflections. This has been done following the methodology described in reference [26].

Let τ_0 denote the time of arrival of the direct signal or, equivalently, the time of the turn-on of the device and τ_j, j = 1, …, R, the time of arrival of the jth reflection resulting from the reflection of the transmitted signal from a boundary of the tank. Then, a model for the measured signal is given by

$$y(t) = \sum_{j=0}^{R} y_j(t), \tag{7.8}$$

where $y_0(t)$ models the response to the direct signal and $y_j(t)$, j = 1, …, R, the response to the jth reflection, with

$$y_j(t) = A_{j,0}\sin\left(2\pi f_0\left(t-\tau_j\right)+\phi_{j,0}\right)H\left(t-\tau_j\right)+\sum_{k=1}^{n_r} A_{j,k}e^{d_k(t-\tau_j)}\sin\left(2\pi f_k\left(t-\tau_j\right)+\phi_{j,k}\right)H\left(t-\tau_j\right), \tag{7.9}$$

and $H(t)$ defined by

$$H(t) = \begin{cases} 0, & t < 0, \\ 1, & t \geq 0. \end{cases}$$

Here, the first term in equation 7.9 is used to describe the steady-state response of the device with f_0 being the drive frequency. The remaining terms in equation 7.9 describe the resonant behaviour with f_k denoting the resonance frequencies and d_k are the damping factors for the device that are related to its Q-factors according to

$$Q_k = -\frac{\omega_k}{2d_k} = -\frac{\pi f_k}{d_k}, \tag{7.10}$$

where $\omega_k = 2\pi f_k$ is the angular frequency.

Note that $y(t)$ reduces to the model

$$y(t) = A_0 \sin\left(2\pi f_0 t + \phi_j\right) + \sum_{k=1}^{n_r} A_k e^{d_k t} \sin\left(2\pi f_k t + \phi_k\right), \quad t \geq 0, \tag{7.11}$$

for the free-time response given in equation 7.2 in the case that there are no reflections (R = 0) and the arrival of the direct signal is zero (τ_0 = 0). In practice, the arrival of the direct signal is not necessarily known exactly, and τ_0 denotes the start of the waveform to be modelled and is set to exceed, but to be close to, this arrival time.

It is assumed that no dispersive or nonlinear effects are present within the system such that the reflected signals have the same frequency content as the direct signal. Consequently, the frequency f_0 of the steady-state response, and the frequencies f_k, $k = 1, \ldots, n_r$, and damping factors d_k, $k = 1, \ldots, n_r$, defining the resonances of the device, are the same for each signal arrival $y_j(t)$. However, the reflected signals may be expected to have attenuated amplitudes and be delayed in time with respect to the direct signal. Hence, the amplitudes $A_{j,k}$, $k = 1, \ldots, n_r$, and phase angles $\phi_{j,k}$, $k = 1, \ldots, n_r$, may be different for each response $y_j(t)$, and so these parameters are indexed using j as well as k.

As before, estimates of the values of the parameters defining the model $y(t)$ are obtained by solving the following nonlinear least-squares problem: given measurement data $\{(t_i, y_i): i = 1, \ldots, m\}$,

$$\text{minimise} \quad \sum_{i=1}^{m} \left(y_i - y(t_i)\right)^2 \tag{7.12}$$

with respect to the parameters of $y(t)$.

One way to determine the arrival times for the reflections is from geometrical considerations. If we measure the positions of the transmitting and receiving devices in relation to each other and we know the speed of the transmitted signal in the medium containing the devices, we can calculate the time it takes for the direct signal to travel between the devices. Similarly, if we measure the positions of the devices in relation to the reflecting surfaces, we can calculate the times it takes for the signal to travel between the devices following reflections at these surfaces. In the case of the waveforms used here, the echo arrival times could be estimated from inspection of the waveform since a small high frequency signal is present at the start of the signal due to the presence of the 20 kHz resonance within the signal (see Section 7.3.2).

Other approaches to determining the arrival times include the application of data processing techniques, such as wavelet analysis, to identify "features" in the measured signal. These approaches have been investigated at NPL, but were not used in the analysis presented here.

Whichever approach is used, the quality of the final results depends on the accuracy to which the arrival times are determined.

7.5.2 Results

The above method was applied to the waveform data for the 2 kHz transducer. Firstly, the arrival times of the first three reflections were determined from close inspection of the waveforms. Figure 7.9 shows the waveform for a frequency of 1.1 kHz, including echo arrival time estimates of 1.52 ms, 1.75 ms and 3.00 ms.

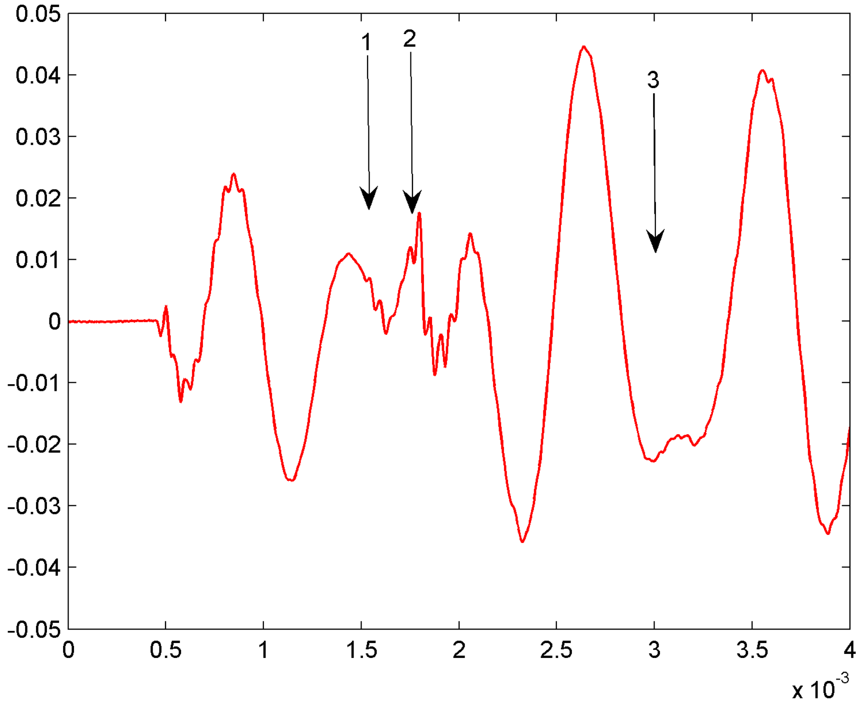

Figure 7.9 Receive waveform for a frequency of 1.1 kHz, including echo arrival time estimates of 1.52 ms, 1.75 ms and 3.00 ms.

The waveforms for each frequency in turn was processed using the extended model with the echo arrival times maintained at these values for all frequencies.

Figure 7.10 shows the improved results obtained using the extended model with three reflections. The agreement is better than before, with the root mean square difference between the free-field vale and the signal modelling value being better than 0.7 dB.

However, the improvement is not as great as might be hoped when compared to work published previously [26]. Unfortunately, when acquiring the longer waveforms containing reflections, the sampling frequency was not increased on the vector signal analyser. This means that although the waveforms containing reflections were of longer time duration, they contained only the same number of waveform points as the waveforms used for the echo-free analysis. It is intended that measurements with greater time resolution will be made in the future to improve the performance of the extended model further for measurements of this transducer.

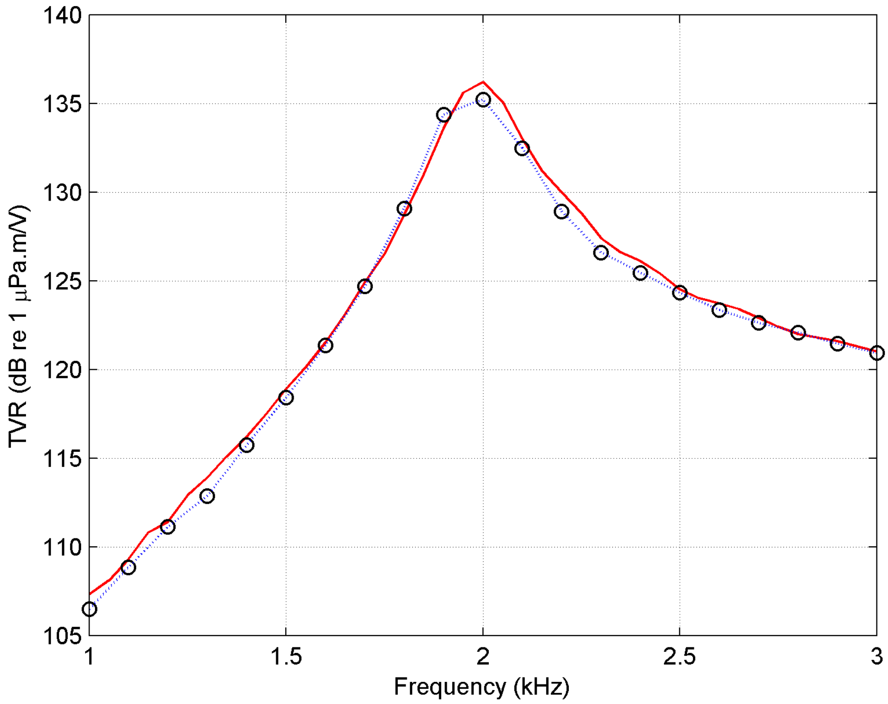

Figure 7.10 Results for TVR for the 2 kHz transducer showing the free-field response determined at the NPL Wraysbury facility (red curve), and the results of the extended signal modelling method (circles and dotted line) including the first three reflections.

8. TRACEABILITY OF OPEN-WATER CALIBRATIONS AT WRAYSBURY

8.1 INTRODUCTION

The NPL open-water underwater acoustic calibration facility is situated on a reservoir at Wraysbury, Middlesex. The temperature of the reservoir water varies according to the time of year, the temperature ranging from around 5 °C in winter up to around 20 °C in the summer months. Since the sensitivities of the reference transducers used at the facility can vary significantly over this temperature range, they have to be re-calibrated up to four times a year when the water temperature reaches pre-determined values. The calibration method used is three-transducer spherical-wave reciprocity, and since there are twelve reference transducers (three of each type to cover four frequency ranges), this is a time-consuming exercise. When a reference transducer is used to calibrate a device under test, the reference sensitivity values from the calibration at the temperature closest to the ambient water temperature are used and an appropriate value for any temperature drift included in the uncertainty budget; no temperature corrections are applied to the reference transducer sensitivity values. The traceability of the calibrations performed at the facility could be improved, and the number of three-transducer spherical-wave reciprocity calibrations required could be reduced, by characterising the reference transducers for their variation with temperature and applying appropriate corrections to the sensitivities.

8.2 REFERENCE TRANSDUCERS

To cover the 1 kHz to 350 kHz frequency range at the Wraysbury facility (the range accredited to ISO17025), four types of reference transducers are used. These are identified by their nominal frequency of resonance. The 8 kHz transducer used for the lower end of the frequency range up to 20 kHz is a seven element vertical stave, each element being 90 mm in diameter. The use of an array gives some directionality in the vertical plane, even down to 1 kHz, helping to reduce the effect of any reflections from the surface or bottom of the reservoir which may be present. The remaining three are: the 50 kHz transducer covering the range 18 kHz to 85 kHz, the 150 kHz transducer covering the range 70 kHz to 220 kHz and the 300 kHz transducer covering the range 200 kHz to 350 kHz. These three higher frequency devices all have a similar construction, appearing externally identical, and consist of a circular phosphor bronze casing, containing a matrix of ammonium dihydrogen phosphate (ADP) crystals on a pressure release backing, which is oil-filled and has a rubber window. The differing frequency responses of the three higher frequency transducers (Figures 8.4, 8.6 and 8.9) are obtained by varying the length of the ADP crystals.

These reference transducers can be seen in the photographs in Figure 8.1. All four transducers are mounted on a single bracket bolted to a hoist station, which in normal use remains lowered to a depth of around 5 metres. This hoist station is shown tilted up out of the water to allow the transducers to be removed for calibration and maintenance. The seven element 8 kHz array can be seen mounted to the bottom of the bracket with the remaining three transducers above in ascending frequency order. This arrangement allows low frequency measurements, where surface reflections are more likely to be a problem, to be performed at a greater depth.

From previous calibrations carried out at various times of the year, an indication of the temperature characteristics of the reference transducers can be obtained. Figure 8.3 shows the difference in sensitivity of an 8 kHz transducer at a range of temperatures when compared to the mean of those calibrations. This device exhibits good temperature stability with a sensitivity variation of less than 0.4 dB for a change of 8 °C over the majority of the frequency range. Similar data is shown for a 50 kHz transducer in Figure 8.5, but this time the response variation is much more changeable with frequency. Below 50 kHz the sensitivity decreases with increasing temperature, up to a maximum of over 2 dB for a 10 °C change, whereas between 50 kHz and 58 kHz the sensitivity increases with increasing temperature. It can be seen that the temperature coefficient changes sign twice more as the frequency increases further. At the frequencies where this occurs the sensitivity of the device will show negligible change with temperature.

Figure 8.1 Wraysbury reference transducers

Figures 8.7 and 8.8 show the temperature variation of two different 150 kHz transducers, and it can be seen that, while their temperature characteristics are similar around the resonant frequency, serial number 1219 exhibits a much greater variation around 70 kHz and 105 kHz. The temperature variation of a 300 kHz transducer is shown in Figure 8.10 and, like the 50 kHz transducer, the temperature coefficient changes sign as the frequency changes. A change in temperature will typically cause a change in the resonant frequency of a transducer, and so the maximum variation in sensitivity with temperature would be expected to occur around the frequency of resonance. By comparing the graphs of frequency response with the temperature variations, it can be seen that this is generally the case, although the 50 kHz transducer also shows large variations at the lower and upper ends of its frequency range.

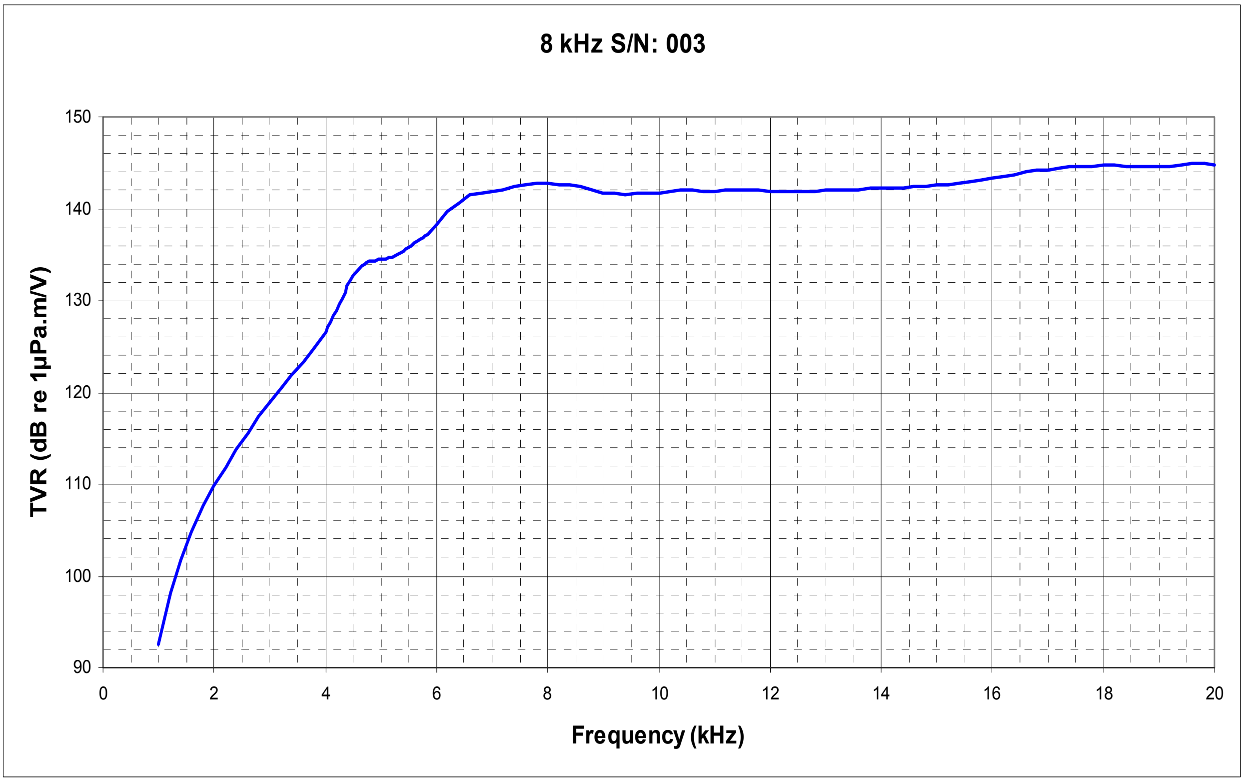

Figure 8.2 Typical frequency response of an 8 kHz reference transducer

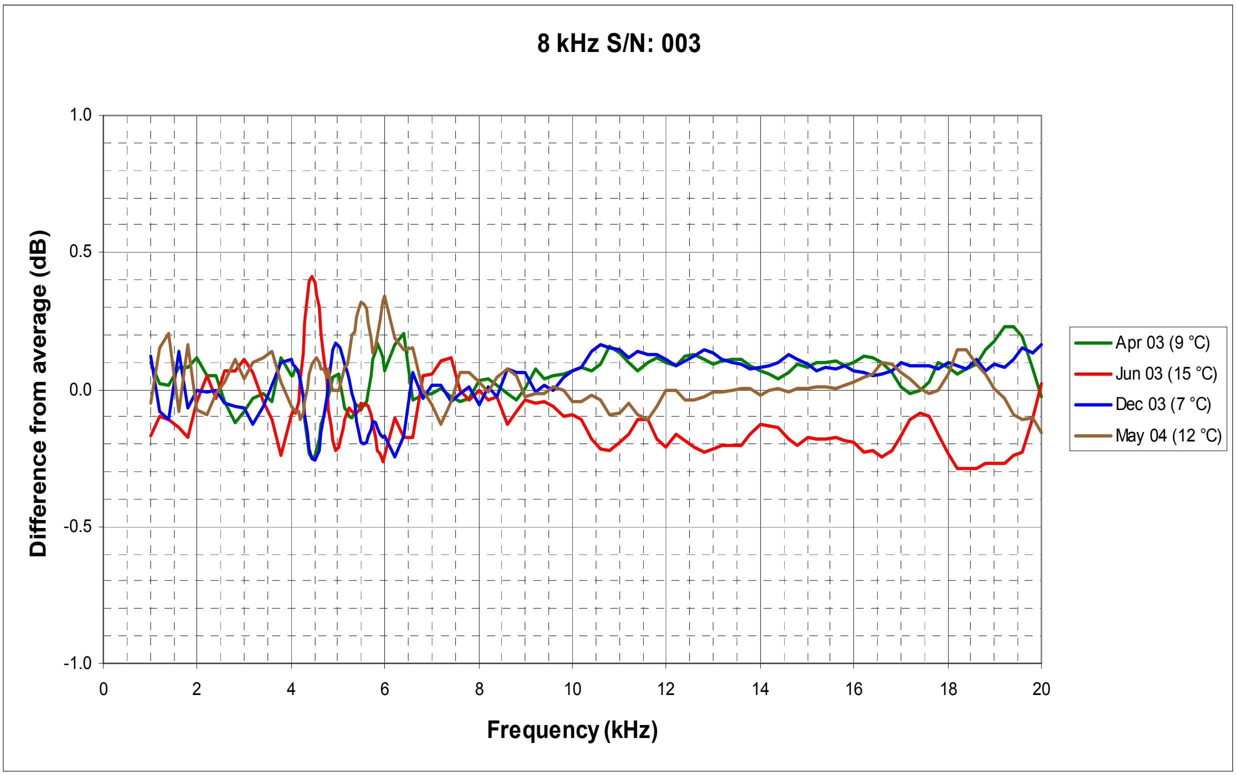

Figure 8.3 Temperature characteristics of an 8 kHz reference transducer

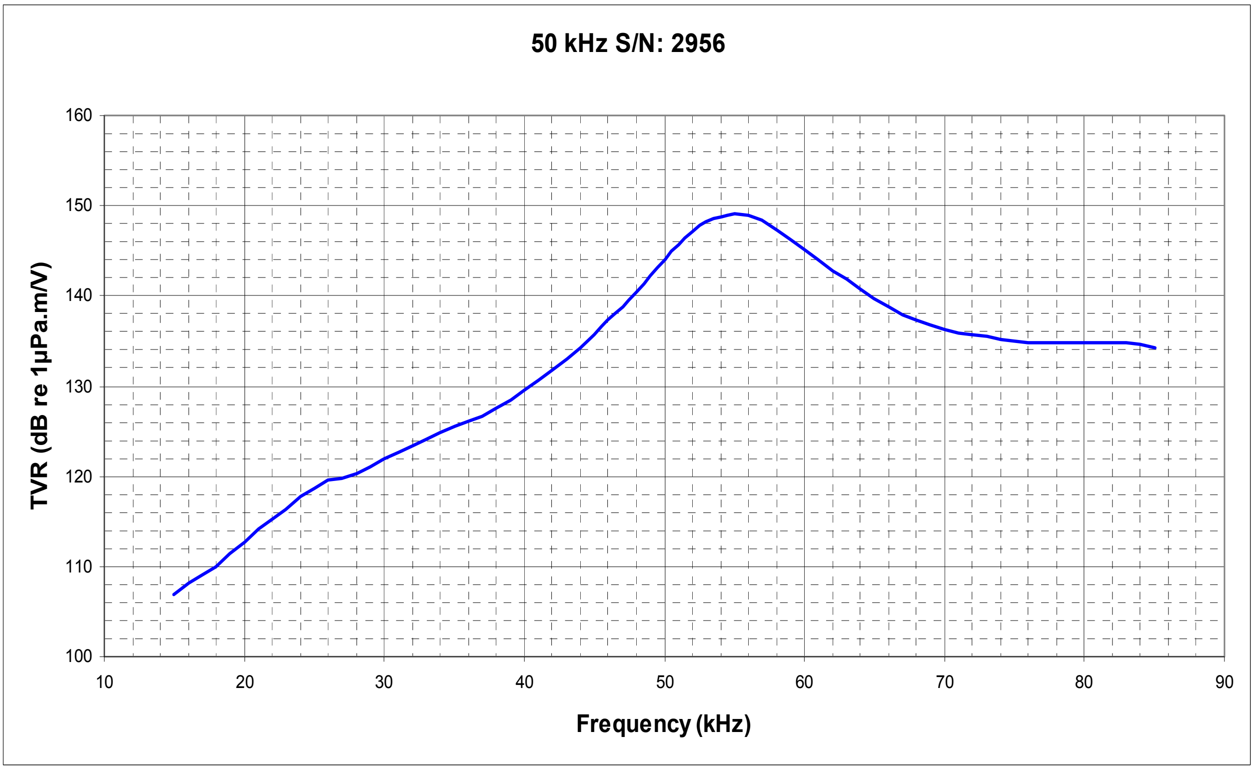

Figure 8.4 Typical frequency response of a 50 kHz reference transducer

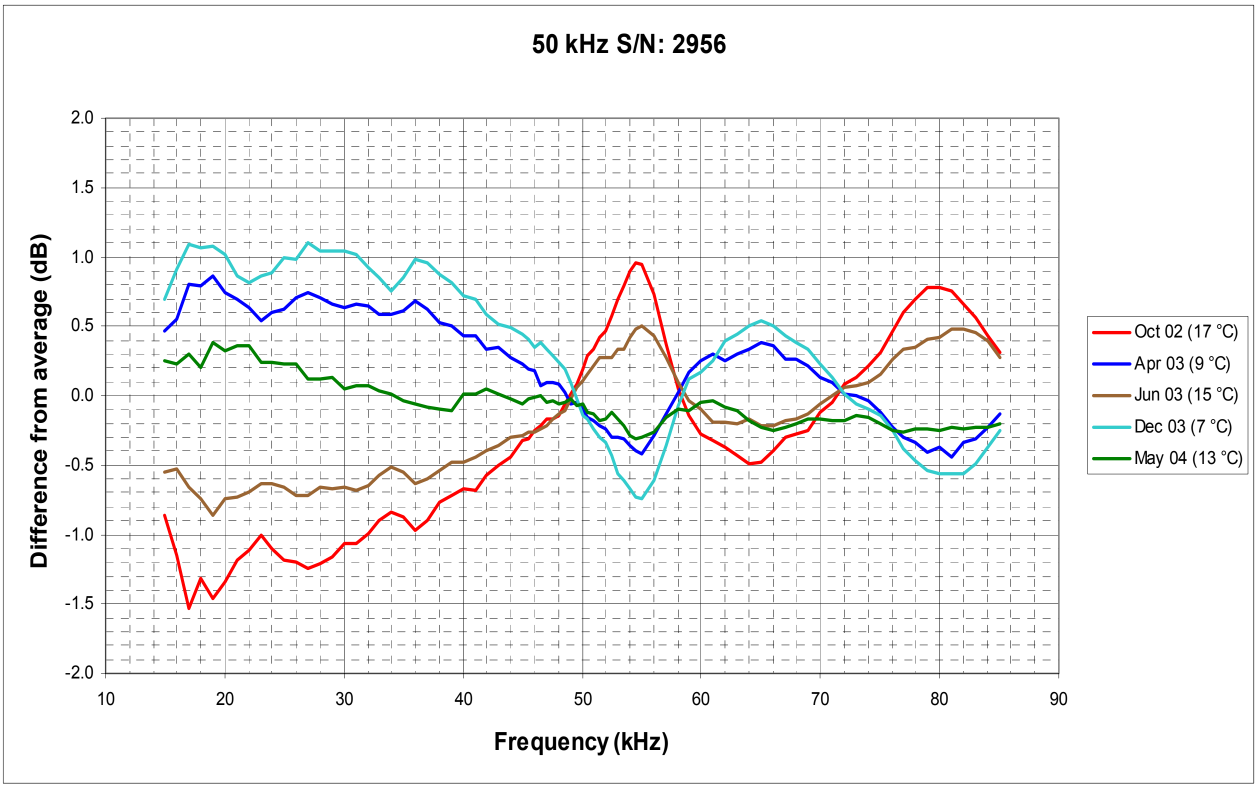

Figure 8.5 Temperature characteristics of a 50 kHz reference transducer

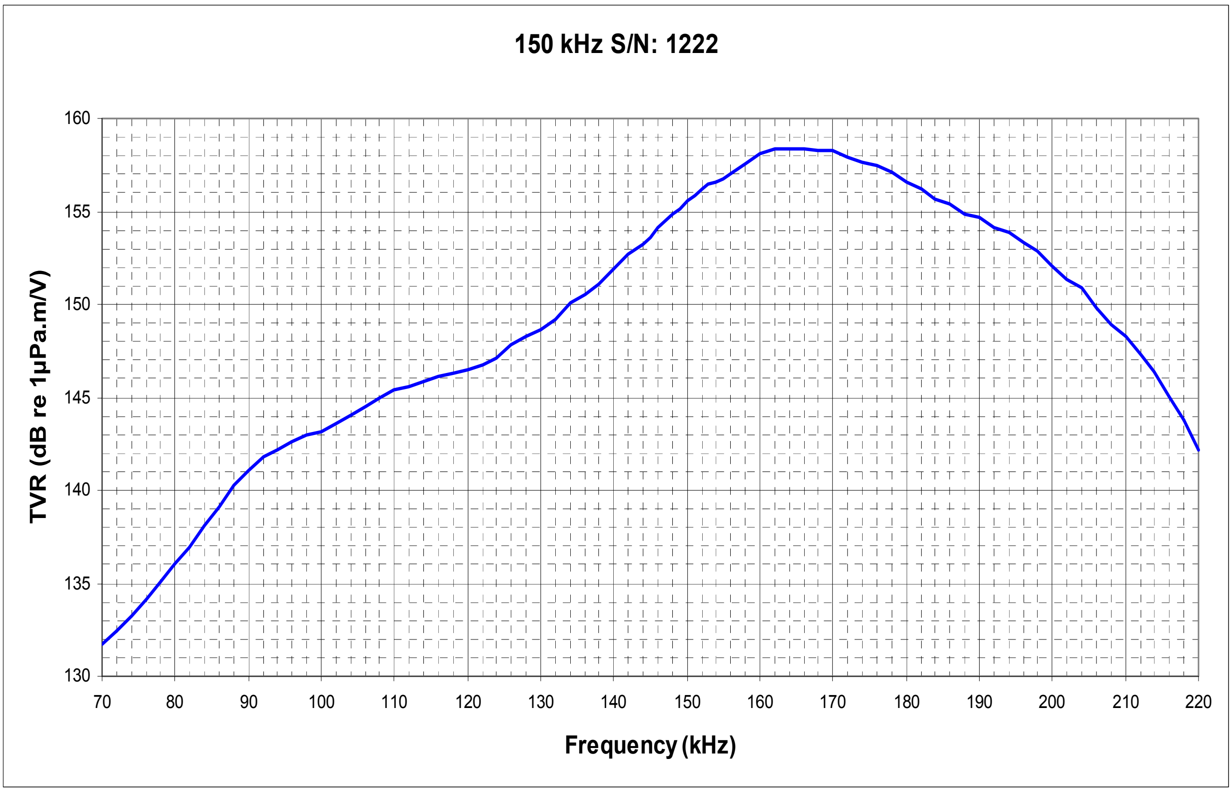

Figure 8.6 Typical frequency response of a 150 kHz reference transducer

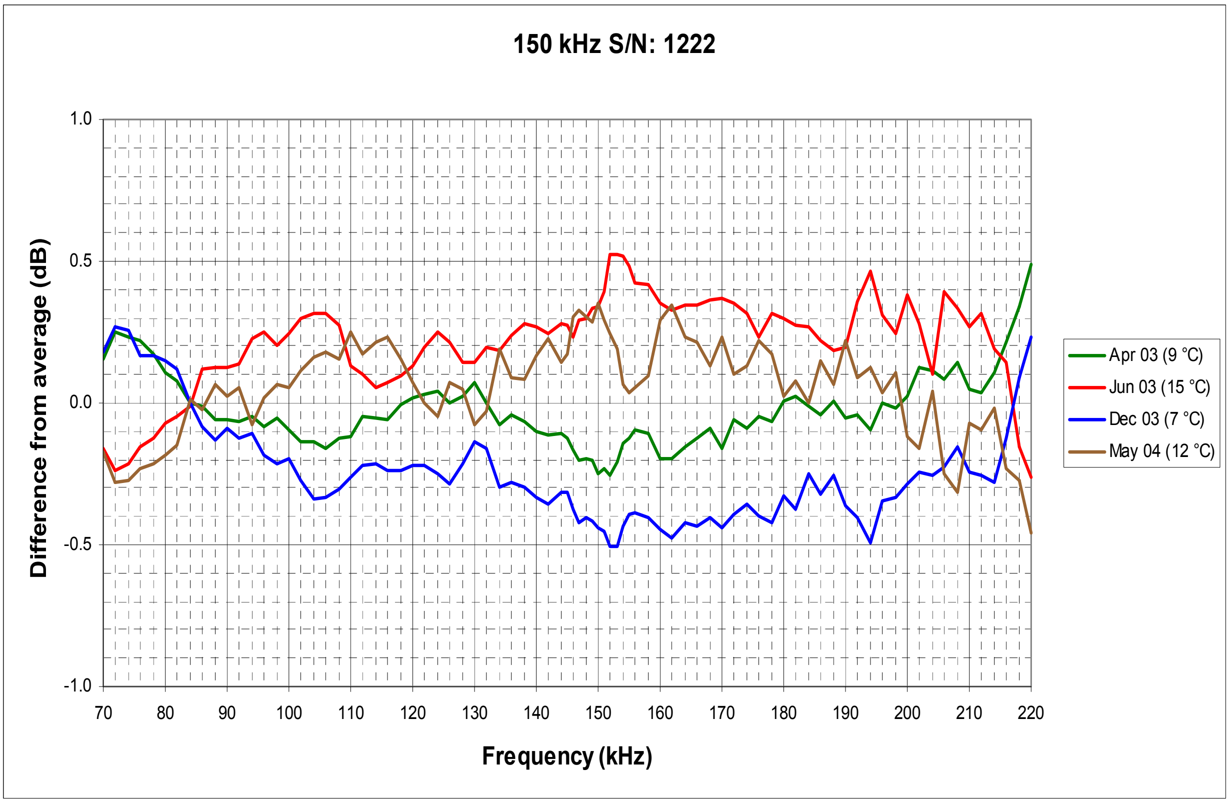

Figure 8.7 Temperature characteristics of a 150 kHz reference transducer

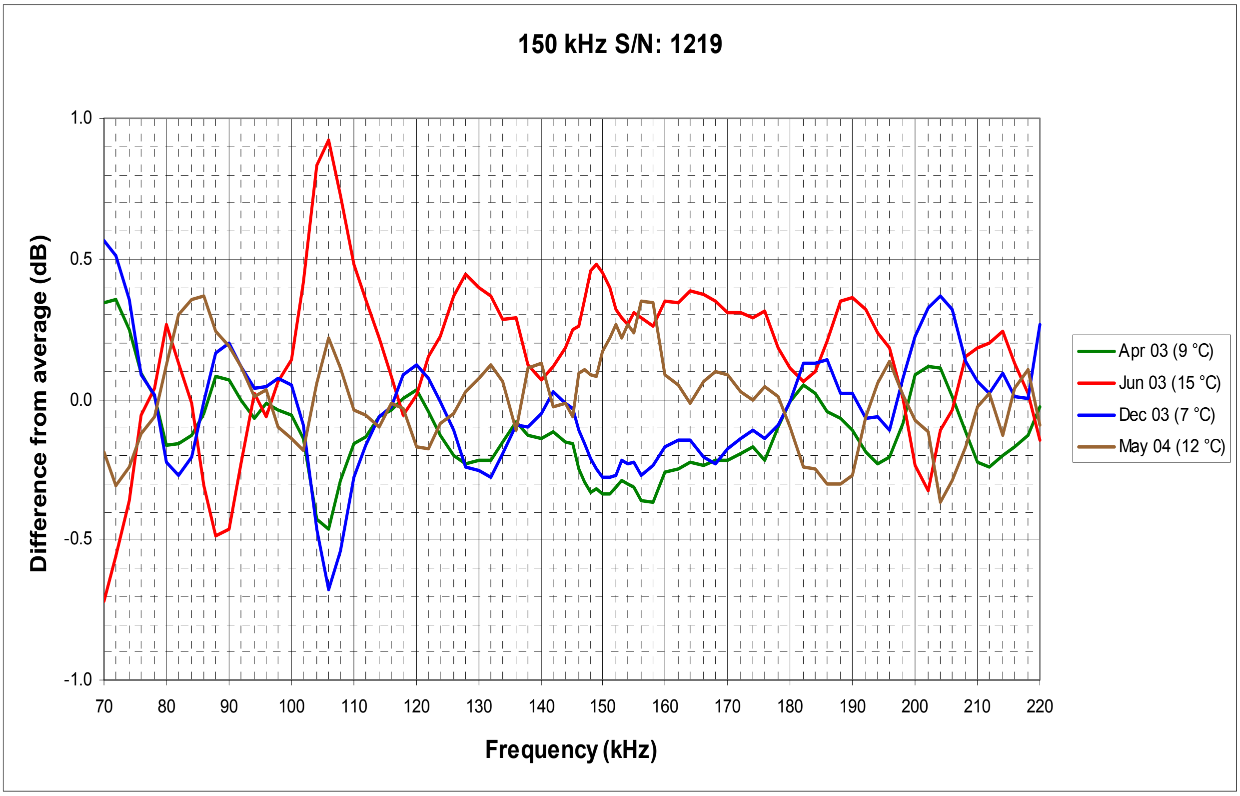

Figure 8.8 Temperature characteristics of a second 150 kHz reference transducer

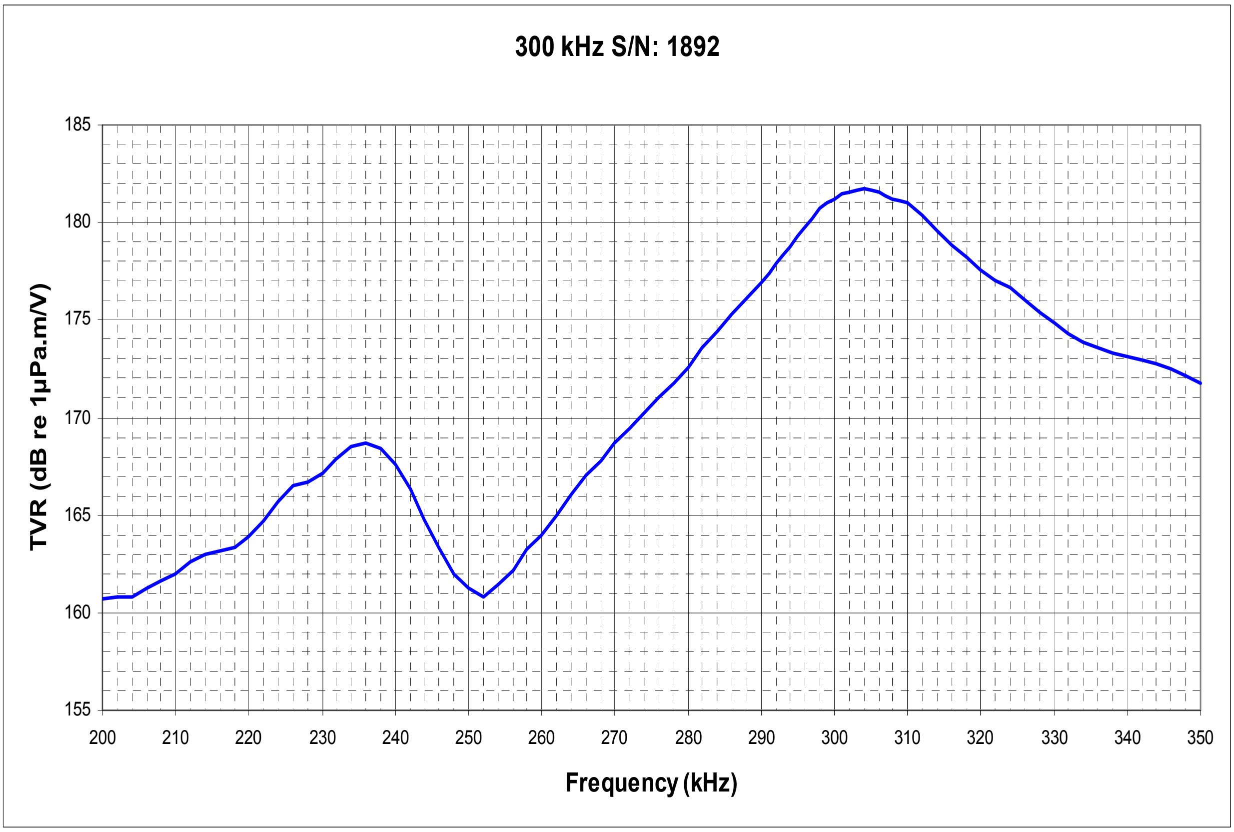

Figure 8.9 Typical frequency response of a 300 kHz reference transducer

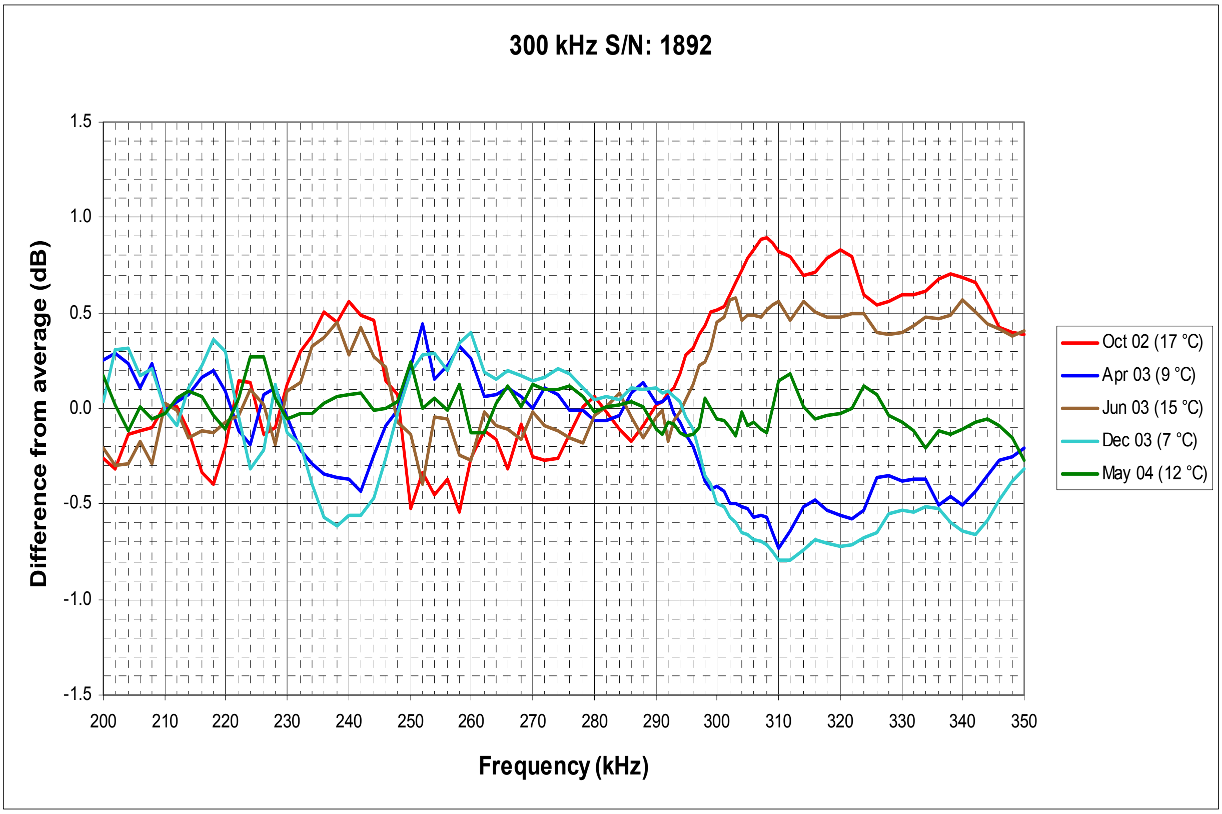

Figure 8.10 Temperature characteristics of a 300 kHz reference transducer

8.3 METHODOLOGY TO IMPROVE TRACEABILITY

As can be seen from Figures 8.7 and 8.8 above, reference transducers of the same type can exhibit significantly different temperature characteristics, and so each of the twelve reference transducers needs to be characterised individually. Normally, the temperature characteristics of a transducer can be measured directly by performing calibrations on the device in the NPL Acoustic Pressure Vessel (APV) at various temperatures, but in the case of all but the 50 kHz Wraysbury reference transducers this is not possible due to their size; the 8 kHz, 150 kHz and 300 kHz all have dimensions and frequency ranges such that the transducer separation required to perform calibrations in the far-field is significantly greater than the maximum 2.5 metres available in the APV.

One solution is to measure the temperature characteristics of the reference transducers *in situ* by using a reference hydrophone which has been previously characterised for its response with temperature in the APV. Calibrations using this hydrophone can be performed on each of the reference transducers as the temperature of the reservoir changes throughout the year, and from these the temperature characteristics of each device can be obtained. A file of temperature coefficients for each reference transducer can then be created enabling corrections to be applied to the reference sensitivities by the measurement software when using the reference transducers to calibrate an unknown device. An absolute calibration of the reference transducers by three-transducer spherical-wave reciprocity would then only need to be performed once a year.

8.4 REFERENCE HYDROPHONE CHARACTERISATION

The reference hydrophone used to perform the temperature characterisation is a Reson TC4014, a broad-band spherical hydrophone with a built-in 26 dB preamplifier. This hydrophone was chosen because, having a usable frequency range of 15 Hz - 480 kHz, it can be used to cover the entire 1 kHz – 350 kHz range of the four types of reference transducers, and also the built-in preamplifier provides signal conditioning for transmission over the long cables required at the Wraysbury facility. From the frequency response graph shown in Figure 8.11, it can be seen that the TC4014 hydrophone shows relatively little variation in sensitivity over this range of frequencies.

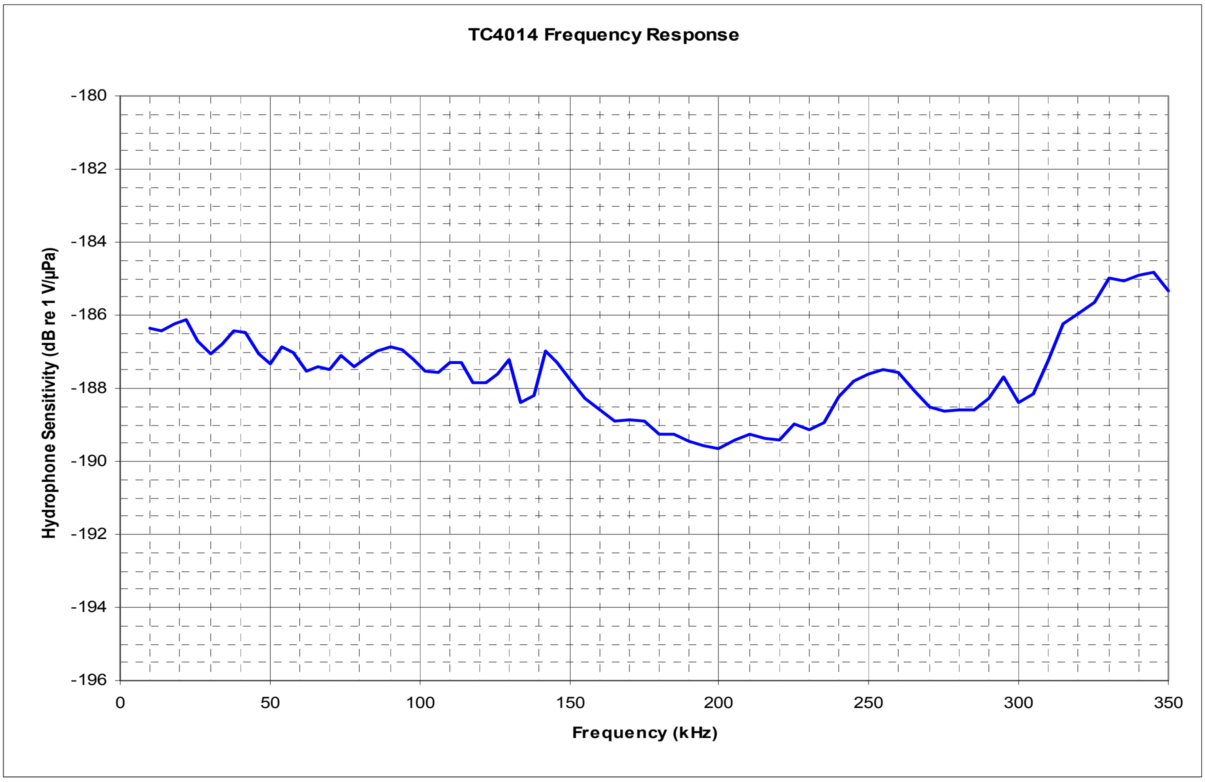

Figure 8.11: Typical frequency response of Reson TC4014 hydrophone

The Reson TC4014 was calibrated in the APV at temperatures of 5, 9, 13, 17 and 21 °C and from these measurements the temperature coefficient of the device was determined by calculating a least squares straight line fit for the data at each frequency. From the graph of these temperature coefficients in Figure 8.12 it can be seen that this hydrophone shows very good temperature stability over a wide range of frequencies.

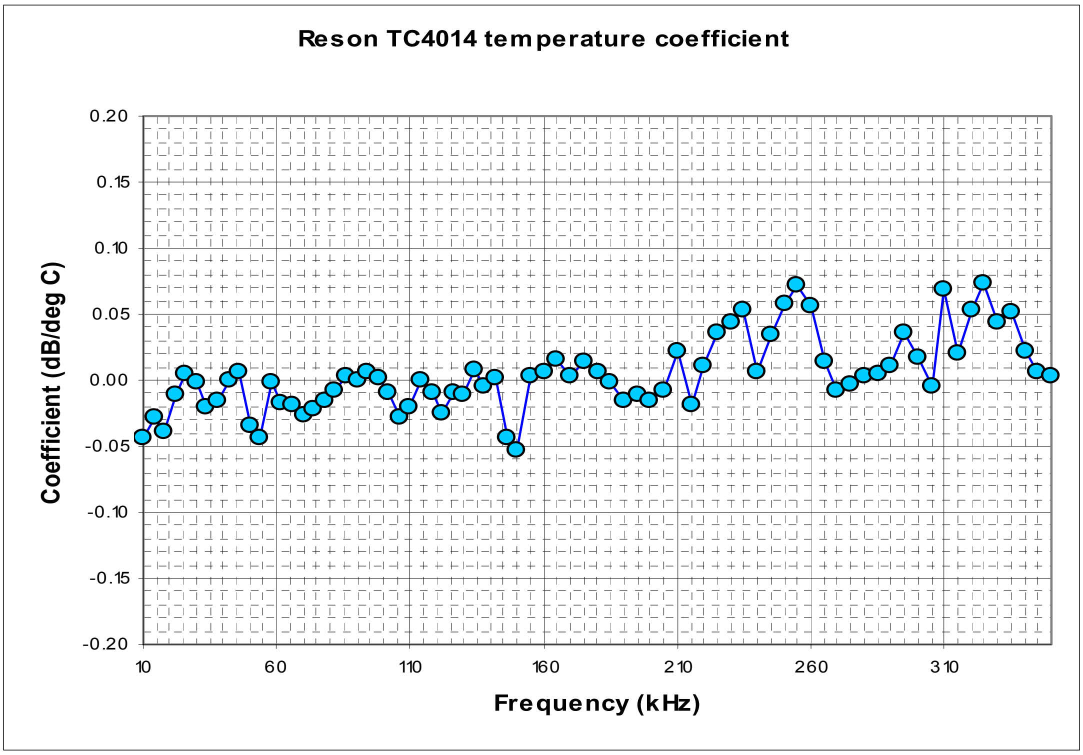

Figure 8.12: Temperature coefficients of Reson TC4014 hydrophone

The above results were obtained using the Calibrated Projector method described in Section 5. The minimum total uncertainty for this method is 0.9 dB for the frequency range 3 kHz – 200 kHz and 1.0 dB for frequencies outside this range. To reduce the uncertainties when the Reson TC4014 is used to calibrate the Wraysbury reference transducers, an absolute calibration of the hydrophone by three-transducer spherical-wave reciprocity was performed using the NPL Open Tank facilities. The minimum total uncertainty for this calibration is 0.5 dB for frequencies of 2 kHz and above and 0.7 dB for frequencies below 2 kHz.

8.5 LOW FREQUENCY CALIBRATIONS

The low frequency limit for free-field measurements when transmitting a tone burst signal from one device to another is determined by the ability to make a measurement on the steady-state portion of the direct signal before it is corrupted by reflections from boundaries. Currently, the low frequency limit for free-field calibrations at the Wraysbury open-water facility is 1 kHz. This limit could be extended downwards by increasing the distance between the devices and any boundaries, thereby allowing more time for the measurement to be made before the reflections arrive at the receiving device, and/or reducing the time required to make the measurement.

The mounting arrangements at the site enable devices to be deployed at depths of between 5 metres and 6.5 metres, depending on the size and weight of the device. With a typical water depth of 20 metres in the reservoir, the optimum depth to deploy devices to avoid reflections from the water surface or reservoir bottom would be 10 metres. This could potentially be achieved by the use of a telescopic extension to the existing hoist stations.

The signal from the receiving device is measured using an Agilent 89410A Vector Signal Analyser. The on-board FFT is used to measure the amplitude of the gated steady-state portion of the tone burst, but this requires a minimum of four cycles of the signal to achieve an accurate measurement. Although the same instrument is used in the underwater acoustic facilities at the NPL Teddington site, the time waveform is transferred from the analyser to the measurement PC for processing. This allows more flexibility in the signal analysis. The analysis software used for the NPL open tanks allows the choice of a number of analysis options, two of which enable accurate measurements to be made on as little as one cycle of the signal. One method performs a discrete Fourier transform on an integer number of cycles of the signal, calculating only the amplitude of the spectral component at the acoustic frequency. The other performs a fit of a sinusoidal waveform using a least-squares estimation in which the frequency of the sinusoidal wave is constrained to be the acoustic frequency and the amplitude of the fitted sine wave provides the measurement of the signal amplitude. Of course, both of these methods assume that the signal to be analysed has reached steady-state conditions.

By deploying devices at greater depth and employing the signal processing methods described above, it is estimated that it would be possible to perform free-field calibrations at frequencies down to around 250 Hz. As the output of the 8 kHz transducer falls off sharply below 1 kHz, a new low frequency source capable of operating down to 250 Hz would be required. However, the use of a comparison calibration method would mean that this would not need to be a calibrated device, as the sensitivity of the hydrophone under test would be compared to that of a previously calibrated reference hydrophone. It is intended that the reference hydrophone used would be calibrated at low frequencies using the NPL coupler primary standard [27], thereby achieving traceability for the low frequency calibrations at the Wraysbury facility. As the range of hydrophones which can be calibrated directly in the coupler is limited by its size, the provision of low frequency free-field calibrations at the Wraysbury facility would provide a future dissemination route for the NPL coupler primary standard.

9. CONCLUSIONS

9.1 SUMMARY

Standards for underwater acoustics at simulated ocean conditions have now been provided in the UK by NPL using the Acoustic Pressure Vessel since July 2000 enabling acoustic measurements to be made at hydrostatic pressures of up to just under 7 MPa (simulating depths of approximately 700 metres) and in the temperature range of 2 ºC to 35 ºC. The report has detailed the limitations of the facility that were present at the start of the 2001-2004 NMS Acoustic Metrology Programme along with how certain of the limitations were addressed.

Extensive improvement to the mechanical handling capabilities for acoustic devices and artefacts within the test chamber has been implemented. In particular, improvements have been made beneath the large lid where the addition of a better mounting capability was made possible by the introduction of the dual hydrophone mount. This has in-turn significantly reduced set-up time before and during measurement routines. The additional functionality of being able to acoustically align transducers in the vertical axis with the aid of the recently commissioned vertical height adjuster is another major improvement to the test chambers hardware. Improved reliability and functionality of the large lid rotator will be a significant enhancement to the existing rotation feature when it is installed shortly.

The ability to conduct electrical impedance measurement using a tone-burst method allows for measurement to be made on low frequency, omni directional devices without interference due to reflections from the APV walls. The speed at which reciprocity calibrations can be conducted in the APV has been increased by approximately a factor of two with implementation of the dual hydrophone mount and amendments being made to the existing measurement software, even if it is still necessary to manually rotate devices during the measurement cycle.

The implementation of relative calibration methods that require the use of a calibrated projector or hydrophone allow calibrations to be performed at a rate of between two and five times faster than is possible with absolute methods, depending on the exact method chosen and the number of frequency points. The accuracy of the relative calibration methods are not as good as for an absolute method, but is particularly useful to maximise the volume of measurements when calibrations are to take place over a range of different environmental conditions as a significant amount of time can be saved.

Work to determine the acoustic properties of the APV has given us the knowledge to make the best use of the APV for conducting free-field measurements within the test chamber. Through this work it has been found that it is possible to conduct measurements in a low-noise environment in the APV. The performance of the acoustic absorbers inside the APV was investigated experimentally and they were found to be most effective at 40 kHz and 80 kHz.

The use of the signal modelling method has been demonstrated for extending the usable frequency range of the APV down in frequency for calibration of high-Q projectors at frequencies of a few kilohertz.

The limitations of the traceability in dissemination of standards via the Wraysbury open-water facility caused by seasonal variation in water temperature have been described. The reference projectors traditionally used at Wraysbury have sensitivities which are dependent on temperature. Improved methods of maintaining traceability over a range of temperatures have been described. The limitations on disseminating standards at frequencies less than 1 kHz have also been described along with potential solutions to allow extension of the frequency range downwards.

9.2 RECOMMENDATIONS

There are a number of areas where further work would be of benefit for the APV:

- Integration of the control and functionality of the vertical height adjuster in the suite of acoustic measurement software - this would allow automatic maximisation of acoustic signal and also allow for scanning to take place in the vertical axis of devices that are attached to the large lid mounting flange.
- Implementation of bulkhead connections that interface with specific NPL reference devices would be of benefit to eliminate the deterioration of the transducer cables that are subjected to the repeated compression gland pressures.
- The capability of scanning a transducer along axes orthogonal to the main tank axis would be an enhancement that would enable near-field measurement techniques to be employed within the test chamber, and would also be valuable when conducting panel measurements.
- The ability to rotate transducers that are attached to the dual hydrophone mount without the need to remove either lid would decrease further the amount of setting-up required during common measurement routines. This would ideally be possible while the test chamber is in a pressurised state there by eliminating the need to de-pressurise during measurement cycles.
- The ability to undertake calibrations at frequencies less than 1 kHz would be a significant extension to the capability. At such frequencies, techniques such as comparison calibrations of hydrophones in a reverberant field, and novel techniques such as the signal modelling methods described in Section 7, offer the opportunity to extend the free-field measurements beyond the free-field limit of the APV.

To improve the traceability of the calibrations undertaken at Wraysbury, the following would be of benefit:

- Improved traceability over a range of water temperatures by use of a stable reference hydrophone calibrated using the free-field primary standard reciprocity method in the open-tank facilities and characterised over the full range of temperatures using the APV.
- Traceability to the primary standard of coupler reciprocity for frequencies less than 1 kHz, using a stable hydrophone calibrated in using the coupler facility over the full range of temperatures.
- Improved dissemination of standards at frequencies less than 1 kHz by use of comparison methods using the reference hydrophone calibrated in the primary coupler

(requiring improved mounting capability at Wraysbury to allow use of greater depths during calibration).

10. ACKNOWLEDGEMENTS

The authors would like to acknowledge the support of the of the National Measurement System Directorate of the UK Department of Trade and Industry which funded this work as part of the 2001-2004 Acoustical Metrology Programme.

The authors would like to thank Professor Victor Humphrey of the Institute of Sound and Vibration Research, University of Southampton, for his assistance with the measurement of the reverberation time of the APV.

The authors would also like to thank Mr Keith Mayne of Ultra Electronics Ltd for the loan of the two flexural disc transducers calibrated in the work described in Section 7, and to Dr Peter M. Harris of NPL (Mathematics and Scientific Computing Group) Division of Enabling Metrology for assistance with the signal modelling work in the same section.

The authors would like to thank the staff of the Engineering Services Group at NPL for invaluable help with the design and manufacture of the hardware for improved transducer positioning in the APV.

11. REFERENCES

1 BOBBER, R.J. *Underwater Electroacoustic Measurements.* USA, Peninsula Press, (2nd edition), 1989.

2 WEYDERT, M. CEC efforts to improve acoustic calibration underwater. *Proceedings of the first European Conference on Underwater Acoustics*, Luxembourg , 1992, 49-51, ed M. Weydert, Pub. No. EUR 14453 EN, Commission of the European Communities, Luxembourg, 1992, pub. Elsevier Applied Science.

3 GOODIER, I. W. Quality assurance of underwater acoustic measurements. *Proceedings of the first European Conference on Underwater Acoustics*, Luxembourg, 1992, 57-59, ed M. Weydert, Pub. No. EUR 14453 EN, Commission of the European Communities, Luxembourg, 1992, pub. Elsevier Applied Science.

4 ROBINSON, S. P. and PRESTON, R. C. A survey of European calibration facilities for underwater acoustics. *NPL Report RSA(EXT)32*, April 1992, NPL, UK.

5 ROBINSON, S. P. and PRESTON, R. C. A survey of European calibration facilities for underwater acoustics – EUROMET project A73. *Proceedings of the first European Conference on Underwater Acoustics*, Luxembourg, 1992, 45-48, ed M. Weydert, pub. Elsevier Applied Science.

6 PRESTON, R.C. and ROBINSON, S. P. Towards new UK underwater acoustical measurement standards in the 21st century. *J. Acoust. Soc. Am.*, **103**, 2754, May 1998.

7 PRESTON, R.C. and ROBINSON, S.P. Progress towards UK underwater acoustical measurement standards for the 21st century. *Proceedings of the sixth International Congress on Sound and Vibration*, **2**, 797-804, ed. Finn Jacobsen, Technical University of Denmark, July 1999.

8 PRESTON, R.C. and ROBINSON, S. P. A new anechoic pressure vessel facility for the UK. *Proceedings of the IOA*, **20**, part 3, 73-78, 1998.

9 BEAMISS, G.A. HAYMAN, G and ROBINSON, S.P. The provision of standards for underwater acoustics at simulated ocean conditions by use of the NPL acoustic pressure vessel. NPL *Report CMAM 76,* National Physical Laboratory, UK, 2001.

10 CRAMER, W.S. Sound-absorbing linings for water-filled tanks. *Sound*, **2**, 18, 1963.

11 DARNER C. L. An anechoic tank for underwater sound measurements under high hydrostatic pressure. *J. Acoust. Soc. Am.*, 1954, **26**, 221.

12 T. J. Esward, V. F. Humphrey, L. C. Evans, G. A. Beamiss and G. Hayman, “Acoustic Characterisation of Panel Materials in Simulated Ocean Conditions using the NPL Acoustic Pressure Vessel”, Proc. ECUA2002, 665-670, 2002.

13 V. F. Humphrey, N. L. Carroll, J. D. Smith, G. A. Beamiss, G. Hayman, T. J. Esward and S. P. Robinson, “Acoustic characterisation of panel materials under simulated ocean conditions”, Proc. I.O.A., **25**, 2003.

14 IEC 60565: 1977. *The calibration of hydrophones.* International Electrotechnical Commission, Geneva.

15 ROBINSON, S.P. and DORÉ, G.R. Uncertainties in the calibration of hydrophone at NPL by the three-transducer spherical-wave reciprocity method in the frequency range 10 kHz to 500 kHz. NPL Report RSA(EXT)054, National Physical Laboratory, UK, 1994.

16 ROBINSON, S.P. PRESTON, R.C. and DORÉ, G.R. Measurement standards for underwater acoustics in the UK. *Proceedings of First European Conference on Underwater Acoustics,* Luxembourg, pages 52-56, Pub. No. EUR 14453 EN, Commission of the European Communities, Luxembourg, 1992.

17 USRD Transducer Catalog, USRD, NUWC, Newport RI, USA, 1982.

18 VAN BUREN, A. L., DRAKE, R. M. and PAOLERO, A. E. Temperature dependence of the sensitivity of hydrophone standards used in international comparisons. *Metrologia*, Vol. 36, pp 281-285, 1999.

19 BIPM, IEC, IFCC, ISO, IUPAC, IUPAC and OIML. *Guide to the Expression of Uncertainty in Measurement*. ISBN 92-67-10188-9, Second Edition, 1995.

20 ROBINSON, S. P. Review of methods for low frequency calibration in reverberant tanks: NPL Report CMAM 034, June 1999.

21 BS EN ISO 3382 – *Measurement of reverberation time of rooms*. British Standards Institute, Chiswick, London.

22 KINSLER, L.E., FREY, A.R., COPPENS, A.B., and SANDERS, J.V., *Fundamentals of acoustics, 1982,* Wiley (3rd edition), USA.

23 AINSLEIGH, P. L. and GEORGE, J. D. Signal modelling in reverberant environments with application to underwater electroacoustic transducer calibration. *J. Acoust. Soc. Am.*, **98**, 270-279, 1995.

24 ROBINSON, S.P. and HARRIS, P.M., Acoustic signal modelling and its application to the calibration of electroacoustic transducers in reverberant laboratory tanks, *Proceedings of the IOA*, **20**, part 3, 13-19, 1998.

25 ROBINSON, S.P. and HARRIS, P.M., Modelling acoustic signals in the calibration of electroacoustic transducers in reverberant laboratory tanks, *NPL CMAM Report 029*, March 1999.

26 ROBINSON, S.P. and HARRIS, P.M., Modelling acoustic signals containing reflections in the calibration of acoustic transducers in reverberant laboratory tanks, *NPL CMAM Report 052*, May 2000.

27 ESWARD, T.J., ABLITT, J., ROBINSON, S.P. and BEAMISS, G.A. Development of a primary standard for hydrophone calibrations in the frequency range from 20 Hz to 2 kHz based on the principle of coupler reciprocity. Proceedings of the Fifth European Conference on Underwater Acoustics (ECUA2000), Lyon, France, Volume II, 1417-1422, 2000.

APPENDIX 1. APV SPECIFICATION

Feature	Description
Frequency Range	1 kHz to 2 MHz
Free volume Provided by Acoustic Lining	1.9 m diameter and 4.1 m long
External Dimensions	2.5 m diameter and 7.6 m long
Access Ports	Two ports 2.4 m apart: one port having access diameter 0.84 m and the other 0.50 m
Measurement Distance	One fixed stage and two movable to give distance range 0.8 m to 2.5 m. Rotation of main shaft through 360 °.
Device Handling	Overhead crane with continuous fine control of speed, comprehensive safe support system for large lid during monitoring procedures, and a versatile lifting platform to aid device attachment
Maximum Weight	For devices under test 350 kg
Hydrostatic Pressure	20 kPa to 6895 kPa, normal rate of change variable from 35 kPa per minute to 1500 kPa per minute (5 psi to 220 psi per minute)
Temperature	2 °C to 35 °C
Environmental Noise	Lower than sea state zero
Cable Specification	Electrical lead-through to take cables from 5 mm to 20 mm diameter and integral connectors up to 38 mm diameter
Signal Power	Analogue Associates MA 5000VZ amplifier (5 kW, DC to 25 kHz); Brüel & Kjær 2713 100 W amplifier (DC to 1 MHz); ENI 240L 200 W amplifier (20 kHz to 10 MHz)
Device Mounting	Full information on the device/flange mounting arrangements is available on request

APPENDIX 2. REFERENCE TRANSDUCERS

A2.1 Acoustic pressure vessel reference devices

Transducers currently selected for reference devices for use in the APV facility are:

USRD H52	ITC 1001
USRD F30	ITC 1032
Reson TC 4034	ITC 1042
	ITC 1089

A2.2 Temperature and pressure coefficients

For each frequency, the data at the various temperatures was used to derive a coefficient of variation with temperature for that frequency by using linear least square fit, the coefficient being derived from the slope of the linear fit and expressed in dB/°C. The temperature coefficient was determined for a range of different hydrostatic pressures. These were then averaged to provide one value of the temperature coefficient at each frequency. The standard deviations of the values were also calculated (these are used to derive uncertainties on the coefficients). This procedure was then repeated for the data at the various hydrostatic pressures, with the pressure coefficient being derived at each of the various temperatures and averaged in the same way, providing a coefficient expressed in dB/MPa [9].

There are a number of potential problems that might be envisaged with the above approach. Use of a linear fit provides quite a crude estimate of the variation in response with temperature (or pressure). The response of some hydrophones has been seen to vary nonlinearly with temperature or pressure, but to characterise such a variation accurately requires more data points than available. However, the choice of a linear approximation does not introduce too great an inaccuracy if, as is the case for the examples here, the response generally varies monotonically with pressure or temperature and only by relatively small amounts over the range of interest. In any case, devices showing a strongly nonlinear variation with temperature or pressure are simply rejected for use as reference hydrophones for simulated ocean conditions.

Another potential problem is that there is an implicit assumption that the variations with temperature and pressure are independent (ie uncorrelated). Hence the pressure coefficients derived at separate temperatures have been averaged to provide one value (and vice versa). Similarly, uncertainties have been calculated assuming that the three values are three independent estimates of the same coefficient. This may not be a valid assumption and there may well be correlation between the pressure and temperature coefficients. However, since for the reference devices shown here the variations in response is relatively small, it is believed that the errors introduced by this assumption are not too great.

Examples of reference device coefficient plots along with the error bars equal to the standard deviations of the measurements are shown below for several devices covering an overall frequency range of 3 kHz to 500 kHz.

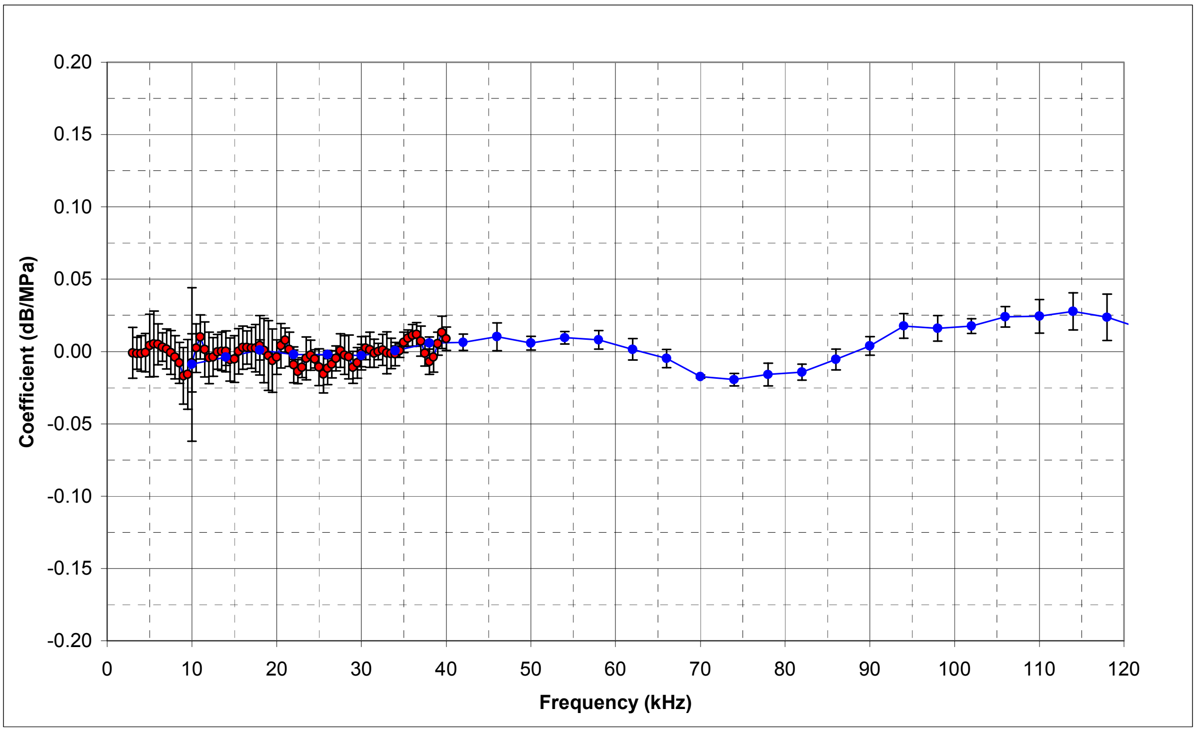

Figure A2.1 Coefficient of variation of hydrophone response with pressure for the H52.

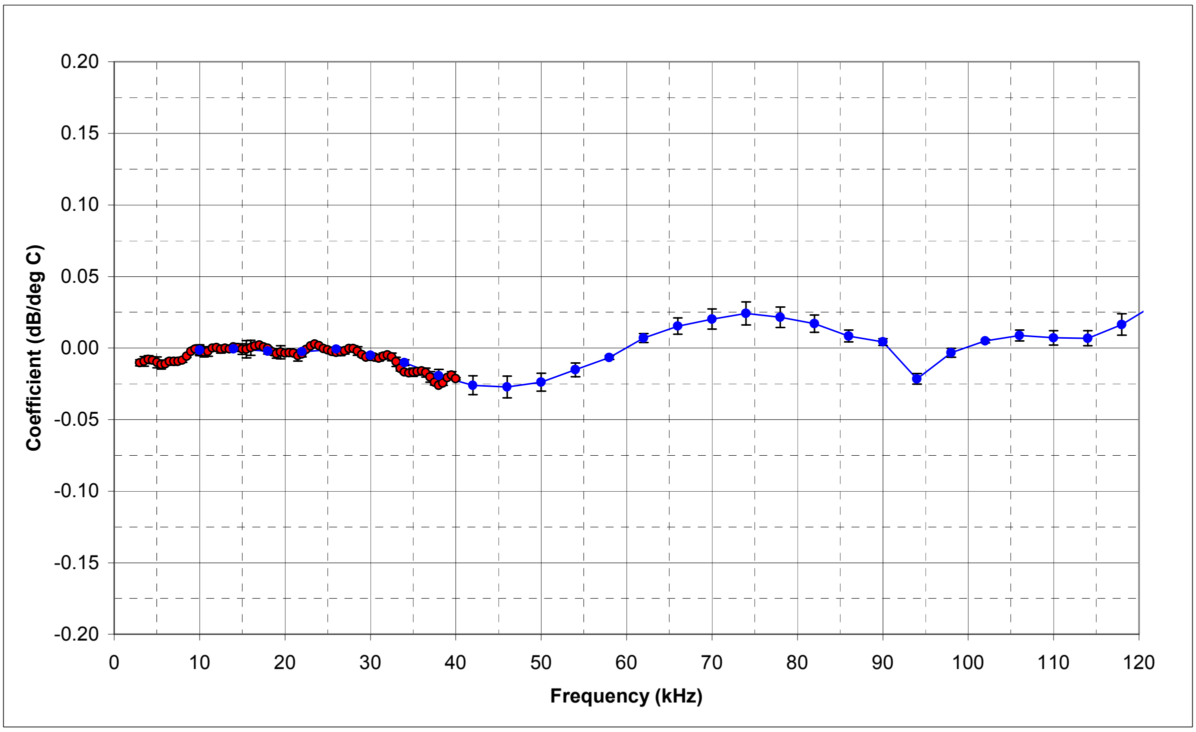

Figure A2.2 Coefficient of variation of hydrophone response with temperature for the H52.

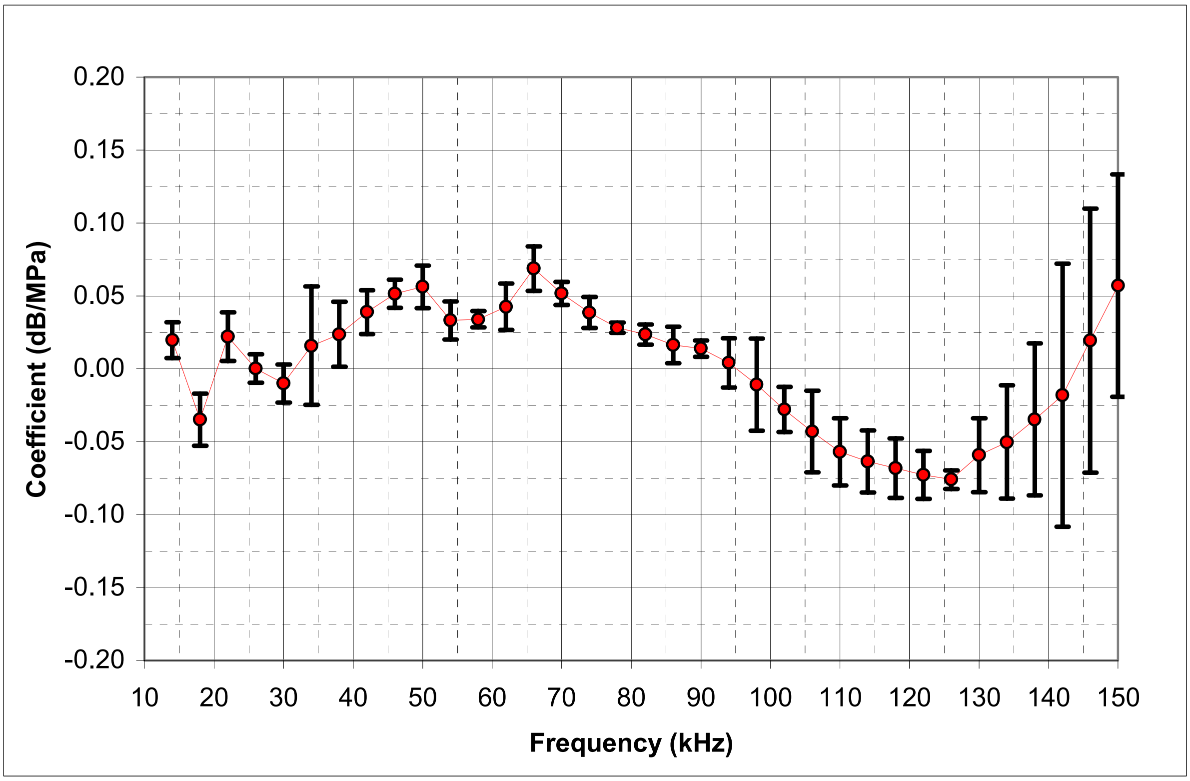

Figure A2.3 Coefficient of variation of hydrophone response with pressure for the F30.

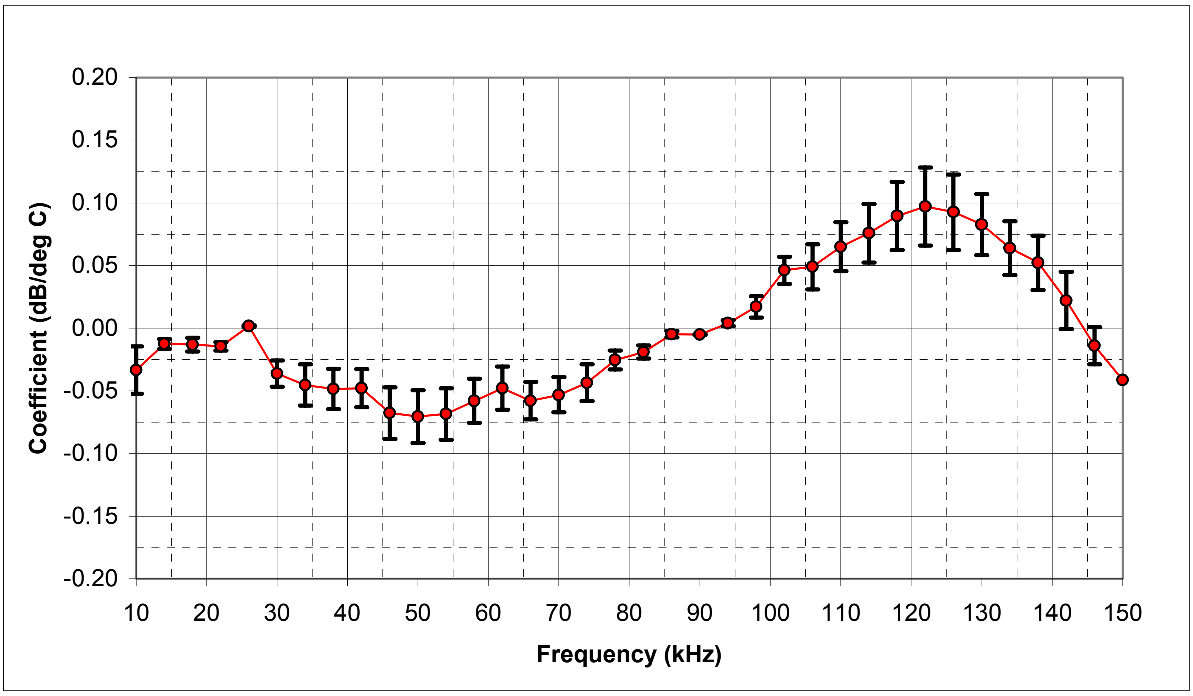

Figure A2.4 Coefficient of variation of hydrophone response with temperature for the F30.

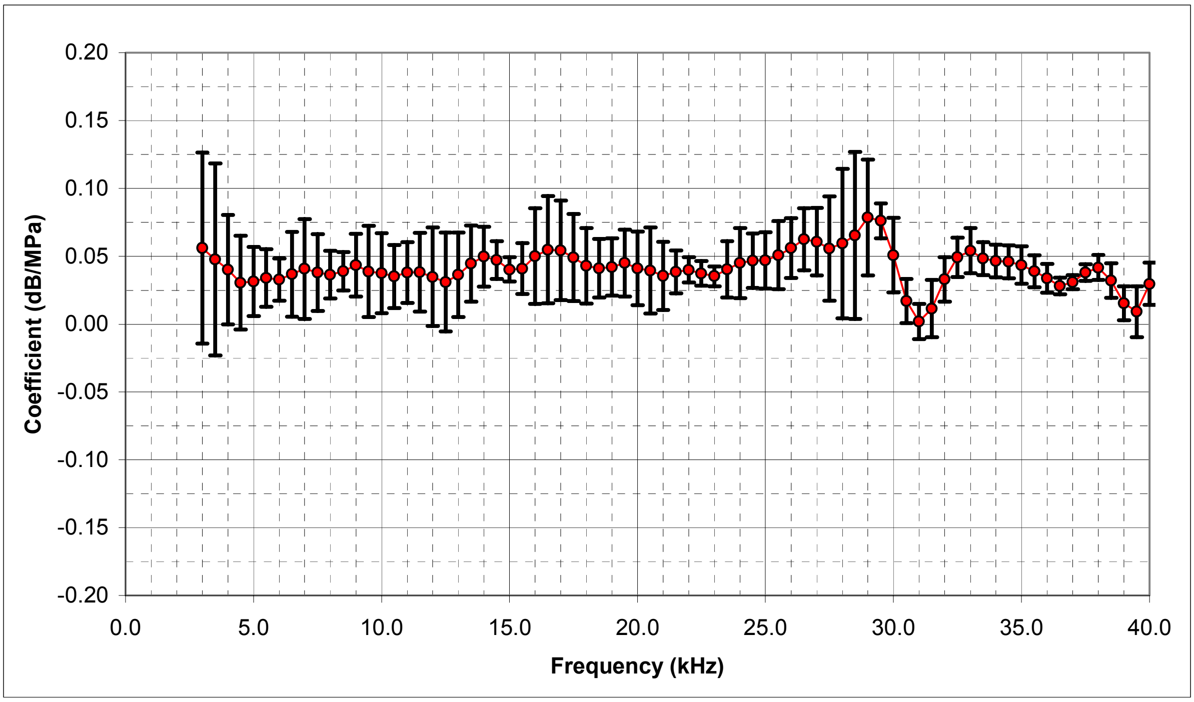

Figure A2.5 Coefficient of variation of hydrophone response with pressure for the ITC1001.

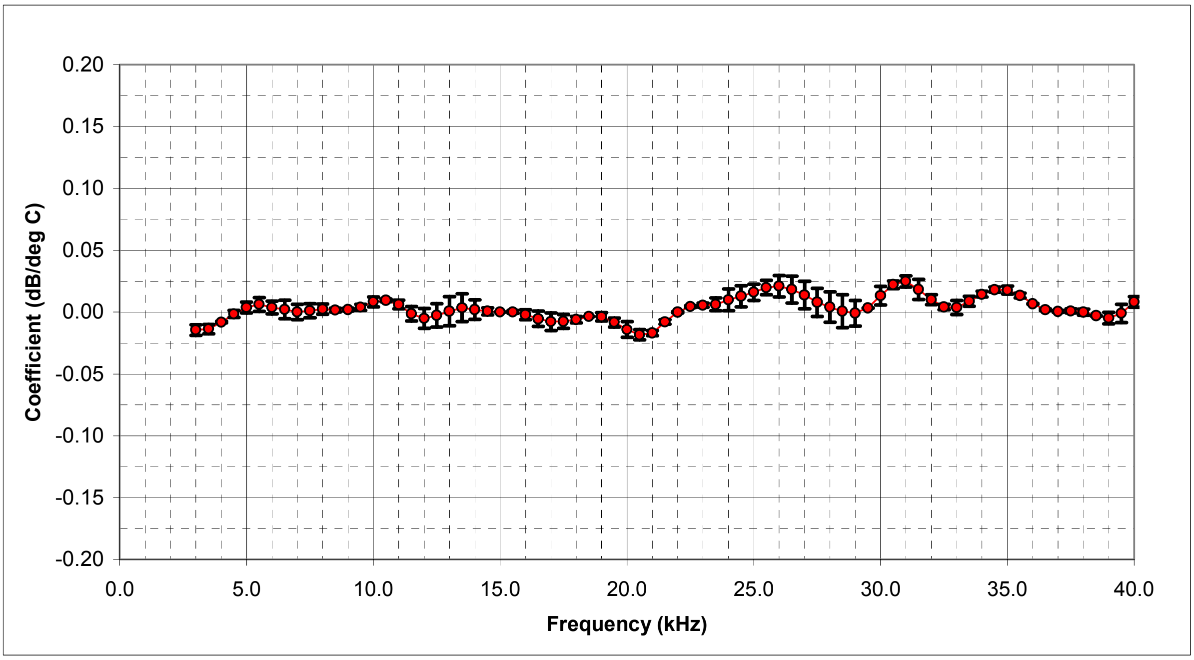

Figure A2.6 Coefficient of variation of hydrophone response with temperature for the ITC1001.

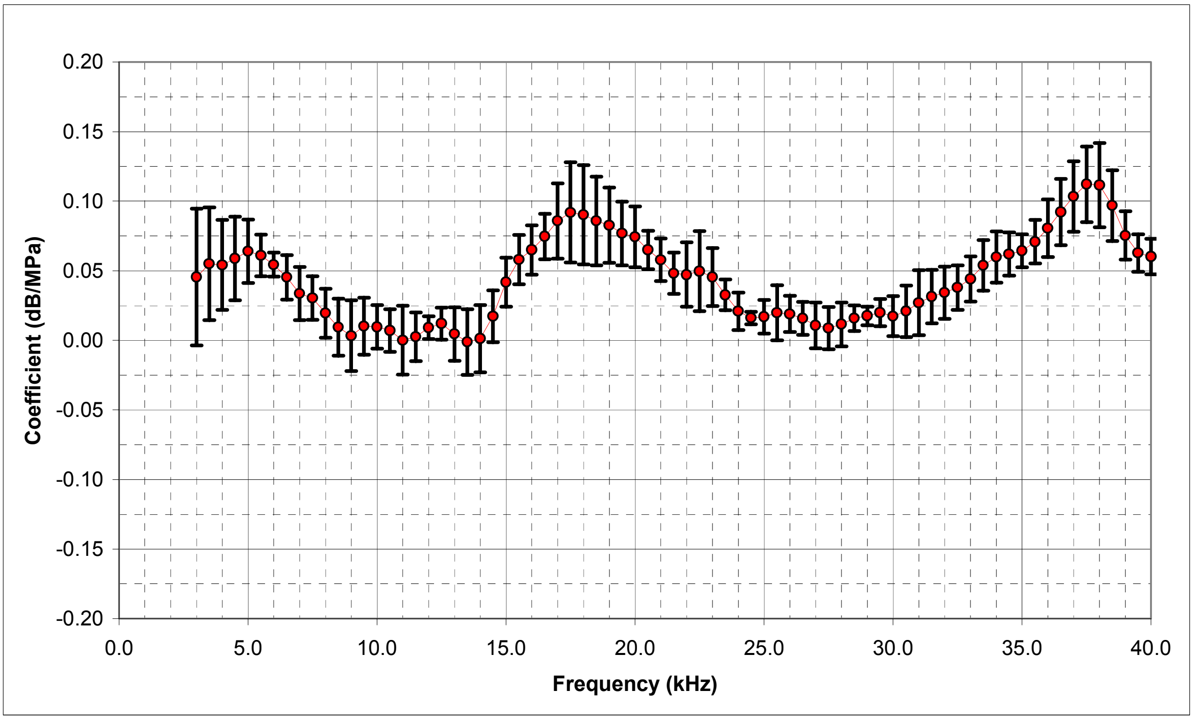

Figure A2.7 Coefficient of variation of hydrophone response with pressure for the ITC1032.

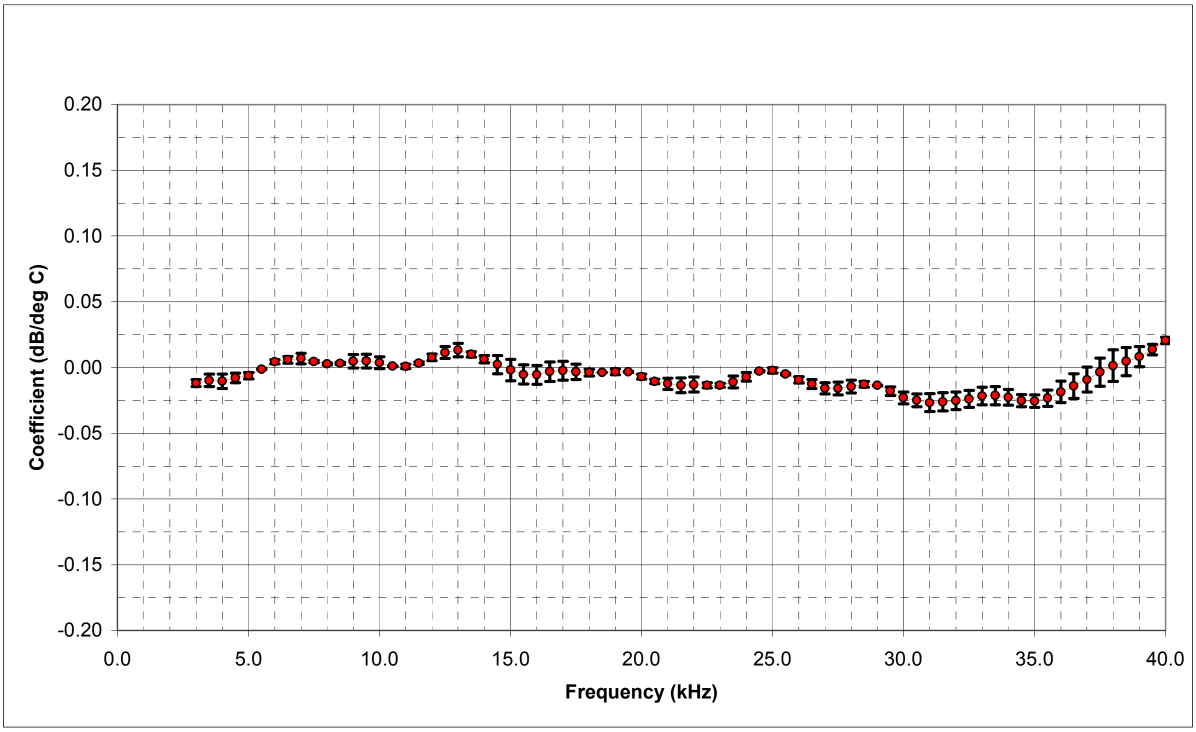

Figure A2.8 Coefficient of variation of hydrophone response with temperature for the ITC1032.

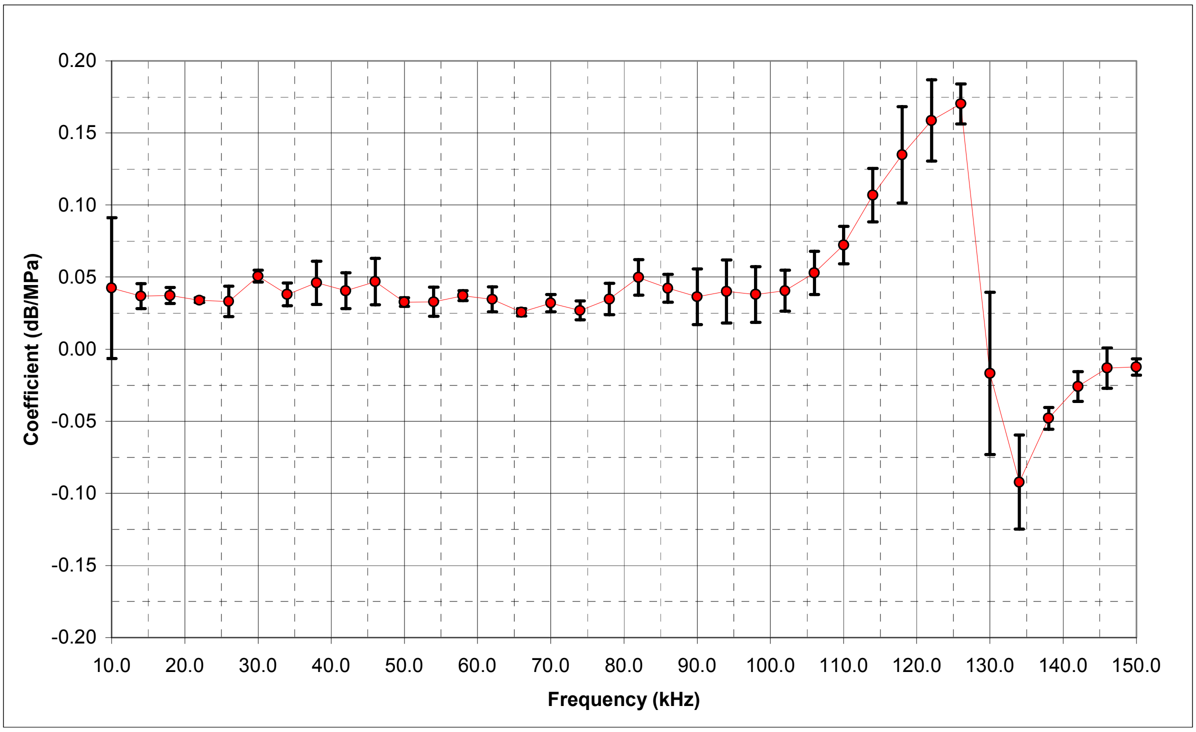

Figure A2.9 Coefficient of variation of hydrophone response with pressure for the ITC1042.

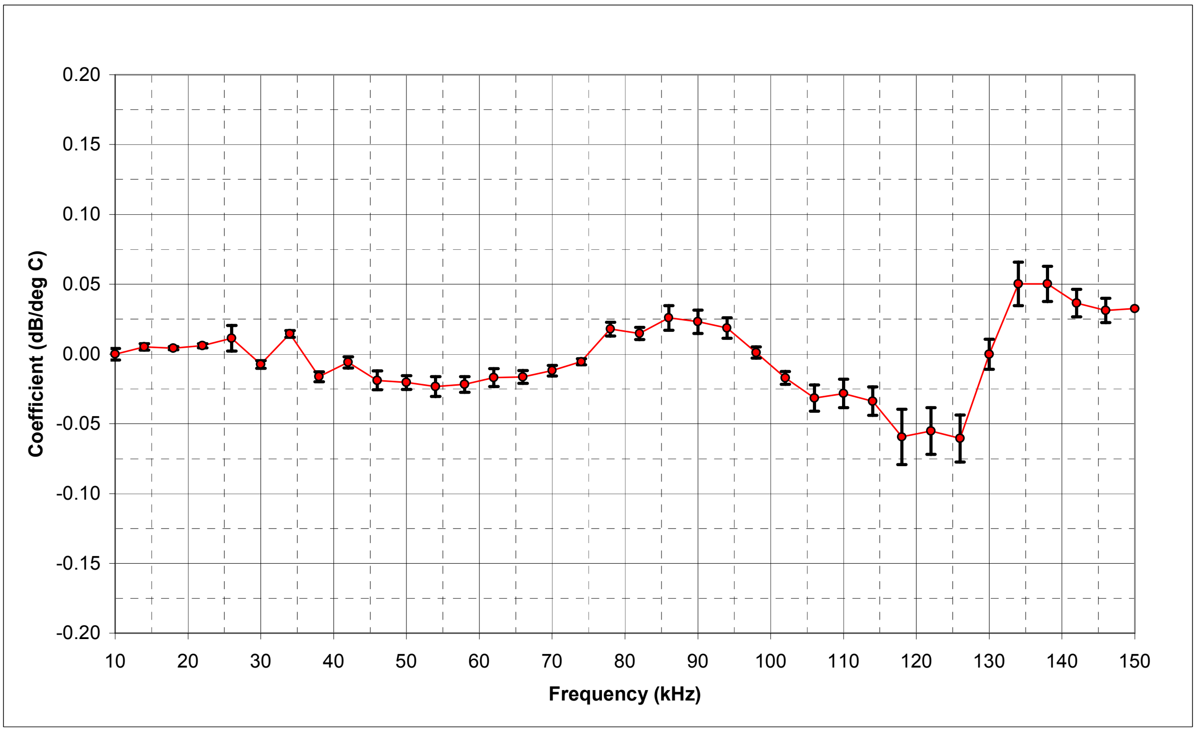

Figure A2.10 Coefficient of variation of hydrophone response with temperature for the ITC1042.

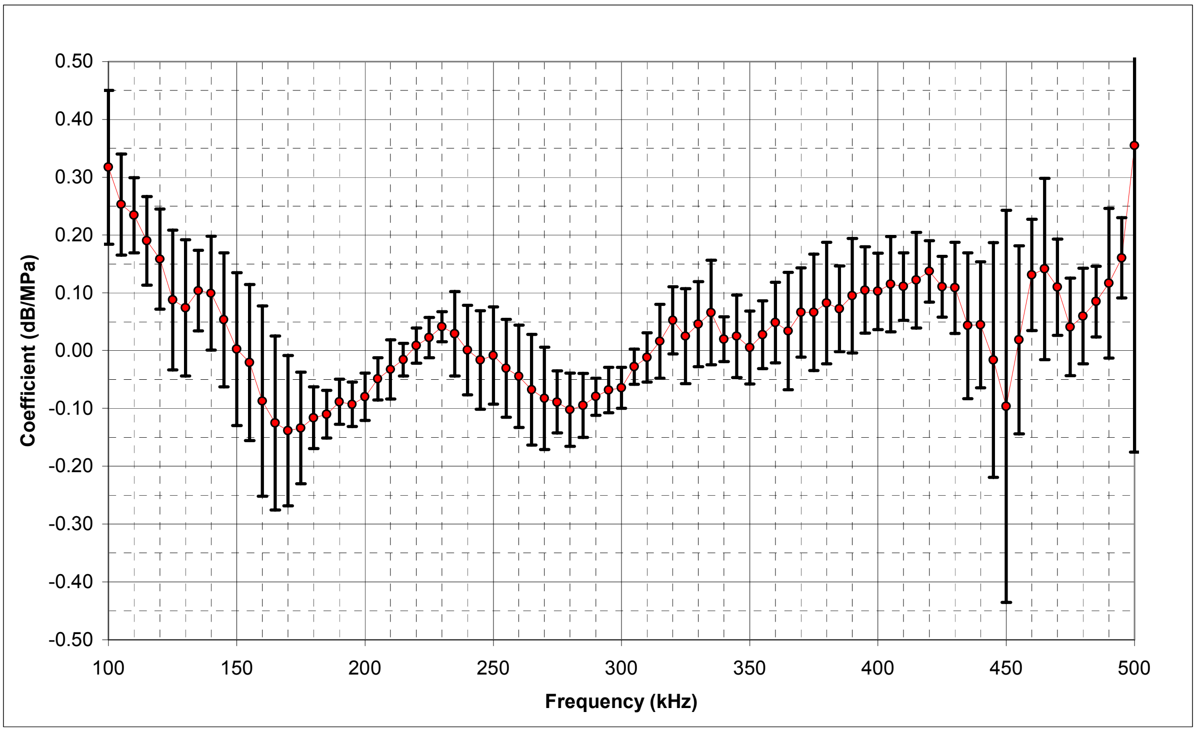

Figure A2.11 Coefficient of variation of hydrophone response with pressure for the Reson TC4034.

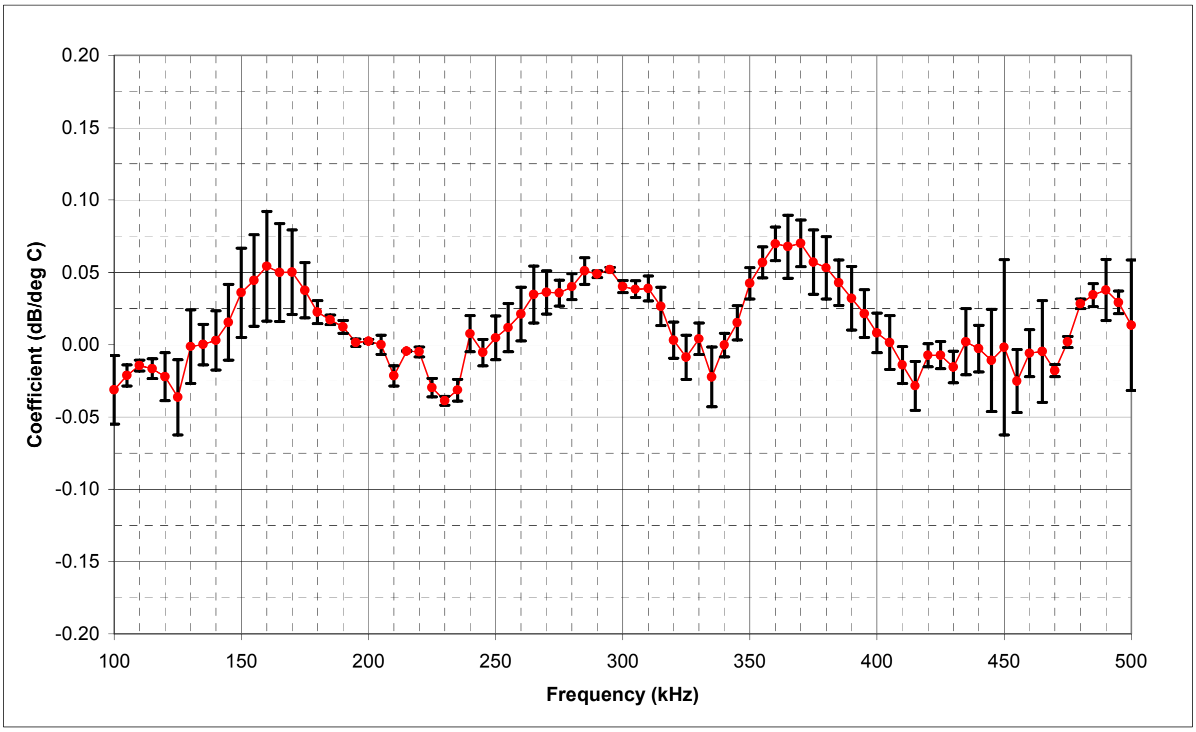

Figure A2.12 Coefficient of variation of hydrophone response with temperature for the Reson TC4034.